Characterization of Non-covalent Interactions in Self-assembling Systems

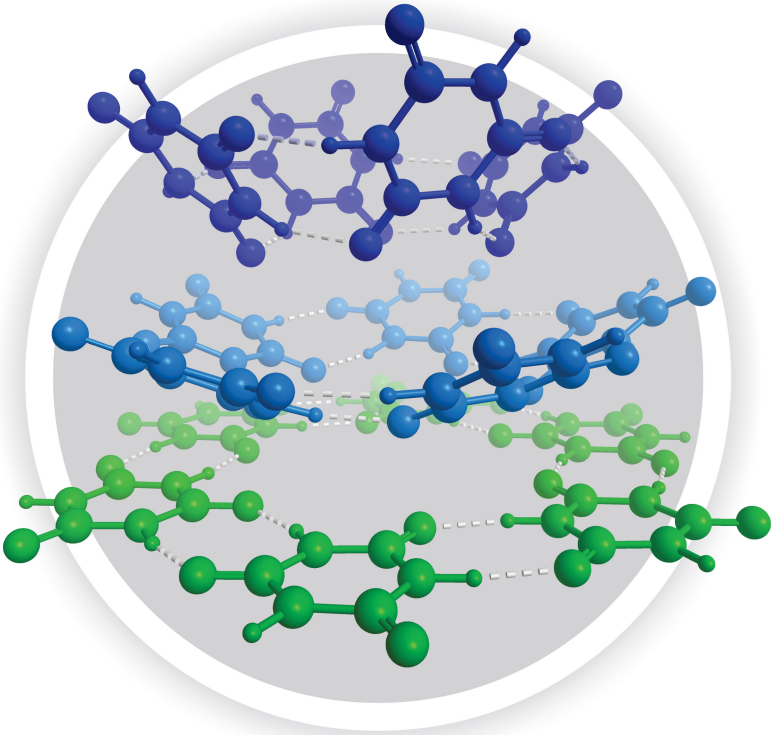

André Nicolai Petelski

Universidad Nacional del Nordeste
Facultad de Ciencias Exactas y Naturales y Agrimensura

Caracterización de las Interacciones no Covalentes en Sistemas Auto-ensamblantes

Tesis Doctoral

André Nicolai Petelski

Tesis presentada para optar por el título de *Doctor de la Universidad Nacional del Nordeste en Química*

Directoras: Prof. Dra. Gladis Laura Sosa

Prof. Dra. Célia Fonseca Guerra

Codirectora: Prof. Dra. Nélida María Peruchena

VRIJE UNIVERSITEIT

Characterization of Non-covalent Interactions in Self-assembling Systems

ACADEMISCH PROEFSCHRIFT

ter verkrijging van de graad Doctor of Philosophy
aan de Vrije Universiteit Amsterdam en Universidad Nacional del Nordeste,
op gezag van de rectores magnifici
prof.dr. V. Subramaniam en prof. M.D. Veiravé,
in het openbaar te verdedigen
ten overstaan van de promotiecommissie
van de Faculteit der Bètawetenschappen
op woensdag 8 mei 2019 om 13.45 uur
in de aula van de universiteit,
De Boelelaan 1105

door

André Nicolai Petelski

geboren te Resistencia Chaco, Argeninië

promotoren:	prof.dr. C. Fonseca Guerra
	prof.dr. G.L. Sosa
copromotoren:	prof.dr. N.M. Peruchena

"Science is a cooperative enterprise spanning the generations.
It is the passing of a torch from teacher to student to teacher.
A community of minds, reaching back to antiquity and forward to the stars."

Neil de Grasse Tyson

Table of Contents

Dedicated to my mother, who taught me the value of the hard work and discipline,
my sister Alexandra, my number one fan,
Guille, a big support and an inspiration,
and Gustavo, my love, thanks for making me shine.

PREFACE

"In other studies you go as far as others have gone before you, and there is nothing more to know, but in a scientific pursuit there is continual food for discovery and wonder."

Mary Shelley, in Frankenstein

The human being is curious by nature, and that is the driving force that has taken it to wonder itself how things work. This thesis is the fruit of the same energy, of the elemental and innocent curiosity of knowing what chemical compound was on the back of ACHETIQ's T-shirt. The Chaqueña Association of Technological Chemical Engineering Students (Asociación Chaqueña de Estudiantes de Ingeniería Química) I belonged back in my student life.

All of that has resulted in this desire of searching the molecular factors that give rise to the fascinating self-assembling systems.

The results are displayed here as part of the requirements to obtain the academic degree of Doctor of the National University of the Northeast in Chemistry, and Doctor of Theoretical Chemistry at the Vrije Universiteit Amsterdam.

The investigations were carried out at the QUITEX UTN Group (Química Teórica y Experimental, Facultad Regional Resistencia, Universidad Tecnológica Nacional), and at the FONSECA GUERRA GROUP (Vrije Universiteit Amsterdam).

SUMMARY

Self-assembling supramolecular chemistry is a branch of chemistry that studies the spontaneous association of molecular species. Since its birth with the Nobel prizes Donald J. Cram, Jean-Marie Lehn and Charles J. Pedersen, chemists have exploited non-covalent interactions to obtain complex molecular structures with specific functions. **This thesis studies different self-assembling systems based on melamine (M), cyanuric acid (CA) and some of their derivatives. The work focuses mainly on systems assembled via hydrogen bonds.**

Within the overlap of supramolecular and organic chemistry non-covalent synthesis has arisen. The merging of this field of chemistry with areas such as materials science and nanotechnology has led to the obtaining of self-assembling materials. This new generation of materials, which is also inspired by the spontaneous processes of nature, has stimulated great interest for its potential technological applications. For instance, in bottom-up methods for the development of more efficient nanotechnology. Within this method, molecules are building-blocks to construct materials block by block. Thus, **one of the main objectives of this thesis is to contribute to the understanding of the nature of self-assembling processes through the structural-electronic characterization of M and CA supramolecules**.

On the other hand, behind experimentation and theory, simulation experiments represent the third pillar of science. The theoretical study of supramolecular systems has allowed researchers to explain many phenomena of this field and it has paved a very promising way for the rational design of materials. Therefore, another of the main **objectives of this thesis is to obtain information about structure and energy that could lead to discern if a molecular system has better self-assembling capabilities than others.**

For the characterization of the different molecular systems studied here, different electronic-structure analyzes have been carried out within the framework of the density functional theory (DFT). By using tools of the Quantum Theory of Atoms in Molecules (QTAIM), an exploratory study of the electronic charge density was

carried out. Charge transfer energies and electronic populations have also been analyzed using the Natural Bond Orbitals (NBO) method. Finally, within the Kohn-Sham Molecular Orbital Theory, an exhaustive analysis of the interaction energies and their energy decomposition has been carried out along with Voronoi Deformation Density analyzes.

This thesis is organized as follows:

In **Chapter I**, a brief historical background of supramolecular chemistry and the specific terms of the field are introduced. The thermodynamics of the self-assembly process is also described. Then, the definition of the hydrogen bond is presented, along with its characteristics like strength, classification and nature. Finally, the aim and the objectives of this thesis are pointed out.

In **Chapter II**, a brief description of the used methods is presented. Firstly, the DFT methods and basis sets that were used in the thesis are presented. Then, basic concepts of the energy decomposition analyzes, and a summary of the QTAIM and the NBO theories are also covered.

In **Chapter III**, some hydrogen- and halogen-bonded supramolecules of M and a selected set of CA derivatives are explored. This includes the trithiocyanuric acid, mono-chlorinated and mono-brominated cyanuric acid. An analysis of the electronic charge density distribution in the framework of QTAIM and NBO analysis was performed in order to characterize their interactions and to investigate how the incoming monomers perturb M. Selected aromaticity indices were computed for the triazine ring of M. The study shows that the analogue with bromine can form complexes that are as strong as those of melamine and cyanuric acid. The interplay of intramolecular interactions is also revealed.

The molecular factors that govern the self-assembly process of the well-known rosette of CA and M are explored in **Chapter IV**. Through a thorough topological analysis we could observed that, despite the system does no show a net cooperative effect, some interactions are more strengthened than others. Our computations are in

line with crystallographic data and the finding of a new phase of these compounds in the solid state.

In **Chapter V** the self-assembling capability of CA is unveiled. It has been shown that the molecule itself can form different supramolecular arrangements when it is deposited as a monolayer, and they can coexist within the same layer. Through a QTAIM and NBO analysis we have shown that while one arrangement shows the presence of cooperativity, the other one shows larger binding energies.

When it comes to M, it is known that the gradual hydrolysis of this compound leads to the obtaining of CA. In **Chapter VI,** through an exhaustive energy analysis, we examine the self-assembling capacity of the first hydrolysis by-product of M, which is called ammeline (AM). The computations reveal that AM is superior than M as a self-assembling building block to form cyclic rosettes (hexamers). This outcome was proved not only by a greater pair interaction in AM but also the presence of a strong synergistic effect.

Given the relevance of M and AM rosettes, we then undertook a computational study of these systems and their interactions with monovalent cations and anions. In **Chapter VII**, we show that M and AM rosettes are potent supramolecules to selectively recognize ions.

Finally, even though every chapter has its own conclusion, in **Chapter VIII** the general conclusion of this thesis is exposed.

RESUMEN

La química supramolecular auto-ensamblante es una rama de la química que estudia la asociación espontánea de especies moleculares. Desde su nacimiento con los premios nobeles Donald J. Cram, Jean-Marie Lehn y Charles J. Pedersen, los químicos han explotado las interacciones no-covalentes para obtener estructuras moleculares complejas y con funciones específicas. **En esta tesis se estudian diferentes sistemas auto-ensamblantes basados en la melanina (M), el ácido cianúrico (AC) y algunos de sus derivados. El trabajo se enfoca pricipalmente en sistemas ensamblados por puentes de hidrógeno.**

En los límites de la química supramolecular con la síntesis orgánica surge lo que hoy se conoce como la síntesis no covalente. La fusión de este campo de la química con áreas como la ciencia de los materiales y la nanotecnología ha dado lugar a la obtención de materiales auto-ensamblantes. Esta nueva generación de materiales, inspirada también en los procesos espontáneos de la naturaleza, ha despertado un gran interés por sus potenciales aplicaciones tecnológicas. Por ejemplo, en los métodos bottom-up (de abajo hacia arriba) para el desarrollo de nanotecnología más eficiente, es decir, la construcción bloque a bloque haciendo uso de moléculas. En este sentido, **uno de los objetivos principales de esta tesis es el de contribuir a la comprensión de la naturaleza de los procesos auto-ensamblantes mediante la caracterización estructural-electrónica de supramoléculas de M y AC.**

Por otro lado, detrás de la experimentación y la teoría, los experimentos de simulación representan el tercer pilar en la ciencia. La simulación de sistemas supramoleculares ha permitido así explicar muchos fenómenos del campo, y además ha pavimentado un camino muy prometedor para el diseño racional de materiales. Por ello, otro de los **objetivos principales de esta tesis es el de obtener información del tipo estructura-energía que permita discernir si un sistema molecular tiene mejores capacidades auto-ensamblantes que otro.**

Para la caracterización de los diferentes sistemas moleculares estudiados en esta tesis, se han realizado diferentes análisis de estructura electrónica en el marco de la teoría del funcional de la densidad (DFT). Se ha realizado un estudio exploratorio de la densidad de carga electrónica utilizando herramientas de la Teoría Cuántica de Átomos en Moléculas (AIM). Se han estudiado también energías de transferencia de carga y poblaciones electrónicas mediante el método de los Orbitales Naturales de Enlace (NBO). Finalmente, haciendo uso de la Teoría de Orbitales Moleculares de Kohn-Sham, se ha realizado un análisis exhaustivo de las energías de interacción y de su descomposición energética, en conjunto con análisis de la Deformación de la Densidad de Voronoi (VDD)

La presente tesis está organizada de la siguiente manera.

En el **Capítulo I**, se introducen brevemente los antecedentes históricos de la química supramolecular, junto con los términos específicos del campo. Además, se describe la termodinámica del proceso de auto-ensamblado. Luego, se presenta la definición de los enlaces de hidrógeno, y también características tales fortaleza, clasificación y naturaleza. Finalmente, se señalan los objetivos de la tesis.

En el **Capítulo II**, se presenta una breve descripción de la metodología utilizada. En primer lugar, se presentan los métodos DFT y los conjuntos base que fueron empleados. Luego, se presentan los conceptos básicos de los análisis de descomposición de la energía, y un resumen de la teoría AIM y NBO.

En el **Capítulo III**, se exploran supramoléculas de M y un conjunto de derivados del AC, los cuales se encuentran unidos mediante puentes de hidrógeno y halógeno. Esto incluye al ácido tritiocianúrico y a derivados mono clorados y bromados del AC. Para caracterizar las interacciones y analizar cómo perturban los monómeros a la M, se realizó un análisis de la densidad de carga electrónica en el marco de la teoría AIM y NBO. También se analizaron algunos índices de aromaticidad en el anillo de la M. El estudio muestra que el análogo bromado del AC puede formar complejos tan estables como los de M-AC. Finalmente, se expone también el papel de las interacciones intramoleculares.

En el **Capítulo IV** se exploran los factores moleculares que gobiernan el proceso de auto-ensamblado de las conocidas rosetas de AC y M. Mediante un profundo análisis topológico se pudo observar que, a pesar de que el sistema no muestra un efecto cooperativo neto, algunas interacciones son más fortalecidas que otras. Los cálculos computacionales se encuentran en buen acuerdo con datos cristalográficos, y con el hallazgo de una nueva fase de estos compuestos en el estado sólido.

En el **Capítulo V** se manifiestan las capacidades auto-ensamblantes del AC. Ha sido demostrado experimentalmente, que el AC puede formar diferentes arreglos supramoleculares cuando es depositado en monocapas, y que además pueden coexistir. Mediante un análisis AIM y NBO se ha mostrado que uno de los arreglos presenta cooperatividad, mientras que el otro presenta fuertes interacciones de enlace.

Finalmente, aunque cada capítulo cuenta con sus conclusiones particulares, en el **Capítulo VIII** se exponen las conclusiones generales de esta tesis.

I. GENERAL INTRODUCTION AND OBJECTIVES

- ***Mr. Rzykruski:*** *Back home, everyone is scientist. Even my plumber wins Nobel Prize. Your country does not make enough scientist. Always needs more. You should be a scientist, Victor.*
- ***Victor Frankenstien:*** *Nobody likes scientists.*
- ***Mr. Rzykruski:*** *They like what science gives them, but not the questions, no. Not the questions that science asks.*
- ***Victor Frankenstien:*** *Actually, I have a question.*
- ***Mr. Rzykruski:*** *That is why you are a scientist.*

Extract from the movie Frankenweenie, directed by Tim Burton

I.1. Supramolecular Chemistry. Historical review and definitions

The general principles of *supramolecular chemistry* (SC) were yet enunciated many years ago, for instance in one of the biggest works of Linus Pauling: *The Nature of the Chemical Bond*.[1,2] Almost 80 years later a new chapter in the SC was introduced by Bruns and Stoddart (Nobel Prize for his molecular machines) with the publication of the book *The Nature of the Mechanical Bond*.[3] The *supramolecule* concept was already introduced in 1937 by Wolf *et al*.[4] in order to describe the interactions in some chemical species like the carboxylic acid dimer. However, it was only in 1987 when the basis of the concept, just as we know it, were set by the chemists Donald J. Cram, Charles J. Pedersen and Jean-Marie **Lehn** who were awarded a Nobel Prize[i] *"for their development and use of molecules with structure-specific interactions of high selectivity"*. Consequently, as from that important event, a new and a solid branch of chemistry was opened, and yet it is still growing and surprising chemists. Nevertheless, the SC is a multidisciplinary field that uses other ones, like organic and inorganic chemistry, physical chemistry and molecular modeling,[5] which, at present, allows the comprehension of the complex behavior of supramolecules.

[i] "The Nobel Prize in Chemistry 1987". *Nobelprize.org*. Nobel Media AB 2014. Web. 14 Feb 2017. http://www.nobelprize.org/nobel_prizes/chemistry/laureates/1987/

The SC was described by J. –M. Lehn as "*the chemistry beyond the molecule*",[6] or, the chemistry of the non-covalent bond. This field studies the complex entities called supramolecules, which are the result of the association of two or more molecules via intermolecular forces.

A very good analogy of SC is the very famous Mecanno® game, as shown in **Figure I.1a**. This construction system consists in a set of small pieces with different forms and sizes, and then by their combination with other junction pieces several models can be constructed, starting from vehicles to robots. In this sense, the SC is just like a Meccano, since there is a vast diversity of building blocks (molecules) that can be interconnected by a diverse "*set*" of non-covalent interactions (e.g., hydrogen bonds, halogen bonds, π–π stacking, etc.), with the final aim of constructing models with a defined structure (see **Figure I.1b**).

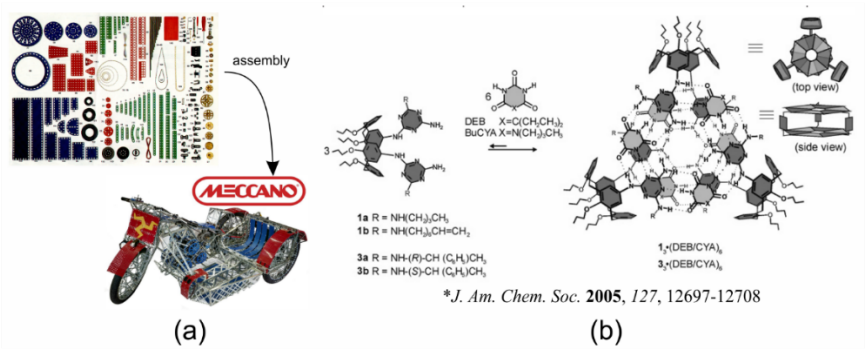

Figure I.1. (a) Meccano Brand construction system: small pieces are assembled to obtain a more complex structure. **(b)** Example of a supramolecular self-assembly: molecular fragments self-assembly in a cage-like structure.

Ongoing the same way, the concept of non-covalent synthesis emerges. A side and an essential field for SC, in which the physicochemical study of molecular interactions acquires a great meaning. Thus, the SC has become a very powerful and highly effective tool to create very complex structures spontaneously.[7–9] In recent years, a growing interest in molecular devices has motivated the research of intra

and intermolecular forces that control and drive the creation of nanostructures in one, two and three dimensions by the self-assembly of small molecular building blocks.[9–11] So that, in 2016 the Royal Swedish *Academy* of Sciences awarded the Nobel Prize in Chemistry to Jean-Pierre Sauvage, Sir J. Fraser Stoddart and Bernard L. Feringa *"for the design and synthesis of molecular machines"*.[ii]

Finally, the SC can be divided into two main categories: *host-guest* and *self-assembly*. Since this thesis is focused on the latter, a special attention will be given to it.

I.1.1. Host-guest supramolecular chemistry

If a molecular species is big enough and contains a cavity to hold another smaller molecule, the first one is called *host* and the second one *guest.* In his Nobel Lecture,[12] Donald Cram has defined these molecules as:

> *"The host component is defined as an organic molecule or ion whose binding sites converge in the complex… the guest component is defined as any molecule or ion whose binding sites diverge in the complex…"*

The binding site is a region within a molecule that must have the correct size and geometry and a specific chemical nature, so the molecules can interact with each other. Classic examples of these complexes are the substrate-enzyme biological systems, in which the host (enzyme) has a binding pocket with a specific chemical activity to welcome the guest (*e.g.* a special drug), as shown in **Figure I.2a**. Other illustrations are coordination complexes like those with ethylenediaminetetraacetic acid (EDTA) or the famous crown ethers, which were synthesized by the previously mentioned Nobel Laureate Charles Pedersen (see

[ii] "The Nobel Prize in Chemistry 2016". *Nobelprize.org.* Nobel Media AB 2014. Web. 15 Feb 2017. <http://www.nobelprize.org/nobel_prizes/chemistry/laureates/2016/>

Figures I.2b,c). In these last cases, the EDTA or the crown ether have specific groups that converged to the guest.

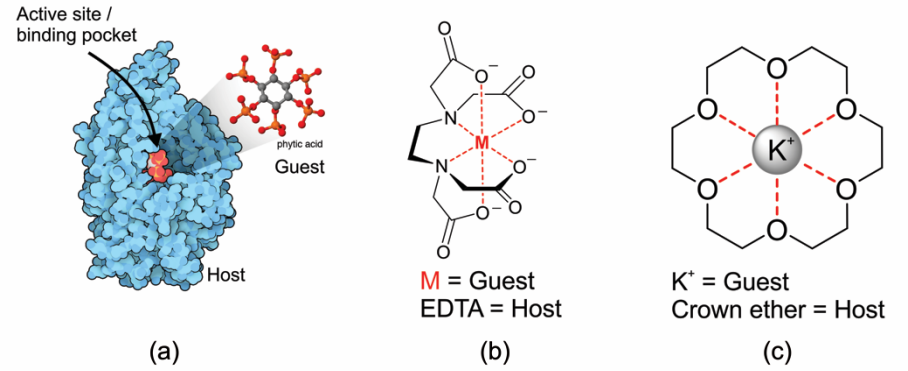

Figure I.2. (a) Substrate-enzyme biological system.[iii] **(b)** EDTA-Metal complex. **(c)** Crown ether/K^+ complex

Despite this division in categories (host-guest and self-assembly), there are several examples that limit between both sub-areas. One of the most representative cases are the inclusion compounds in the solid state, in which atoms, ions or guest molecules are trapped inside the cavities that other molecules create as a consequence of the crystal packing. Such compounds are called *clathrates*. One of the most well-known examples is the xenon/hydroquinone clathrates, as shown in **Figure I.3**.

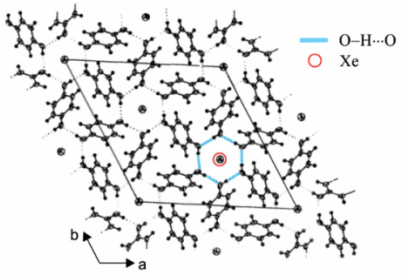

Figure I.3. Unit cell of β-hydroquinone/Xe clathrate. Taken from ref.: *Acta Cryst.* **1989**, *C45*, 944-946

[iii] Taken from www.pdb.org DOI: 10.2210/rcsb_pdb/mom_2018_9

I.1.2. Self-assembling supramolecular chemistry

Self-assembly can be defined as the *spontaneous and reversible association of molecular species to form bigger and more complex supramolecular entities according to the intrinsic information that is contained in the constituent molecules.*[13–15] It should be pointed out that there is a big difference between the concepts molecular and supramolecular self-assembly. The former refers to the formation of covalent bonds in a conventional synthesis, while the latter denotes the molecular association by non-covalent forces, which is mediated by molecular recognition.

In an article of the *New Journal of Chemistry*,[7] Lindsey has exposed an ultimate classification of different types of self-assembly as follow:

1. *Strict self-assembly:* the final product, which is thermodynamically reversible, is formed completely spontaneously when the components are mixed under specified conditions.
2. *Irreversible self-assembly:* it involves the formation of a stable product by the formation of covalent bonds under kinetic control.
3. *Precursor modification followed by self-assembly:* it involves molecules that that cannot self-assemble unless they are modified chemically or activated by some other changes.
4. *Self-assembly with post-modification:* in this process, the self-assembled product is then covalently modified and finally it becomes irreversible.
5. *Assisted self-assembly:* in this case, external factors are employed, which are not part of the final ensemble, and they are involved in mediating the assembly process alike a catalyst.
6. *Directed self-assembly:* this class involves a template that can be part of the final product or not.
7. *Self-assembly with intermittent processing:* this class incorporates processes of the aforementioned classes.

Whitesides, one of the pioneers in the field of supramolecular chemistry, has deeply studied complexes of cyanuric acid (1,3,5-triazine-2,4,6-trione) and melamine (2,4,6-triamine-1,3,5-triazine)[16–18] by employing preorganization and steric hindrance techniques. These methods are also called non-covalent synthesis.[19] In **Figure I.1a** it can be seen a supramolecular complex made of melamine and cyanuric acid, which were covalently modified, in order to direct the assembly of a particular structure, in this case, a complex with a cage-like arrangement that can also host small molecules inside.[20]

Finally, it is common within self-assembling systems for there to be more than one type of interaction present. Therefore, self-assembly processes can be classified as *Single-interaction self-assembly* and *multiple-interaction self-assembly.* The former refers to systems in which only one specific interaction is present (*e.g.* N–H···N hydrogen bonds, or N···Cu coordination interactions). The letter refers to processes in which more than one interaction of any kind is present (*e.g.* N···Cu and N···Pd interactions, or N–H···N and N–H···O hydrogen bonds). Multiple-interaction assemblies can be sub-divided into *unimediated* and *multimediated* assemblies, depending on whether there is more than one category of interaction present (*e.g.* N···Cu interactions and N–H···N hydrogen bonds).

It is noteworthy that nature has already overcome chemists. A vast number of examples in biology amazes and inspires researchers to construct new and more efficient molecular systems. The most well-known case is the double helix of DNA, which is formed by two independent polymeric chains that are hydrogen-bonded. However, the concept of *self-assembly* itself was conceived from the study of tobacco mosaic virus, the "holy grail" of supramolecular chemistry. This virus is made of an RNA chain encapsulated in a protein shell, which is built from 2130 identical monomers, as shown in **Figure I.4**.

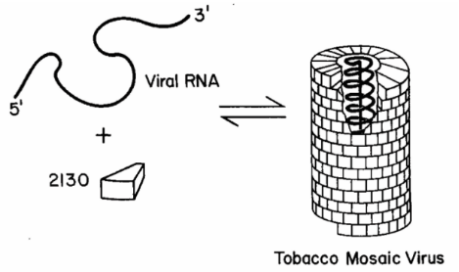

Figura I.5. Self-assembly scheme of tobacco mosaic virus. Taken from J. S. Lindsey. *New. J. Chem.* **1991**, *15*, 153-180.

Research has shown that the virus can be dissociated into its constituent parts and then re-assembled to rebuild the intact virus, under specific conditions as a chemical reaction.

I.1.2.1 Thermodynamic of the self-assembly

Self-assembly processes are reversible and dynamic by nature. This allows them to correct all the "errors" during the successive assemble steps in order to gradually reach thermodynamically most stable product. When a large number of molecules bind non-covalently, there is more than one possibility of binding. Nevertheless, it is a fact that only one product will prevail according to thermodynamics. Any self-assembled system can be understood as a *dynamic combinatorial library*: many products are able to be formed and broke up continuously, and this process tends to the most stable thermodynamic product.

Enthalpic and entropic considerations

Figure I.5 shows six molecules that can assembled via hydrogen bonds into two main structures: a cyclic and an open structure.

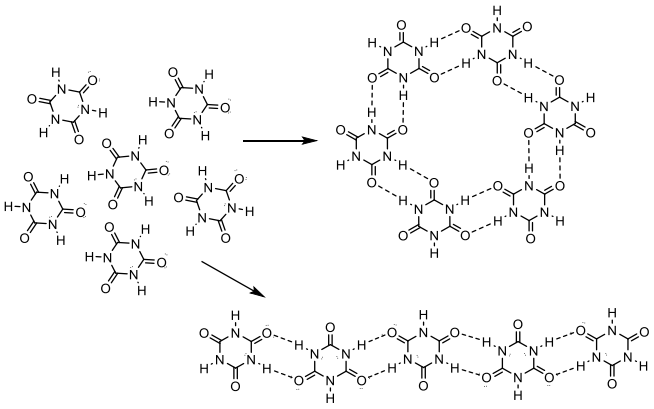

Figure I.5. Possible aggregation states in a self-assembly process.

Lawrence *et al.*[21] has claimed that the preferential self-assembling of discrete architectures over open oligomers is related to the widely known phenomenon of enthalpic-entropic compensation. When each interaction is formed, the enthalpic benefit is balanced by the entropic cost. This implies losing degrees of freedom, which leads to a greater loss of entropy.

In an effort of elucidating the thermodynamic parameters that determine the relative stabilities of cyclic and linear aggregates of melamine-cyanuric acid complexes, Reinhoudt *et al.*[22] have developed a novel thermodynamic model that considers the possible stereoisomers and their equilibrium constants, and including steric hindrance. Their study shows that the thermodynamics of the assembly is controlled by two variables: the association constant of the dimer and the association constant of the cyclic rosette via the linear isomer.

I.1.2.2 Technological applications

In nature, several biological and chemical processes occur every second within the nanoscale. The main idea of this area is that, in principle, we could construct complex molecular systems with a minimal effort, in the same way nature constructs proteins, copies DNA or transports endorphins. This implies less use of chemicals

and more efficient chemistry, but there are still many challenges, which researchers are struggling with.

Supramolecular self-assembly and non-covalent synthesis are still at a very early stage. In general, scientists are creating fascinating supramolecules and showing to the scientific community, what they can do. However, several advances and applications are growing every year. For example, the self-assembly of small molecular units unto surfaces, like gold or graphite, can originate self-assembled monolayers (SAMs). This could be used to produce different nano-coatings over surfaces with different functions, and these new surfaces could have the ability to capture atoms,[23,24] small molecular fragments,[25] or even cells.[26] In addition, one could modified covalently the original building blocks in order to add new functional groups with different physical, chemical, electrochemical, and biochemical properties. This process in conjunction with chemical etching techniques could be useful to produce nanoelectronics devices and sensors.[26]

Concerning nanotechnology, *bottom-up* techniques will replace the *top-down* ones in the near future. Researchers can now fabricate many nano-molecular structures with self-assembling techniques, i.e.: nanowires, nanorings, and complexes with several forms (square, rectangular, pyramidal, etc.).[24]

Finally, in the area of material science, hydrogels have emerged from self-assembly chemistry. These materials have a semi-solid elastic state with a very complex network. Their gel-like properties are gaining considerable attention for their future applications.[27–29]

I.1.3. Key interactions in supramolecular chemistry

Molecular interactions are the backbone of the non-covalent synthesis. As long as they are completely understood and described, a rational design of materials with specific functionalities will be achieved. That is, probably, one of the reasons why the hydrogen bond is still under study.

Non-covalent bonds have an energy that ranges from around 2 $kJ.mol^{-1}$, for dispersive interactions, to 300 $kJ.mol^{-1}$, for ion-ion type interactions. This range in energy can be used, in principle, to fine-tune the stability of a particular complex structure over another one. In addition, the use of different interactions with different strengths can also be understood as an intrinsic information of the molecules with a set of instructions to be read by the self-assembly process.

In this vast sea of interactions, it is not very straightforward to summarize a whole pallet with all the non-covalent bonds with their ranges in strength. Some excellent text books on supramolecular chemistry[3,5,14] have done this work, but they differ in the strength energies. Therefore, for a more in-depth discussion, the reader is thus referred to them. Nevertheless, a good approximation is the summary given in **Table I.1**.

Since this thesis is focused on the study of hydrogen-bonded supramolecules, this interaction will be described with more detail.

Definition

The IUPAC Gold Book has two definitions about hydrogen bonds:[iv]

> *"A form of association between an electronegative atom and a hydrogen atom attached to a second, relatively electronegative atom. It is best considered as an electrostatic interaction, heightened by the small size of hydrogen, which permits proximity of the interacting dipoles or charges. Both electronegative atoms are usually (but not necessarily) from the first row of the Periodic Table, i.e. N, O or F. Hydrogen bonds may be inter-molecular or intra-molecular. With a few exceptions, usually involving fluorine, the associated energies are less than 20 – 25 kJ mol^{-1} (5 – 6 kcal mol^{-1})."*

[iv] http://goldbook.iupac.org

Table I.1. Different types of bonds and typical ranges of energies[a]

Bond type		Energy Range (kcal mol^{-1})
Weak	Dispersion Forces	≤ 1
	Dipole–Dipole Interactions	0.5 – 2
	Hydrogen Bonds	1 – 10
	Halogen Bonds	1 – 40
	Ion-Pairing	2 – 50
Strong	Coordinate/Dative Bonds (M–X)	10 – 100
	Organic Covalent Bonds (C–X)	60 – 100
	Ionic Lattice	250 – 4000

[a] taken from ref. [3]

Hydrogen bond in theoretical organic chemistry:

"A particular type of multicenter (three center - four electron) X–H···Y in which the central hydrogen atom covalently linked to an electronegative atom X (C, N, O, S...) forms an additional weaker bond with atom Y (N, O, S..) in the direction of its lone electron pair orbital. The energy of hydrogen bonds, which is usually in the range of 12 – 65 kJ mol^{-1} (3 – 15 kcal mol^{-1}), results from the electrostatic interaction and also from the orbital interaction of the antibonding σ(XH)* MO *of the molecule acting as the hydrogen donor and the non-bonding lone electron pair* MOn_Y *of the hydrogen acceptor molecule."*

The second definition is more open and extended than the first one, since it also considers the covalent component resulting from the charge transfer. However, a new definition of hydrogen bonds has been recommended in the scientific journal of IUPAC:[30]

> *"The hydrogen bond is an attractive interaction between a hydrogen atom from a molecule or a molecular fragment X–H in which X is more electronegative than H, and an atom or a group of atoms in the same or a different molecule, in which there is evidence of bond formation."*

In this article, the authors set a list of criteria and some characteristics of the interactions. They define hydrogen bonds as a result of electrostatic, charge transfer and dispersion components. But, it should be pointed out that the Pauli repulsion, which is responsible for any steric hindrance, could also be a decisive factor for relative hydrogen-bonding strengths and lengths.[31] In general, it is accepted in the literature that the nature of hydrogen bonds can be described, in principle, by the interplay of five contributions:

1. Electrostatic or coulomb energy
2. Exchange repulsion
3. Polarization energy
4. Charge-transfer energy or attractive orbital interactions
5. Dispersion forces.

It is worth stressing that there exist different approaches in which to decompose the interaction energy, and yet there is no solid consensus about it. For instance, some decomposition schemes compute the polarization and charge transfer contributions, but, as Timothy Clark has pointed out, they are part of the same phenomenon and separating them does not lead to a more predictive model.[32] Moreover, Wolters and Bickelhaupt[33] have indicated that one can get insight into these contributions by a detailed orbital analysis. Elangannan Arunan has also claimed that besides those energy components "*all that can be experimentally measured is the interaction energy*" (or more precisely, the binding energy[34]), and "*all the methods for decomposing them are models, and we should not forget that.*"[v]

[v] https://www.chemistryworld.com/news/do-hydrogen-bonds-have-covalent-character/2500428.article

Finally, chemistry uses models to explain nature, and as long as they have predictive power, there is nothing wrong with them. That is the way science works, and models will continue to be improved in order to understand observable nature better every time.

Hydrogen bond geometry

The hydrogen bond is usually depicted as X–H···Y–Z, where X–H is the H-bond donor (also called Lewis acid, electron acceptor) and Y–Z is the H-bond acceptor (Lewis base, electron donor). The hydrogen bond can also be represented as D–H···A (D for H-bond donor and A for H-bond acceptor). The geometry may also be described in terms of the distances *d, D* and *r,* and angles θ and ϕ, as shown in **Figure I.7a**. If $\theta = 180°$ the hydrogen bond is perfectly linear. There are also situations in which a donor can interact with more than one acceptor and vice versa (see **Figures I.7c-f**). All of these geometries are of particularly importance in self-assembly and they will be discussed in subsequent chapters.

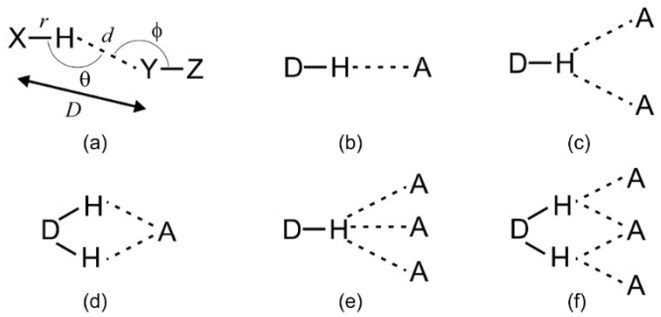

Figure I.7. Different geometries of hydrogen bonds: **(a)** bent, with geometrical parameters **(b)** linear, **(c)** donating bifurcated, **(d)** accepting bifurcated, **(e)** trifurcated, **(f)** three center bifurcated.

Hydrogen bond strength

George Jeffrey has classified them into three general categories: strong, medium and weak, according to the energy of the interaction.[35] General properties of the

three classes of hydrogen bond are given in **Table I.2**. The strength of a hydrogen bond should be expressed more exactly by their enthalpies as: strong (14–40 kcal mol^{-1}), moderate (5–15 kcal mol^{-1}), or weak (0–5 kcal mol^{-1}).

Table I.2. Properties of D–H···A hydrogen bonds[a]

	Strong	Moderate	Weak
Bond energy (kcal mol^{-1})	15 – 40	4 – 15	< 4
Bond lengths (Å)			
H···D	1.2 – 1.5	1.5 – 2.2	2.2 – 3.2
A···D	2.2 – 2.5	2.5 – 3.2	3.2 – 4.0
Bond angles (°)	175 – 180	130 – 180	90 – 150
IR ν_s relative shifts	25%	10 – 25%	< 10%
^{1}H NMR chemical shift downfield (ppm)	14 – 22	< 14	-
Examples	HF complexes Super acids	Acids Alcohols	C–H···A and O–H···π hydrogen bonds

[a] adapted from references [13,15]

Hydrogen bond arrays

When a direct interaction between the donor group and the acceptor group occurs, the geometry is usually named as *primary hydrogen bond interaction.* Besides, when multipoint hydrogen bonds occurs, in a contiguous array, secondary electrostatic interactions between neighboring groups could have a significant effect on the stability of a supramolecular complex.[36] Thus, hydrogen bond arrays could be double (DD-AA or DA-AD), triple (*e.g.* DDD-AAA, DDA-AAD, ADA-DAD), quadruple (*e.g.* DDAA-AADD, DADA-ADAD, etc.), and so on. In these cases, the partial charges on adjacent atoms could be destabilizing, due to repulsion between

similar charges, or stabilizing by virtue of attraction between opposite charges (see **Figure I.8**).

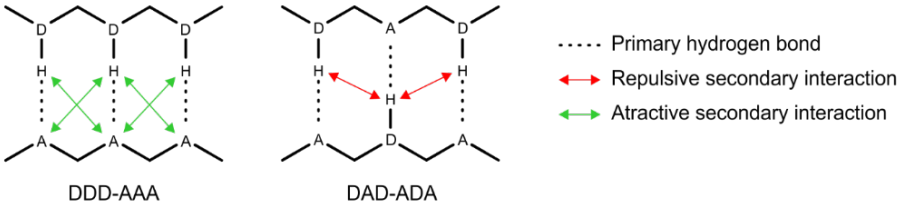

Figure I.8. Secondary interactions in DDD-AAA and DAD-ADA arrays.

These secondary effects could be used, in principle, in empirical methods for predicting complex stabilities and trends in association constants.[37,38] In addition, computational chemistry can assist experiments by the calculation of free energies of complexations.[39]

Hydrogen-bonded synthons

In crystal engineering, supramolecular *synthons* are usually defined as spatial arrangements of non-covalent bonds between molecules (the building block of organic crystals, also called *tectons*), in order to form different interaction patterns within a solid state structure.[14,15,40] Gautam Desiraju introduced the term in 1995 as:[41]

> *"Structural units within supermolecules which can be formed and/or assembled by known or conceivable synthetic operations involving intermolecular interactions."*

Supramolecular synthons are the main tool in crystal engineering to predict and design synthetic methods of novel crystalline structures, and by manipulating functional groups of molecules.

Many authors have claimed that hydrogen bonds are the master key of supramolecular chemistry. There are a vast number of hydrogen-bonded synthons in crystal, and it would be impossible to cover all of them in this chapter. However, the most common arrangements are rings and linear patterns. **Figure I.9** shows all the synthons that were studied in this thesis.

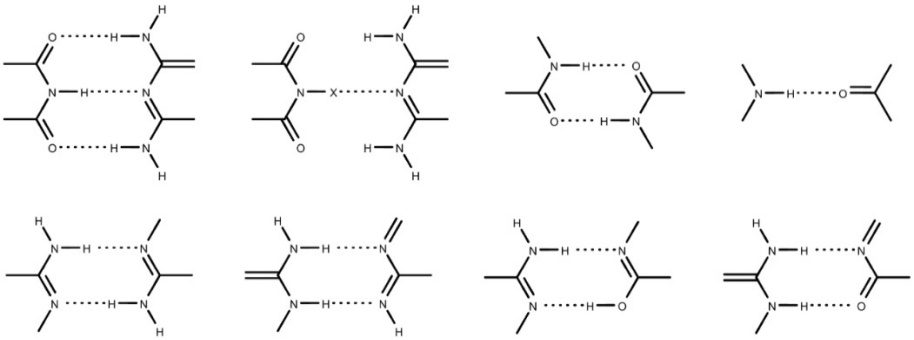

Figure I.9. Synthons that are discussed in this thesis. X = Cl, Br.

Cooperativity in hydrogen bonds

To some extent, hydrogen bonds are like fire ants, since they show group behavior.[42] A single ant is weak, hard to see and easy to kill. However, when they act as a group, they do it in a cooperative way and they can be strong enough to kill small animals, or to form islands over water and make ant bridges. H-Bonds work in the same manner; they can show the phenomenon of cooperativity. In a very simple way, this means that in a molecular cluster the whole is greater than the sum of the parts, or even simpler "1+1 is greater than 2". This effect has a tremendous importance to explain many macroscopic properties in water, materials or proteins.

The synergy effect in molecules has been extensively studied for many authors. It has been shown that the general trend in cooperativity is:

- shorter D···A distance,
- longer D–H distance,
- larger chemical shift,

- large red-shifts of the D–H vibrational frequency.

The many-body interaction is a major source of the cooperativity in molecular clusters of small molecules. However, the origin of the cooperativity has been recently established to be originated in the σ electron system, due to donor-acceptor interactions. The charge transfer from molecule to molecule causes a charge separation, which is the origin of the synergy. In **Chapter V**, the source of cooperativity in cyanuric acid clusters is also elucidated.

I.2. Aim of the thesis:

Understanding the nature of non-covalent interactions in self-assembling systems is extremely important for two main reasons:

1. To link the molecular properties of a system to their potential macroscopic properties, so that one can have a true scientific understanding of matter; and,
2. once we know the interplay between interactions we could design supramolecular materials in a more rational way and also, we could then tune the properties at our will.

The general aim of this thesis is to gain insight into the self-assembly phenomenon by the static characterization of the non-covalent forces between small molecular entities.

The particular objectives are summarized as follows:

- To describe the structural, energetic and electronic properties of small supramolecules.
- To describe the characteristics of the hydrogen bonds and other interactions that are involved in the self-assembly of small building blocks.
- To gain information about the structure and energy that allows us to decide which system will perform better as a self-assembling molecule.

- To gain information about the most important factors that drive the mechanism of the self-assembling phenomenon.

I.3. References

(1) Pauling, L. The Nature of the Chemical Bond. II. The One Electron Bond and Three Electron Bond. *J. Am. Chem. Soc.* **1931**, *53*, 3225–3237.

(2) Pauling, L. *The Nature of the Chemical Bond*; C.U. Press.: Ithaca, New York, 1939.

(3) Bruns, C. J.; Stoddart, J. F. *The Nature of the Mechanical Bonds. From Molecules to Machines*; John Wiley & Sons, Inc.: Hoboken, New Jersey, 2017.

(4) Wolf, K. L.; Frahm, H.; Harms, H. The State of Arrangement of Molecules in Liquids. *Z Phys Chem. Abt. B* **1937**, *36*, 237–287.

(5) *Analytical Methods in Supramolecular Chemistry*; Schalley, C. A., Ed.; WILEY-VCH: Weinheim, 2007.

(6) Lehn, J.-M. Supramolecular Chemistry—Scope and Perspectives Molecules, Supermolecules, and Molecular Devices(Nobel Lecture). *Angew. Chemie Int. Ed. English* **1988**, *27* (1), 89–112.

(7) Lindsey, J. S. Self-Assembly in Sinthetic Routes to Molecular Devices. Biological Principles and Chemical Perspectives: A Review. *New J Chem* **1991**, *15*, 153–180.

(8) Ariga, K.; Hill, J. P.; Lee, M. V; Vinu, A.; Charvet, R.; Acharya, S. Challenges and Breakthroughs in Recent Research on Self-Assembly. *Sci. Technol. Adv. Mater.* **2008**, *9* (1), 14109.

(9) Stupp, S. I.; Palmer, L. C. Supramolecular Chemistry and Self-Assembly in Organic Materials Design. *Chem. Mater.* **2014**, *26*, 507–518.

(10) Paraschiv, V.; Crego-Calama, M.; Fokkens, R. H.; Padberg, C. J.; Timmerman, P.; Reinhoudt, D. N. Nanostructures via Noncovalent

Synthesis: 144 Hydrogen Bonds Bring Together 27 Components. *J. Org. Chem.* **2001**, *66* (25), 8297–8301.

(11) Yagai, S.; Nakajima, T.; Karatsu, T.; Saitow, K.; Kitamura, A. Phototriggered Self-Assembly of Hydrogen-Bonded Rosette. *J. Am. Chem. Soc.* **2004**, *126* (37), 11500–11508.

(12) Cram, D. J. The Design of Molecular Hosts, Guests, and Their Complexes. *Angew. Chem. Int. Ed. Engl.* **1988**, *32* (10), 1009–1112.

(13) Atwood, J. L.; Steed, J. W. *Encyclopedia of Supramolecular Chemistry, Volume 1*; CRC Press, 2004.

(14) Steed, J. W.; Turner, D. R.; Wallace, K. J. *Core Concepts in Supramolecular Chemistry and Nanochemistry*; John Wiley & Sons, Ltd: England, 2007.

(15) Steed, J. W.; Atwood, J. L. *Supramolecular Chemistry*, Second Edi.; John Wiley & Sons, Ltd: United Kingdom, 2009.

(16) Seto, C. T.; Whitesides, G. M. Synthesis, Characterization, and Thermodynamic Analysis of a 1 + 1 Self-Assembling Structure Based on the Cyanuric Acid·melamine Lattice. *J. Am. Chem. Soc.* **1993**, *115* (4), 1330–1340.

(17) Mathias, J. P.; Simanek, E. E.; Whitesides, G. M. Self-Assembly through Hydrogen Bonding: Peripheral Crowding - A New Strategy for the Preparation of Stable Supramolecular Aggregates Based on Parallel, Connected CA3.cntdot.M3 Rosettes. *J. Am. Chem. Soc.* **1994**, *116* (10), 4326–4340.

(18) Cheng, X.; Gao, Q.; Smith, R. D.; Simanek, E. E.; Mammen, M.; Whitesides, G. M. Characterization of Hydrogen-Bonded Aggregates in Chloroform by Electrospray Ionization Mass Spectrometry. *J. Org. Chem.* **1996**, *61* (6), 2204–2206.

(19) Whitesides, G. M.; Simanek, E. E.; Mathias, J. P.; Seto, C. T.; Chin, D. N.; Mammen, M.; Gordon, D. M. Noncovalent Synthesis: Using Physical-Organic Chemistry to Make Aggregates. *Acc. Chem. Res.* **1995**, *28*, 37–44.

(20) Kerckhoffs, J. M. C. a; ten Cate, M. G. J.; Mateos-Timoneda, M. a; van Leeuwen, F. W. B.; Snellink-Ruël, B.; Spek, A. L.; Kooijman, H.; Crego-Calama, M.; Reinhoudt, D. N. Selective Self-Organization of Guest Molecules in Self-Assembled Molecular Boxes. *J. Am. Chem. Soc.* **2005**, *127* (36), 12697–12708.

(21) Lawrence, D. S.; Jiang, T.; Levett, M. Self-Assembling Supramolecular Complexes. *Chem. Rev.* **1995**, *95* (6), 2229–2260.

(22) Bielejewska, A. G.; Marjo, C. E.; Prins, L. J.; Timmerman, P.; Jong, F. De; Reinhoudt, D. N. Thermodynamic Stabilities of Linear and Crinkled Tapes and Cyclic Rosettes in Melamine - Cyanurate Assemblies: A Model Description. *J. Am. Chem. Soc.* **2001**, *123*, 7518–7533.

(23) Li, Y.; Zhao, K.; Yang, Y.; Deng, K.; Zeng, Q.; Wang, C. Functionalization of Two-Component Molecular Networks: Recognition of Fe3+. *Nanoscale* **2012**, *4*, 148–151.

(24) Mayoral, M. J.; Bilbao, N.; González-Rodríguez, D. Hydrogen-Bonded Macrocyclic Supramolecular Systems in Solution and on Surfaces. *ChemistryOpen* **2016**, *5* (1), 10–32.

(25) Kudernac, T.; Lei, S.; Elemans, J. A. A. W.; De Feyter, S. Two-Dimensional Supramolecular Self-Assembly: Nanoporous Networks on Surfaces. *Chem. Soc. Rev.* **2009**, *38* (2), 402–421.

(26) *Supramolecular Materials and Technologies Perspectives in Supramolecular Chemistry Volume 4*; Reinhoudt, D. N., Ed.; John Wiley & Sons, Ltd.: Chichester, 1999.

(27) Roy, B.; Bairi, P.; Saha, A.; Nandi, A. K. Variation of Physical and Mechanical Properties in the Bicomponent Hydrogels of Melamine with Positional Isomers of Hydroxybenzoic Acid. *Soft Matter* **2011**, *7* (18), 8067–8076.

(28) Roy, B.; Bairi, P.; Nandi, A. K. Metastability in a Bi-Component Hydrogel of Thymine and 6-Methyl-1,3,5-Triazine-2,4-Diamine: Ultrasound Induced

vs. Thermo Gelation. *Soft Matter* **2012**, *8* (8), 2366–2369.

(29) Kohlmeier, A.; Vogel, L.; Janietz, D. Multiple Hydrogen Bonded Mesomorphic Complexes between Complementary 1,3,5-Triazine and Pyrimidine Derivatives. *Soft Matter* **2013**, *9* (39), 9476–9486.

(30) Arunan, E.; Desiraju, G. R.; Klein, R. A.; Sadlej, J.; Scheiner, S.; Alkorta, I.; Clary, D. C.; Crabtree, R. H.; Dannenberg, J. J.; Hobza, P.; et al. Definition of the Hydrogen Bond (IUPAC Recommendations 2011). *Pure Appl. Chem.* **2011**, *83* (8), 1637–1641.

(31) van der Lubbe, S. C. C.; Fonseca Guerra, C. Hydrogen-Bond Strength of CC and GG Pairs Determined by Steric Repulsion: Electrostatics and Charge Transfer Overruled. *Chem. - A Eur. J.* **2017**, *23* (43), 10234.

(32) Clark, T. Polarization, Donor–acceptor Interactions, and Covalent Contributions in Weak Interactions: A Clarification. *J. Mol. Model.* **2017**, *23* (10).

(33) Wolters, L. P.; Bickelhaupt, F. M. The Activation Strain Model and Molecular Orbital Theory. *Wiley Interdiscip. Rev. Comput. Mol. Sci.* **2015**, *5* (4), 324–343.

(34) Biedermann, F.; Schneider, H. J. Experimental Binding Energies in Supramolecular Complexes. *Chem. Rev.* **2016**, *116* (9), 5216–5300.

(35) Jeffrey, G. A. *An Introduction to Hydrogen Bonding.*; Oxford University Press: Oxford, 1997.

(36) Jorgensen, W. L.; Pranata, J. Importance of Secondary Interactions in Triply Hydrogen Bonded Complexes: Guanine–cytosine vs Uracil-2,6-Diaminopyridine. *J. Am. Chem. Soc.* **1990**, *112*, 2008–2010.

(37) Blight, B. A.; Hunter, C. A.; Leigh, D. A.; McNab, H.; Thomson, P. I. T. An AAAA-DDDD Quadruple Hydrogen-Bond Array. *Nat. Chem.* **2011**, *3* (3), 244–248.

(38) *Molecular Self-Assembly Organic Versus Inorganic Approaches*; Fujita, M., Ed.; Springer-Verlag Berlin Heidelberg: New York, 2000.

(39) Kirchner, B.; Reiher, M. Theoretical Methods for Supramolecular Chemistry. In *Analytical Methods in Supramolecular Chemistry*; Schalley, C. A., Ed.; WILEY-VCH Verlag GmbH & Co. KGaA: Weinheim, 2007; pp 419–463.

(40) Wang, L.-C.; Zheng, Q.-Y. Hydrogen Bonding in Supramolecular Crystal Engineering. In *Hydrogen Bonded Supramolecular Structures, Lecture Notes in Chemistry 87*; Li, Z.-T., Wu, L.-Z., Eds.; Springer-Verlag: Berlin, Heidelberg, 2015; pp 69–113.

(41) Desiraju, G. R. Supramolecular Synthons in Crystal Engineering—A New Organic Synthesis. *Angew. Chemie Int. Ed. English* **1995**, *34* (21), 2311–2327.

(42) Tennenbaum, M.; Liu, Z.; Hu, D.; Fernandez-Nieves, A. Mechanics of Fire Ant Aggregations. *Nat. Mater.* **2015**, *15* (1), 54–59.

II. THEORY AND METHODS

"In so far as quantum mechanics is correct, chemical questions are problems in applied mathematics."

Henry Eyring

II.1. Computational chemistry

Quantum Mechanics (QM) was born at the beginning of the XX century with the introduction of Max Planck's idea that the energy was quantized. QM describes mathematically the movement of electrons by a simple postulate, which establishes that the energy can be transferred between particles in specific quantities. With this idea, in conjunction with other ones from many physicists such as Einstein, Schrödinger, Bohr, Heisenberg, Dirac, and so on; and with a series of experiments that questioned the foundations of Classical Physics, one of the most complete and predictive theories was conceived, and which has been most tested throughout history. In the years that followed, this theoretical basis slowly began to be applied to small molecules, reactions and chemical bonds; thus, QM applied to chemistry is known as *theoretical chemistry*.[1,2]

On the other hand, from the decade of the 50s, the development of computers introduced a third methodology to scientific research: *computational simulation*. This is commonly known as numerical experiments. Thus, *computational chemistry* (CC) can be defined as a branch of chemistry that makes use of mathematical models (of the QM and also of classical mechanics) to simulate the interactions between the atoms and molecules of substances and matter in general, and thus be able to solve problems of a chemical nature, making intensive use of computers. Additionally, CC offers useful information to rationalize or interpret trends and to enunciate structure-activity relationships, so it has a powerful predictive power.

Nowadays, thanks to the accelerated development of technology, computational simulation has become an essential calculation tool, both for experimentalists and for theorists. In this context, Professor Dominic Tildesley, who is one of the presidents of the Royal Society of Chemistry (RSC), a former chief scientist at

Unilever and a current director of the European Center for Atomic and Molecular Calculus, has said:

> *"The speed and development of computers is now so rapid, and the advances in modelling and informatics are so dramatic that in 15 years' time, no chemist will be doing any experiments at the bench without trying to model them first."*

II.2. Electronic structure methods

Electronic structure methods are based on QM principles, which were developed to study small molecular systems in gas phase. However, their expansion to biochemical systems and materials has required the development of approximations and other methodologies that can consider systems that are more complex.

Within the formalism of the QM, a system is described by its wave function Ψ(x,y,z,t), since it includes all its information. This wave function can be obtained by the corresponding solution of the time-dependent Schrödinger equation or, more commonly, by time-independent equation (**Equation II.1**). This equation represents, in simple words, an energetic quantum-mechanic balance, and it is solved by obtaining the eigenfunctions of the Hamiltonian operator $\hat{H}$.

$$\hat{H}\Psi(x,y,z,t) = E\Psi(x,y,z,t) \qquad \text{(II.1)}$$

The $\hat{H}$ operator describes the potential and kinetic energy of an electron, and E is the total energy of the electron.

All the electronic-structure methods are characterized by the different mathematical approaches that are used in the $\hat{H}$ operator to solve **Eq. II.1**. All the calculations performed in this thesis were carried out with Density Functional Theory (DFT) Hamiltonians.

The popular B3LYP (Becke, three-parameter, Lee-Yang-Parr) exchange-correlation functional, was used as a test in almost all the systems. However, this

functional cannot describe long-range dispersion interactions, which are important in hydrogen-bonded systems. Therefore, three functionals that include dispersion correction were used:

- **ω-B97XD:** this functional was developed by Head-Gordon *et al.*,[3] and it includes a version of Grimme's D2 dispersion. Within their versions (D, D2 and D3), the Grimme's dispersion method simply add a correction term to the original DFT Hamiltonian.
- **B3LYP-D3:**[4] this functional includes the refined version of Grimme dispersion, which has more accuracy, broader range of applicability, and less empiricism.
- **BLYP-D3(BJ):** this is the hybrid Becke, one-parameter, Lee-Yang-Parr with the improvement D3(BJ). This includes Grimme's D3 dispersion and embodies the Becke-Johnson damping function.

II.2.1. Basis sets

A basis set is defined as a set of monoelectronic functions in which the molecular orbitals (MO) are expanded. These are the basis functions χ, conventionally called atomic orbitals (MO = LCAO, Linear Combination of Atomic Orbitals),

All the calculations begin with the selection of the basis set, and after the Hamiltonian, it is one of the most important factors for obtaining good results.

In this thesis, two types of basis set were used:

- **Slater type functions** (STO, Slater type orbital): these functions are more accurate, since they mirror the exact orbitals for the hydrogen atom. In this thesis, two STOs were used: first, *Triple Zeta plus Double Polarization* (**TZ2P**), which contains six *s*-functions and three *p*-functions for the first row elements and contains two set of polarization functions. Secondly, a *Double Zeta plus Polarization* (**DZP**) type basis.

- **Gaussian type functions** (GTO, Gaussian type orbital): These basis sets have some problems, i.e. in representing the proper behavior near the nucleus; therefore, more GTOs are necessary for achieving a certain accuracy compared with STOs. However, in terms of computational efficiency, GTOs are generally more preferred. In chapters **III**, **IV** and **V**, the split valence 6-311++G(d,p) basis set is applied. In this GTO, the core is described by one contracted GTO (CGTO) composed of six primitive GTOs; three GTOs for contracted valence orbitals and two different sizes of GTOs for extended valence orbitals; two diffuse basis functions (*s*- and *p-type* for heavy atoms and *s* for H); and, two polarization functions (*d*-type orbitals for heavy atoms and *p*-type orbitals for hydrogen).

II.2.2. Analysis of molecular properties:

II.2.2.1. Energetic analysis

Electronic structure methods allow the calculation of the electronic energy of a molecular system given, with a specific nuclear configuration.

In supramolecular systems, the energetic analysis of molecular aggregates is vitally important. In order to obtain the interaction energy of a system, a chemical reaction is defined according **Equation II.2**.

$$A + B \rightarrow [A\cdots B]_{complex} \qquad (II.2)$$

Figure II.1 represents **equation II.2** and displays the interaction between monomers A and B. When the isolated monomers are brought together to interact, they undergo geometrical deformations (bond distances, angles, dihedrals) which go along with energy changes. When the adduct is formed, three types of energies can be defined.

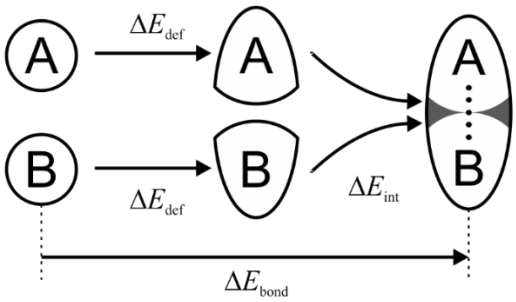

Figure II.1. Scheme of a bimolecular complex formation and the associated energy changes.

Deformation energy: or preparation energy, is the energy needed to deform the monomers from their isolated structures to that they acquire within the complex (see also **Fig. II.1**).

$$\Delta E_{def}^{A} = E_{A}^{AB} - E_{A}^{A} \quad \text{(II.3)}$$

$$\Delta E_{def}^{B} = E_{B}^{AB} - E_{B}^{B} \quad \text{(II.4)}$$

In this equation, the subscripts indicate the system and the superscripts the considered geometry.

Interaction energy: is the difference between the energy of the complex and the energy of the monomers with the same structures they have in the complex. In other words, the interaction energy is the actual energy of the complex.

$$\Delta E_{int} = E_{AB}^{AB} - E_{A}^{AB} - E_{B}^{AB} \quad \text{(II.5)}$$

Bonding energy: is the difference between the energy of the complex and the energy of the isolated monomers (**Equation II.4**). That is, the energy change produced when two isolated molecules are brought together from the infinite in order to form a stable complex.

$$\Delta E_{bond} = E_{AB}^{AB} - E_{A}^{A} - E_{B}^{B} \quad \text{(II.4)}$$

This equation can be obtained by adding up equations II.3-5:

$$\Delta E_{bond} = \Delta E_{int} - \sum \Delta E_{def} \quad \text{(II.7)}$$

Cooperativity – synergy

As was mentioned in Chapter I, hydrogen bonds show what is called *cooperative* or *synergetic effect*. Strictly speaking, this implies that *the whole is greater than the sum of the parts*. In simple words, 1 + 1 is more than 2.

The cooperativity in supramolecules can be evaluated by what is commonly known as *many body energy analysis*. This analysis is performed by subtracting the sum of energies of all the possible pairs to the total interaction energy:

$$\Delta E_{coop} = \Delta E_{int} - \sum_{j}^{n} \sum_{i<j}^{n} \Delta E_{ij} \quad \text{(II.8)}$$

Therefore, if $\Delta E_{coop} < 0$, the synergy is present and the cooperativity is positive. In the opposite case, $\Delta E_{coop} > 0$, the cooperative effect is negative. For instance, in order to study the effect of adding a monomer ***C*** to the dimer ***AB*** to form a complex ***ABC***, the cooperativity can be calculated as:

$$\Delta E_{coop} = E_{AB}^{AB} - E_{A}^{AB} - E_{B}^{AB} - (\Delta E_{AB} + \Delta E_{AC} + \Delta E_{BC}) \quad \text{(II.7)}$$

Energy correction

As the use of *ab-initio* calculations progressed to improve accuracy and to address problems such as weak van der Waals interactions or hydrogen bond interactions, it became clear that the use of an incomplete basis set results in significant errors in the calculation of potential energy curves.

The so-called *basis set superposition error* (BSSE) is caused by the tendency of electrons, which are associated with a given atom, to use the basis functions of a neighboring atom to decrease its energy. Consequently, the interaction energy is

overestimated. In addition, the weaker the interaction the more dramatic is the error.

The *counterpoise* (CP) method of Boys and Bernardi[5] is one of the most used techniques to remove the BSSE. There is controversy in the literature regarding the effectiveness of the CP method to correct the BSSE. For example, there are situations in which CP correction over-corrects energy, especially when using small basis sets.[6,7] On the other hand, in systems dominated by dispersion it was found that the corrected values are higher. Contrarily, van Duijneveldt *et al.*[8] have pointed out that the CP correction does not over-correct, and that the poor agreement with experimental values or high levels calculations is a reflection of the *basis set incompleteness error* (BSIE). At the limit of the complete base set, the BSSE and BSIE would be reduced to zero. However, Schwenke and Trulhar,[9,10] found that the reliability of the CP correction does not increase with increasing the size of the base, and concluded that the extra cost required by the correction method does not guarantee obtaining a more accurate result. Frisch *et al.*[11] came to a similar conclusion in a later study.

In this thesis, the BSSE was computed for B3LYP, ω-B97XD and B3LYP-D3 calculations. For the BLYP-D3(BJ) functional, the BSSE was not calculated because the dispersion correction was developed such that small BSSE effects were absorbed into the empirical potential.[12]

Energy Decomposition Analysis (EDA)

The EDA is a theoretical method that partitions the intermolecular interaction energy into energy components such as electrostatic, polarization, charge transfer, exchange and correlation contributions and dispersion. Many possible ways exist in which the interaction energy can be decomposed. In this thesis, the EDA scheme implemented in the Amsterdam Density Functional (ADF) program was used.

Within this approach, the interaction energy, which is examined in the framework of the Kohn–Sham Molecular Orbital model, is quantitatively decomposed into physically meaningful terms: electrostatic interaction, Pauli-

repulsive orbital interactions, and attractive orbital interactions:

$$\Delta E_{int} = \Delta V_{elstat} + \Delta E_{Pauli} + \Delta E_{oi} + \Delta E_{disp} \quad \text{(II.8)}$$

The term ΔV_{elstat} corresponds to the classical electrostatic interaction between the unperturbed charge distributions of the prepared (that is, deformed) units and it is usually attractive. The Pauli repulsion ΔE_{Pauli} comprises the destabilizing interactions between occupied orbitals and is responsible for any steric repulsion. The orbital interaction ΔE_{oi} accounts for charge transfer (that is, donor–acceptor interactions between occupied orbitals on one moiety with unoccupied orbitals of the other, including the HOMO–LUMO interactions) and polarization (empty/occupied orbital mixing on one fragment due to the presence of another fragment). The term ΔE_{disp} accounts for the dispersion corrections. For planar systems with C_S symmetry, the orbital interaction energy was further decomposed into the contributions from each irreducible representation Γ of the interacting system.

$$\Delta E_{oi} = \Delta E_{\sigma} + \Delta E_{\pi} \quad \text{(II.9)}$$

II.2.2.2. Quantum Theory of Atoms in Molecules.

The *Atoms in Molecules Theory* (AIM) developed by Bader *et al.*[13–15] provides the theoretical basis of the molecular structure hypothesis, which recognizes the molecule as a group of atoms hold together by a bond network.

AIM is an interpretive theory that helps to recover chemical concepts through a topological and rigorous study of the electron density $\rho(\mathbf{r})$. The theory is almost independent on any method of calculation or experimental, and as a starting point only needs the electronic density of the system, which can be obtained by quantum chemical calculations or experimental techniques. Over the years, the AIM theory

has evolved into a program that establishes a bridge between modern *ab initio* wave functions and chemical knowledge.[16]

The approach of the AIM theory is a quantum chemical model that characterizes the bond of a system based only on the *topology of the electronic charge density*. The first step is to compute the critical points of the $\rho(\mathbf{r})$ function (nuclear, bond, ring and cage critical points). The analysis of these points reveals that the properties of the density at the critical point contain information about the characteristics of the interaction between two atoms, which also are of great physical-chemical interest.[17] The pair of gradient paths that originate in the BCP and end in the neighboring nuclei define a line, called the atomic interaction line, through which the electronic density $\rho(\mathbf{r})$ is a maximum with respect to any neighboring line. The network of link paths in a molecule, in a given nuclear configuration, defines a *molecular graph*. A molecular graph of the cyanuric acid molecule is shown in **Figure II.2**.

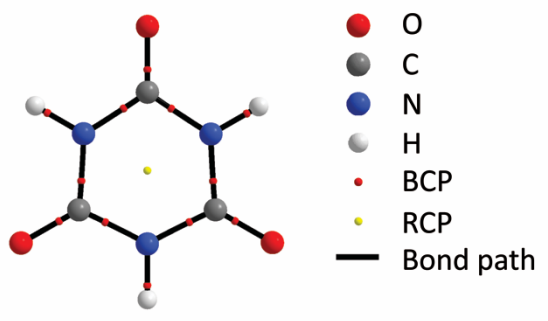

Figure II.2. Molecular graph of cyanuric acid. BCP: bond critical point, RCP: ring critical point.

II.2.2.3. Natural Bond Orbital (NBO) analysis.

The NBO approach[18,19] is a population analysis technique, which provides a localized representation of the electron density in a molecule, from electronic wave functions. The localized orbitals can be identified with bonds, lone pairs and anti-bonds. The strength or energy of the delocalization interactions between orbitals $E^{(2)}$ is estimated by the second order perturbation theory and depend on the relative

orientation of the orbitals and the energy difference between the donor and acceptor orbitals. This energy represents the estimation of the non-diagonal elements of the Fock NBO matrix. It can be deduced from the second-order perturbation approach:

$$E^{(2)} = \Delta E_{ij} = q_i \frac{F(i,j)^2}{\varepsilon_j - \varepsilon_i} \quad \text{(II.10)}$$

where q_i is the donor orbital population; ε_i, ε_j, are the elements of the diagonal (orbital energies) and F(i,j) is the Fock NBO matrix of non-diagonal elements.

Despite that NBO analysis overestimate charge-transfer energies,[20] is not itself a method to quantify these magnitudes as those obtained by a decomposition analysis. The NBO approach is implemented in **Chapters 3 – 5**.

II.4. References

(1) Levine, I. N. *Química Cuántica*, 5ta. ed.; Pearson Eduaction, S. A.: Madrid, 2001.

(2) *Química Teórica y Computacional*; Andrés, J., Beltrán, J., Eds.; Publicacions de la Universität Jaume I: Castello de la Plana, 2000.

(3) Chai, J.-D.; Head-Gordon, M. Long-Range Corrected Hybrid Density Functionals with Damped Atom-Atom Dispersion Corrections. *Phys. Chem. Chem. Phys.* **2008**, *10*, 6615–6620.

(4) Grimme, S.; Antony, J.; Ehrlich, S.; Krieg, H. A Consistent and Accurate Ab Initio Parametrization of Density Functional Dispersion Correction (DFT-D) for the 94 Elements H-Pu. *J. Chem. Phys.* **2010**, *132* (15), 154104.

(5) Boys, S. F.; Bernardi, F. The Calculation of Small Molecular Interactions by the Differences of Separate Total Energies. Some Procedures with Reduced Errors. *Mol. Phys.* **1970**, *19*, 553–559.

(6) Liedl, K. R. Dangers of Counterpoise Corrected Hypersurfaces. Advantages of Basis Set Superposition Improvement. *J. Chem. Phys.* **1998**, *108*, 3199.

(7) Dunning, T. H. A Road Map for the Calculation of Molecular Binding Energies. *J. Phys. Chem. A* **2000**, *104* (40), 9062–9080.

(8) van Duijneveldt, F. B.; van Duijneveldt-van de Rijdt, J. G. C. M.; van Lenthe, J. H. State of the Art in Counterpoise Theory. *Chem. Rev.* **1994**, *94* (7), 1873–1885.

(9) Schwenke, D. W.; Truhlar, D. G. Systematic Study of Basis Set Superposition Errors in the Calculated Interaction Energy of Two HF Molecules. *J. Chem. Phys.* **1985**, *82* (5), 2418–2426.

(10) Schwenke, D. W.; Truhlar, D. G. Erratum: Systematic Study of Basis Set Superposition Errors in the Calculated Interaction Energy of Two HF Molecules [J. Chem. Phys. **8 2** , 2418 (1985); **8 4** , 4113(E) (1986)]. *J. Chem. Phys.* **1987**, *86* (6), 3760–3760.

(11) Frisch, M. J.; Del Bene, J. E.; Binkley, J. S.; Schaefer, H. F. Extensive Theoretical Studies of the Hydrogen-bonded Complexes $(H_2O)_2$, $(H_2O)_2H^+$, $(HF)_2$, $(HF)_2H^+$, F_2H^-, and $(NH_3)_2$. *J. Chem. Phys.* **1986**, *84*, 2279.

(12) Grimme, S.; Ehrlich, S.; Goerigk, L. Effect of the Damping Function in Dispersion Corrected Density Functional Theory. *J. Comput. Chem.* **2011**, *32* (7), 1456–1465.

(13) Bader, R. F. W.; Gillespie, R. J.; MacDougall, P. J. A Physical Basis for the VSEPR Model of Molecular Geometry. *J. Am. Chem. Soc.* **1988**, *110* (22), 7329–7336.

(14) Bader, R. F. W. *Atoms in Molecules. A Quantum Theory*; Clarendon: Oxford, U.K., 1990.

(15) Popelier, P. L. A. *Atoms in Molecules. An Introduction*; Prentice-Hall: Manchester, U.K., 2000.

(16) Matta, C. F.; Boyd, R. J. *The Quantum Theory of Atoms in Molecules: From Solid State to DNA and Drug Design*; Wiley-VCH: Weinheim, 2007.

(17) Bianchi, R.; Gervasio, G.; Marabello., D. Experimental Electron Density Analysis of $Mn_2(CO)_{10}$: Metal–metal and Metal–ligand Bond Characterization. *Inorg. Chem.* **2000**, *39*, 2360–2366.

(18) Reed, A. E.; Curtiss, L. a; Weinhold, F. Intermolecular Interactions from a Natural Bond Orbital, Donor-Acceptor Viewpoint. *Chem. Rev. (Washington,*

DC, United States) **1988**, *88* (6), 899–926.

(19) Weinhold, F.; Landis, C. R. *Valency and Bonding: A Natural Bond Orbital Donor-Acceptor Perspective*; Cambridge UniversityPress: Cambridge, 2005.

(20) Stone, A. J. Natural Bond Orbitals and the Nature of the Hydrogen Bond. *J. Phys. Chem. A* **2017**, *121* (7), 1531–1534.

III. HYDROGEN AND HALOGEN BONDS IN THE SELF-ASSEMBLY OF MELAMINE

"Curiosa. Quiero seguir siendo curiosa, no perder eso de querer ver qué pasa"
(Curious. I want to remain curious, not lose that of wanting to see what happens)

Narda Lepes

Part of this chapter previously appeared as:

Petelski, A. N.; Duerte, D. J. R.; Pamies, S. C.; Peruchena, N. M.; Sosa, G. L. Intermolecular perturbation in the self-assembly of melamine. *Theor. Chem. Acc.* **2016**, *135*, 65. (Topical Collection QUITEL 2015.)

III.1. Introduction

In the field of supramolecular self-assembling, 1,3,5-triazine-2,4,6-triamine, also known as melamine (M), and their derivatives have gained special attention in the last 20 years. Following the elucidation of the crystal structure of M,[1] considerable research has been conducted on this compound. Dewar *et al.*[2] performed the first electronic structure study of M tautomeric forms. Later on, Meier and Coussens studied M molecular structure by *ab initio*, semiempirical, and molecular mechanics methods.[3] Wang *et al.*[4] studied the isolated M and two M derivatives through *ab initio* calculations, predicting that the three M amino groups have a pyramidal structure, two up and one down. Recently, Li *et al.*[5] studied the structural and spectral aspects of various M clusters by DFT calculations. Furthermore, experimental and theoretical studies of M structures on the Au(111) surface[6] have shown that M can form two different networks arranged by hydrogen bonds (HB) on the surface, and the networks coexist despite the fact that one of them is less favored energetically.

On the other hand, several studies have been made regarding M interacting with other compounds due to their potential utility as self-assembly structures in nanotechnology and molecular electronics. Chis¸ *et al.*[7] have analyzed the vibrational and electronic aspects of M complexes with a perylene derivative and

also the M dimer. Atalay *et al.*[8] have shown theoretical studies of the molecular structure and vibrational spectra of M diborate. Moreover, numerous studies have been reported in the solid state. Thomas *et al.*[9] have researched the structure of the 1:1 cocrystallized complex of M and uracil; Makowski *et al.*[10] reported two novel co-crystals between M and N–heterocycles; Xu *et al.*[11] reported a 3D structure through multiple HBs and stacking interactions of pure M with halogen acids; and recently, Prior *et al.*[12] obtained an accurate measurement of the structure of the M–Cyanuric acid (CA) co-crystal after the first elucidation of its structure in 1990.[13]

Research to date has tended to focus on structure itself rather than on the interactions and the mutual effects among molecules, which govern the processes of molecular recognition and self-assembly.[14] Hence, an atomic level comprehension of the chemical nature, strength, and directionality of non-covalent interactions would lead to obtain major advantages to master the controlled design of new materials. In this chapter the examination of intermolecular interactions between selected complexes bonded via HBs and XBs, which were assembled with M and a set of CA derivatives, is emphasized. In order to characterize these interactions and their mutual effects, an analysis of the electronic charge density distribution in the framework of the atoms in molecules (AIM) theory[15] and the natural bond orbital (NBO) analysis[16] was performed. A set of 12 complexes was selected, comprising M, cianuric acid (CA), and three derivatives of CA that can potentially be assembled with M, that is, trithiocyanuric acid (TCA) and two mono-halogenated derivatives of CA, a chlorinated (CACl) and a brominated (CABr; see **Figure III.1**), that is: $M/(CA)_n$, $M/(TCA)_n$, $M/(CACl)_n$, $M/(CABr)_n$, with n = 1, 2 and 3.

Finally, in order to obtain more information about the intermolecular perturbation on M, its aromaticity in each complex through various well-known aromaticity indices was evaluated: one index based on structural criteria, the harmonic oscillator model of aromaticity[17,18] (HOMA), and two indices based on the QTAIM, the para-delocalization index[19] (PDI) and the fluctuation aromatic index[20] (FLU). They have been tested for a great variety of compounds and have shown good correlation with other indices. In addition, two charge density descriptors were used: the curvature of electron density perpendicular to ring plane (λ_3) at the ring critical point (RCP) and the electron density (ρ) at the RCP. In their

study of benzenoid hydrocarbons, Howard and Krygowski[21] reported that these properties correlate well with the HOMA index aromaticity.

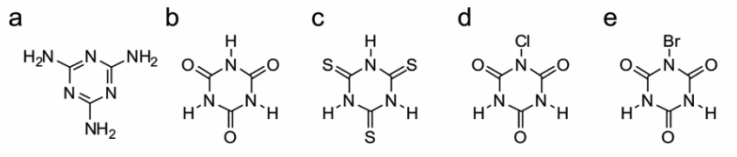

Figure III.1. Molecular structures of **(a)** melamine, **(b)** cyanuric acid, **(c)** trithiocyanuric acid, **(d)** 1-cloro-1,3,5-triazine-2,4,6-trione **(e)** 1-bromo-1,3,5-triazine-2,4,6-trione.

III.2. Methods

The complexes were assembled placing M with each molecule of the selected set in order to form a dimer, and then the HB sites of M were saturated with each compound to form a trimmer and finally a tetramer. Calculations were performed using the Gaussian 03 suite of programs.[22] The geometries of all monomers and complexes were fully optimized without any constraint, using the ω-B97XD hybrid functional from Head-Gordon *et al.*[23] with the 6-311++G(d,p) basis set. Since this functional includes empirical dispersion and correction on long-range interactions, it is potentially suitable for the description of hydrogen bonds.[5] Furthermore, it has been shown that the ω-B97XD functional is also suitable for the description of halogen bonds.[24] The minimum energy nature of the optimized structures was verified using the vibrational frequency analysis.

Binding energies (ΔE_{bond}) were obtained at the same level of theory using the supermolecular approach, which is calculated as the difference between the total energy of the complex and the sum of total energies of the isolated monomers (**Equation III.1**). Binding energies have also been corrected for the basis set superposition error (BSSE) within the approach of Boys and Bernardi (ΔE_{bond}^{BSSE}).[25]

$$\Delta E_{bond} = E_{M/C_n} - (E_M + n \times E_C) \qquad \text{(III.1)}$$

where n is the number of monomers around melamine, the sub-index M refers to melamine and C refers to either the subunit CA or its derivatives (TCA, CACl or

CABr). With these values, the ΔE_{bond} per monomer added (ΔE_{PM}) was also calculated by **Equation III.2**.

$$\Delta E_{PM} = E_{M/C_n} - E_{M/C_{n-1}} - E_C \quad \text{(III.2)}$$

The topology analysis was carried out within the QTAIM with the AIMAll program,[26] using the wave functions generated from the ω-B97XD/6-311++G(d,p) calculations. The optimized geometries were also used to perform a NBO analysis with NBO 3.1 program[27] as implemented in Gaussian 03.[22]

The aromaticity of the M ring was evaluated using geometric criteria by means of HOMA[17,18] taking R_{C-N} = 1.334 Å as reference value; topological criteria by means of PDI[19] and FLU[20] (taking a delocalization index $\delta_{ref}(C,N)$ = 1.566 as reference value); and two charge density descriptors: λ_3 and ρ at the RCP. All aromaticity descriptors were calculated with Multiwfn program.[28]

III.3. Results and discussion

Energetic and geometrical parameters

Figure III.2 shows the optimized geometries for the complexes studied in this work; for simplicity, an example of the M/$(CA)_n$ set of complexes is shown. Binding energies with BSSE correction are given in **Table III.1** and the selected optimized geometrical parameters of D–X···A interactions (where D = donor, X = H, Cl o Br, and A = acceptor) are given in **Table III.2**. These parameters refer to the X···A intermolecular distance, the D–X bond length, and the α equilibrium angles, D–X···A. Δd_{VdW}(X···A) represents the difference between the sum of A and X Van der Waals radii[29] and the X···A intermolecular distances, and $\Delta d_{(D-X)}$ represents the variations in the bond donor distance upon complexation, that is, the difference between the distance d(D–X) in the complexes and in the isolated monomers.

As can be seen in **Table III.1**, through the binding energy analysis, all these complexes are stabilized by HBs and XBs interactions. In the bimolecular complexes, the strength of these interactions decreases in the following order: M/CA > M/TCA > M/CABr > M/CACl. This order is kept as the number of monomers around M increases. The most stabilized system is M/CA, probably due to the

special set of highly directional HBs. It is worth noting that upon addition of monomers to the bimolecular complex, the average interaction energy decreases (see ΔE_{PM} values), which means that the total interaction energies of tri and tetramolecular complexes are smaller than the sum of the individual binding energies of the respective adducts. These results suggest that an anti-cooperative effect is operating.

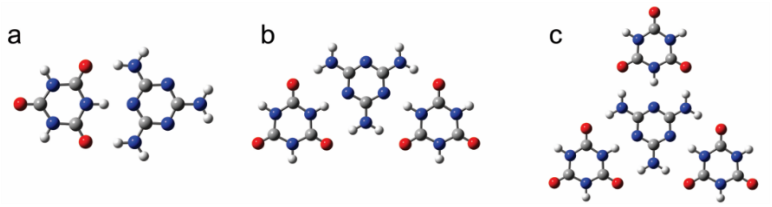

Figure III.2. Optimized geometries of **(a)** M/CA, **(b)** M/$(CA)_2$, and **(c)** M/$(CA)_3$ complexes at ω-B97XD/6-311++G** level of theory.

Observation of geometrical parameters reported in **Table III.2** shows that in all cases a penetration of electronic densities of atoms A and X is evidenced, by interpreting Δd_{VdW}(X···A) values. The highest values of Δd_{VdW} (X···A) are reached in the M/CABr systems followed by M/CA systems. It can be seen from **Table III.2a–d** that in all complexes, as the number of CA monomers increases, the X···A distance of the D–X···A interactions increases linearly. This does not correspond with the cooperative effect of HBs and XBs interactions expected in self-assembly systems, i.e., X···A distances decrease as the cluster size increases.[30–33] Thus, both energetic and geometrical criteria suggest a negative cooperativity of the interactions in these systems.

On the other hand, an elongation of distances D–X (positive values of Δd(D–X)) is observed in all complexes. The stretchiness of D–X lengths correlates fairly well with the binding energies, taking into account the N–X···N interaction. The values of Δd(D–X) are higher in the halogenated compounds. In addition, it can be seen that when the cluster size increases, distance length DX decreases, contrarily, again, to the cooperativity of HBs.

Table III.1 Binding energies (in kcal/mol) calculated at ω-B97XD/6-311++G** level and corrected by counterpoise.

Complejo	ΔE_{bond}	ΔE_{bond}^{BSSE}	ΔE_{PM}
M/AC	-20.21	-19.33	-20.21
$M/(AC)_2$	-39.75	-37.98	-19.54
$M/(AC)_3$	-58.57	-55.87	-18.82
M/ATC	-15.38	-14.33	-15.38
$M/(ATC)_2$	-29.97	-27.76	-14.58
$M/(ATC)_3$	-40.94	-37.81	-10.98
M/ACCl	-8.91	-8.05	-8.91
$M/(ACCl)_2$	-17.44	-15.79	-8.53
$M/(ACCl)_3$	-25.70	-23.12	-8.26
M/ACBr	-13.78	-13.06	-13.78
$M/(ACBr)_2$	-25.77	-24.38	-11.99
$M/(ACBr)_3$	-36.68	-34.67	-10.91

Table III.2 Selected Geometric[a] Parameters of **(a)** $M/(AC)_n$, **(b)** $M/(ATC)_n$, **(c)** $M/(ACCl)_n$ y **(d)** $M/(ACBr)_n$ complexes calculated at ω-B97XD/6-311++G(d,p) level of theory.

Complex	D–X···A	d(X···A)	Δd_{VdW}(X···A)	d(D–X)	Δd(D–X)	α D–X···A
(a)						
M/CA	N–H···N	1.768	0.982	1.058	0.048	179.99
	N–H···O	1.938	0.782	1.013	0.009	175.29
	N–H···O	1.938	0.782	1.013	0.009	175.29
$M/(CA)_2$ [b]	N–H···N	1.786	0.964	1.054	0.045	179.99
	N–H···O	1.930	0.790	1.013	0.010	176.00
	N–H···O	1.948	0.772	1.013	0.010	177.73
$M/(CA)_3$ [c]	N–H···N	1.801	0.949	1.052	0.043	179.97
	N–H···O	1.939	0.781	1.013	0.010	178.66
	N–H···O	1.939	0.781	1.013	0.010	178.66
Complex	D–X···A	d(X···A)	Δd_{VdW}(X···A)	d(D–X)	Δd(D–X)	α D–X···A
(b)						
M/TCA	N–H···N	1.779	0.971	1.057	1.057	179.98
	N–H···S	2.510	0.490	1.011	1.011	157.47
	N–H···S	2.511	0.489	1.011	1.011	157.36

M/$(TCA)_2$[b]	N–H···N	1.816	0.934	1.051	1.051	179.30
	N–H···S	2.489	0.511	1.012	1.012	159.61
	N–H···S	2.522	0.478	1.012	1.012	154.61
M/$(TCA)_3$	N–H···N	1.812	0.938	1.051	0.041	178.00
	N–H···S	2.487	0.513	1.011	0.008	162.34
	N–H···S	2.614	0.386	1.011	0.007	144.99
	N–H···N	1.819	0.931	1.051	0.041	179.76
	N–H···S	2.508	0.492	1.011	0.007	156.39
	N–H···S	2.522	0.478	1.012	0.009	154.67
	N–H···N	2.358	0.392	1.027	0.017	177.33
	N–H···S	2.363	0.637	1.012	0.008	170.00
	N–H···S	2.364	0.636	1.012	0.008	169.50
(c)						
M/CACl	N–Cl···N	2.526	0.774	1.728	0.034	179.81
M/$(CACl)_2$[b]	N–Cl···N	2.554	0.746	1.723	0.029	176.99
M/$(CACl)_3$[c]	N–Cl···N	2.568	0.732	1.721	0.026	179.97
(d)						
M/CABr	N–Br···N	2.399	1.001	1.927	0.078	179.97
	N–H···Br	2.737	0.313	1.006	0.003	120.46
	N–H···Br	2.739	0.311	1.006	0.003	120.44
M/$(CABr)_2$ [b]	N–Br···N	2.447	0.953	1.910	0.061	179.62
	N–H···Br	2.746	0.304	1.007	0.003	121.64
	N–H···Br	2.754	0.296	1.007	0.003	122.29
M/$(CABr)_3$ [c]	N–Br···N	2.500	0.900	1.898	1.898	179.92
	N–H···Br	2.765	0.285	1.007	1.007	123.53
	N–H···Br	2.764	0.286	1.007	1.007	123.52

[a]Distances in Å and angles in (°). [b,c]All other interactions are essentially equal.

One final point concerning geometry is that all systems show coplanarity except the set of M/$(TCA)_n$ complexes. This finding results are interesting, since Ranganathan *et al.*[34] have found that the crystal of the adduct M/TCA has the same spatial arrangement of molecules as the M/CA crystal, that is, all rings are coplanar. Our calculations, however, have shown that the M/TCA coplanar adduct is a

transition state, since an imaginary frequency is observed, whereas the anticoplanar adduct is a minimum (see **Figure III.3a**). This behavior could be explained by a close packing process of molecules in the crystal state. The first and the second molecule of TCA are bound to M almost perpendicularly (see **Figures III.3a–c**) with regard to the M ring, and the angle between the two ring planes is 130°. This allows a greater approach between molecules leading to a N···N intermolecular distance (2.929 Å) shorter than in the coplanar dimer (3.430 Å), as indicated by our calculations, while the experimental distance value is 2.88 Å.[34] It is worth emphasizing that despite the fact that coplanar dimer is a transition state, the third molecule of TCA interacts with M coplanarly (see **Figures III.3e, f**). In this last case, amino groups adopt a pyramidal form that probably contributes to this geometry.

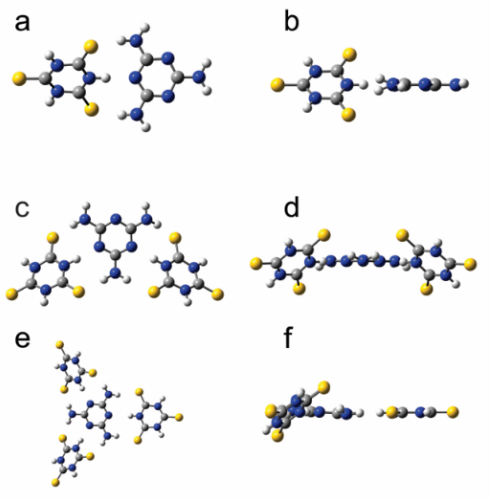

Figure III.3. M/$(TCA)_n$ complexes. **(a)** Top view and **(b)** side view of M/TCA complex. **(c)** Top view and **(d)** side view of M/$(TCA)_2$ complex. **(e)** Top view and **(f)** side view of M/$(TCA)_3$ complex

Local topological properties

As was aforementioned in Chapter II, the Quantum Theory of Atoms in Molecules (QTAIM) of Bader[15] provides a good definition of the chemical concepts of atoms, bonds, and structure. This theory has been used successfully for the characterization of HBs and XBs interactions through a set of local topological

properties calculated at bond critical points (BCP) of electron charge density and a set of integrated atomic properties on atomic basins.[35,36] In this work, the electron charge density $\rho(\mathbf{r}_c)$, which measures the accumulation of charge between the bonded nuclei and reflects the bond strength; the Laplacian of the electron density $\nabla^2\rho(\mathbf{r}_c)$ that provides information about the local charge concentration ($\nabla^2\rho(\mathbf{r}_c) < 0$) or depletion ($\nabla^2\rho(\mathbf{r}_c) > 0$); the densities of kinetic energy, $G(\mathbf{r}_c)$; the densities of potential energy, V(rc); and the total electronic energy density $H(\mathbf{r}_c) = V(\mathbf{r}_c) + G(\mathbf{r}_c)$, were used to analyze the nature of the interactions that occur in the different complexes.

The molecular graphs of all complexes are displayed in **Figure III.4**, and the local properties calculated at BCP are given in **Tables III.3a–d**. In all the complexes studied here, the criteria proposed by Popelier[36] that describe HB formation are fulfilled; that is, BCP properties present $\rho(\mathbf{r}_c)$ values relatively low which range from 0.01 to 0.06 au; positive values of $\nabla^2\rho(\mathbf{r}_c)$ that range from 0.02 to 0.1 au. Thus, BCP values are typical of closed shell interactions and correlate fairly well with values reported for similar interactions.[37–39]

As can be seen in **Fig. III.4a**, in complex mediated hydrogen bonds, three HB interactions occur for every added monomer. The sum of densities at these BCP, decreases: 0.0960 au; 0.0940 au; 0.0925 au in the bimolecular, trimolecular, and tetramolecular complexes, respectively. The same is observed in complexes with sulfur. Considering that it has been established that the density at the BCP is a good indicator of the strength of the bond,[35,40,41] these results are contrary to what is expected of the cooperative effect of HBs. However, a reinforcement of the outer N–H···O interactions is observed, when going from M/CA to M/$(CA)_2$, which is marked by the increase in $\rho(\mathbf{r}_c)$ values (from 0.0247 to 0.0252 au, see **Table III.3a**). In **Fig. III.4c** it can also be seen that in the complex with chlorine, M/CACl, a single interaction of the type N–Cl···N is observed.

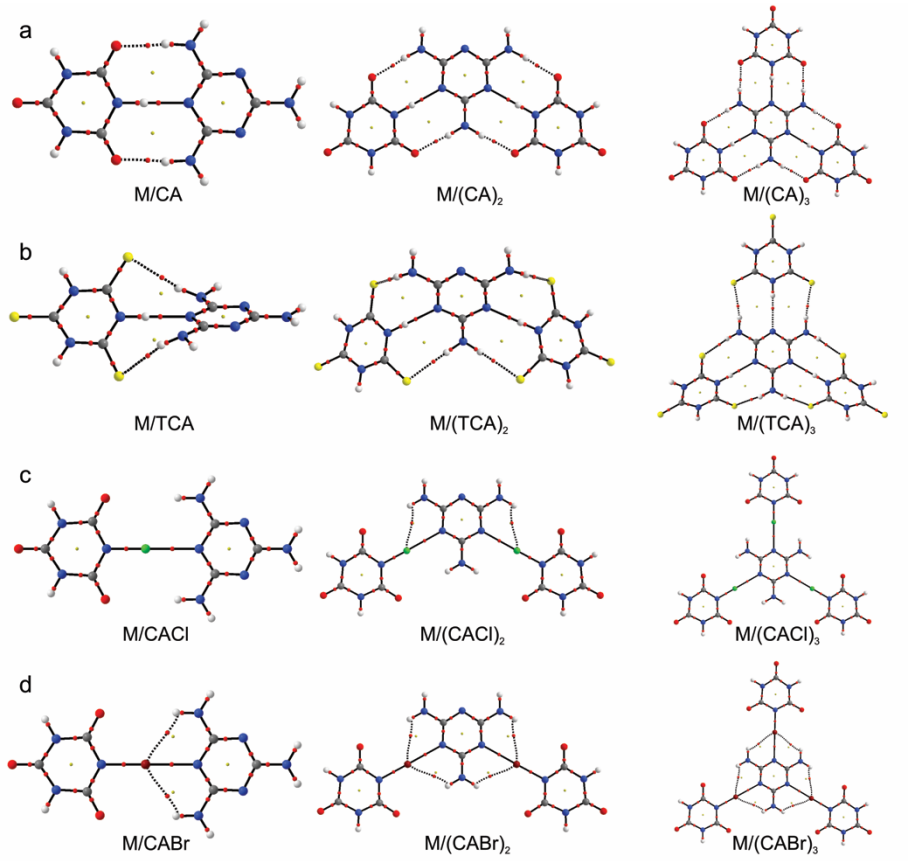

Figure III.4. Molecular graphs (network of bond paths linking pairs of neighboring nuclei) of Melamine complexes. Small red dots indicate bond critical points and yellow dots indicate ring critical points. **(a)** $M/(CA)_n$, **(b)** $M/(TCA)_n$, **(c)** $M/(CACl)_n$, and **(d)** $M/(CABr)_n$

When the trimolecular complex is formed, two interactions of HB type, N–H···Cl, appear and disappear again in the tetramolecular complex. Contrarily, in the system M/CABr, in addition to XB, two HBs interactions occur, and these persist to pass to tri- and tetramolecular complexes. Also, in these halogenated systems, an anti-cooperative effect is observed.

Table III.3 Local Properties at D–X···A Bond Critical Points in **(a)** $M/(AC)_n$, **(b)** $M/(ATC)_n$, **(c)** $M/(ACCl)_n$ y **(d)** $M/(ACBr)_n$[a]

Complexes	Interaction	$\rho(r_c)$	$\nabla^2\rho(r_c)$	$V(r_c)$	$H(r_c)$
(a)					
M/AC	N–H···N	0.0466	0.0951	-0.0391	-0.0077
	N–H···O	0.0247	0.0927	-0.0183	0.0024
	N–H···O	0.0247	0.0927	-0.0183	0.0024
$M/(AC)_2$	N–H···N	0.0446	0.0948	-0.0368	-0.0065
	N–H···O	0.0252	0.0942	-0.0188	0.0024
	N–H···O	0.0242	0.0905	-0.0178	0.0024
$M/(AC)_3$	N–H···N	0.0446	0.0948	-0.0368	-0.0065
	N–H···O	0.0252	0.0942	-0.0188	0.0024
	N–H···O	0.0242	0.0905	-0.0178	0.0024
(b)					
M/ATC	N–H···N	0.0453	0.0942	-0.0374	-0.0069
	N–H···S	0.0152	0.0401	-0.0076	0.0012
	N–H···S	0.0151	0.0400	-0.0076	0.0012
$M/(ATC)_2$	N–H···N	0.0413	0.0929	-0.0329	-0.0048
	N–H···S	0.0149	0.0396	-0.0075	0.0012
	N–H···S	0.0158	0.0412	-0.0080	0.0012
$M/(ATC)_3$	N–H···N	0.0411	0.0925	-0.0326	-0.0047
	N–H···S	0.0150	0.0396	-0.0075	0.0012
	N–H···S	0.0152	0.0403	-0.0077	0.0012
	N–H···N	0.0417	0.0933	-0.0334	-0.0050
	N–H···S	0.0127	0.0349	-0.0063	0.0012
	N–H···S	0.0157	0.0411	-0.0079	0.0012
	N–H···N	0.0126	0.0353	-0.0058	0.0015
	N–H···S	0.0202	0.0514	-0.0113	0.0008
	N–H···S	0.0202	0.0514	-0.0113	0.0008
(c)					
M/ACCl	N–Cl···N	0.0327	0.1061	-0.0237	0.0014
$M/(ACCl)_2$	N–Cl···N	0.0306	0.1012	-0.0222	0.0016
	N–H···Cl	0.0077	0.0306	-0.0045	0.0016
$M/(ACCl)_3$	N–H···Cl	0.0297	0.0990	-0.0215	0.0016

Complexes	Interaction	$\rho(r_c)$	$\nabla^2\rho(r_c)$	$V(r_c)$	$H(r_c)$
(d)					
M/ACBr	N–Br···N	0.0493	0.1233	-0.0391	-0.0041
	N–H···Br	0.0097	0.0357	-0.0055	0.0145
	N–H···Br	0.0097	0.0356	-0.0055	0.0144
$M/(ACBr)_2$	N–Br···N	0.0442	0.1181	-0.0343	-0.0024
	N–H···Br	0.0094	0.0345	-0.0053	0.0017
	N–H···Br	0.0092	0.0338	-0.0052	0.0016
$M/(ACBr)_3$	N–Br···N	0.0397	0.1112	-0.0301	-0.0011
	N–H···Br	0.0090	0.0327	-0.0050	0.0016
	N–H···Br	0.0089	0.0325	-0.0050	0.0016

[a] All quantities are in atomic units (au)

It is known that the ΔE_{bond} is a magnitude that cannot be partitioned when more than one interaction is involved in the same complex, for this reason, several studies have been accomplished with the purpose of measuring the strength of individual interactions in a binary complex involving more than one interaction[42]. Matta and co-workers[43] have based their studies on the methodology of Espinosa et al.[40]. This method has stated that for the hydrogen bond X–H···O (where X = C, N, O), there is a relationship between bond energy of the HB (named E_{HB}) and the potential energy density $V(\mathbf{r}_c)$ at the corresponding BCP, which can be approximately described as $E_{HB} = V(\mathbf{r}_c)/2$. Moreover, Reiher and co-workers correlated the strength of the HB with the two-center shared-electron number[44]. Later on Szatyłowicz *et al.* employed the NBO energy in order to explore the strengths of interactions in DNA base pairs complexes[42]. In this work, the concept of Espinosa and co-workers[40] was used in order to evaluate the relationship between $V(\mathbf{r}_c)$ and the ΔE_{bond}, by considering the sum of the E_{HB} in each individual interaction of complexes, that is: $\Sigma V(\mathbf{r}_c)/2$. Then, these values were plotted versus the bonding energies of **Table III.1** (See **Fig. III.5**). Despite there are different systems, results show a good linear correlation, as it is evidenced in the value of the correlation coefficients ($R^2 = 0.973$), even though this evaluation was limited just to H···O bonds. Therefore, this methodology could be considered suitable to quantify the contribution of individual interactions to the total ΔE_{bond}.

Finally, according to Cremer and Kraka[45], when $H(\mathbf{r}_c)$ is negative at a BCP, the interaction is indicative of being shared and its magnitude could be used as a measure of the covalent character. However, Angelina and co-workers[46,47] have indicated that the decrease of $H(\mathbf{r}_c)$ is mainly due to the increase in the electrostatic character of the interaction and in lesser extent to the increase in its covalent character. Therefore, negative values of H could be considered as an indicator of strengthening or stabilization of the interaction[46]. As can be seen in Table 3a in the set of three interactions, the central interaction N–H···N has a negative value while the side ones are positive, which is also observed in the M/TCA system (See **Table III.3b**). Regarding the set of complexes with XBs, $H(\mathbf{r}_c)$ is positive for N–Cl···N interactions (See **Table III.3c**) which would explain why it is the least energetically favored system. In the M/CABr set of complexes, Table 3d, the $H(r_c)$ at N–Br···N BCP reaches the least negative value among all complexes studied (-0.0041 au). Furthermore, by comparing M/$(CA)_n$ with M/$(CABr)_n$ systems, the $H(\mathbf{r}_c)$ property at the central interaction is reduced by around 26% and 73% respectively, when going from the simple adduct up to the tetramolecular complex, showing that the strength or stability is less affected in the M/CA set of complexes. However, $\rho(\mathbf{r}_c)$ in the M/$(CABr)_n$ system is greater than in the M/$(CA)_n$ system, indicating stronger interactions in the former. Hence, the greatest binding energy in the M/CA system is explained by $\rho(\mathbf{r}_c)$ and $H(\mathbf{r}_c)$ values.

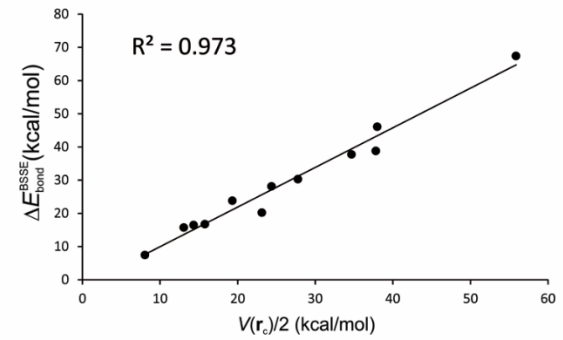

Figure III.5. Linear correlation between ΔE_{bond}^{BSSE} and $\Sigma V(\mathbf{r}_c)/2$. All values are in kcal/mol.

Integrated Atomic Properties

In **Table III.4** changes in the integrated atomic properties for the three atoms involved in the interactions of adducts M/CA, M/TCA, M/CACl and M/CABr are shown. Such properties are the electronic population, N, the total energy of the atom, E, the dipolar polarization, M, and the atomic volume, *v*. The changes were calculated by subtracting the property value of the atom in the isolated compound to the value of the corresponding property in the complex. The criteria for the hydrogen bond formation,[29,48] based on the integrated properties of the hydrogen atom, involve loss of electron population, ($\Delta N < 0$), energetic destabilization, ($\Delta E > 0$), decrease of dipolar polarization ($\Delta M < 0$), and decrease of hydrogen atoms volume ($\Delta V < 0$).

Table III.4 Changes in Atomic Properties[a] for three atoms involved in intermolecular interactions of bimolecular complexes.

Complex	Interaction	Atom	ΔN(Ω)	ΔE(Ω)	Δ*v*(Ω)	ΔM(Ω)
M/CA	N–H···N	N	0.0551	-0.0385	0.2766	-0.0256
		H	-0.0806	0.0610	-11.7608	-0.0444
		N	0.0267	-0.0022	-14.6366	-0.0590
	N–H···O	N	0.0332	-0.0310	-0.0585	0.0064
		H	-0.0565	0.0295	-9.2387	-0.0376
		O	0.0197	-0.0007	-7.2081	-0.0258
	N–H···O	N	0.0330	-0.0310	-0.1222	0.0055
		H	-0.0565	0.0295	-9.2323	-0.0376
		O	0.0196	-0.0007	-7.1885	-0.0258
M/TCA	N–H···N	N	0.0423	-0.0135	0.5217	-0.0309
		H	-0.0753	0.0570	-12.6372	-0.0475
		N	0.0259	-0.0155	-15.6212	-0.0740
	N–H···S	N	-0.0230	0.0121	-1.1994	0.0044
		H	-0.0025	0.0083	-3.7356	-0.0060
		S	0.0446	-0.0299	-7.4819	-0.0097
	N–H···S	N	-0.0230	0.0122	-1.2098	0.0045
		H	-0.0025	0.0082	-3.7445	-0.0059

Complex	Interaction	Atom	ΔN(Ω)	ΔE(Ω)	Δ*v*(Ω)	ΔM(Ω)
		S	0.0445	-0.0298	-7.4561	-0.0095
M/CACl	N–Cl···N	N	0.0427	-0.0346	1.1134	-0.0323
		Cl	-0.0080	0.0076	-12.9247	-0.1434
		N	-0.0018	-0.0247	-19.3408	-0.1384
M/CABr	N–Br···N	N	0.0554	-0.0450	2.8414	-0.0396
		Br	-0.0043	0.0153	-19.8834	-0.3044
		N	0.0034	-0.0245	-24.5173	-0.1649
	N–H···Br	N	0.0050	-0.0110	-1.3707	0.0060
		H	-0.0208	0.0134	-2.0542	-0.0097
		Br	-0.0043	0.0153	-19.8834	-0.3044
	N–H···Br	N	0.0049	-0.0111	-1.4052	0.0060
		H	-0.0209	0.0135	-2.1383	-0.0098
		Br	-0.0043	0.0153	-19.8834	-0.3044

[a]All quantities are in au.

As can be seen in **Table 4**, these criteria are satisfied for the hydrogen bonded adducts (M/CA and M/TCA). In addition, on the other two atoms involved in the HBs, A and D atoms, the atomic volume decreased on the A atom and increased on the D atom for the M/CA dimer. Whereas this behavior is observed just in the central interaction in the M/TCA dimer, in the side ones a decrease in the atomic volumes is evidenced in the three atoms involved D–H···A.

In halogen complexes, M/CACl and M/CABr, the general trend in the XB donor is a loss of electron population, a decrease of the dipolar polarization, a decrease of the atomic volume, and an energetic destabilization, in contrast with values reported for halogen bonds[37]. However, this trend agrees with values reported for I···N interactions.[38] The energetic destabilization is greater in the chlorinated complex, which is in line with the lowest value of BE. On the other hand, the XB acceptor (nitrogen atom), shows a loss of N(Ω) in M/CACl complex, while in the M/CABr complex the XB acceptor shows a gain of electron population ($\Delta N > 0$).

Natural Bond Orbital (NBO) Analysis

The results of NBO analysis conducted on clusters are given in **Table III.5a-d**. The values reported in this table are the changes in NBO occupation numbers for the σ^*_{D-X} antibonds and n_A lone pairs (LP) of D–X···A interactions upon complexation, that is, the difference between the values in the complex and in the isolated molecules. Additionally, the second-order perturbation energies $E^{(2)}$ (donor $\rightarrow$ acceptor) are reported.

An analysis of the results in **Table III.5** shows that the hyperconjugative energy of charge transfer follows the same order as the binding energies. Moreover, they correlate fairly well with the electron density values at BCP of the corresponding interactions. Besides, there is an acceptable correlation between the binding energies and the sum of the $E^{(2)}$ energies at each complex (R^2 = 0.938, see **Fig. III.6**). Therefore, these results also support the idea proposed by Szatyłowicz and Sadlej-Sosnowska[42] based on NBO energies.

Table III.5 Changes in NBO populations of lone pairs (n_A) and antibonds (σ^*_{D-X}) from, and Second-Order Perturbation Energies $E^{(2)}$ ($n_A \rightarrow \sigma^*_{D-X}$).* See full table in Supplementary Material.

Complex	D–X···A	Δn	$E^{(2)}$	$\Delta\sigma^*$
M/CA	N–H···N	-0,0550	41,1	0,0808
	N–H···O	0,0079	7,8	0,0199
	N–H···O	0,0079	7,8	0,0199
M/TCA	N–H···N	-0,0559	41,2	0,0804
	N–H···S	-0,0004	4,5	0,0200
	N–H···S	-0,0004	4,4	0,0200
M/CACl	N–Cl···N	-0,0630	19,1	0,0745
M/CABr	N–Br···N	-0,1284	47,4	0,1508
	N–H···Br	-0,0056	1,3	0,0020
	N–H···Br		1,3	0,0020

*Populations in e and energies in kcal/mol

It is important to note that upon complex formation, all antibonds increase their occupation number, as indicated by positive values of $\Delta\sigma^*$, which range from 0.007

to 0.2 e in halogen complexes, and from 0.01 to 0.09 e in hydrogen complexes. Moreover, as reflected in the Δn values, all LP lost occupation number as it is expected, except LPs of oxygen atoms in the M/CA system (see **Table III.5a**), which gain occupation number even though there is a charge outflow, as it is evidenced from the charge transfer values. This unusual behavior is explained by analyzing the intra molecular charge transfers.

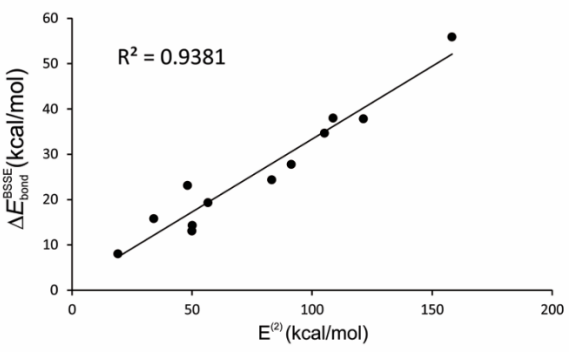

Figure III.6. Linear correlation between BE_{corr} versus $\Sigma E^{(2)}$. All values are in kcal/mol.

It is also worth mentioning correlations of Δn versus $\Delta\sigma^*$ values. By correlating these values from $M/(CA)_n$ $M/(TCA)_n$, $M/(CACl)_n$ and $M/(CABr)_n$ systems, good linear relationships are observed (plots not shown), with R^2 = 0.9986, 0.9804, 0.9988 and 0.9999 respectively (see **Fig. III.7**). These results show that all of the charge that the donor orbital lost was consequently gained by the acceptor orbital. However, as was aforementioned, LPs of oxygen atoms in the M/CA system gain occupation number.

Despite the fact that oxygen atoms of CA act as donors, they also act as acceptors in the intramolecular charge transfer $\Delta n_N \rightarrow \Delta\sigma^*_{C=O}$ (see **Figs. III.8a,b**), that is, six $\Delta n_N \rightarrow \Delta\sigma^*_{C=O}$ CTs which increase in energy upon complex formation (See **Table III.6**). Therefore, it may be suspected that the gain of occupation number of oxygen LP comes from this transfer, which is the most relevant one within the CA molecule. Consequently, intermolecular charge transfers improve the intramolecular ones and the net charge flow (**Fig. III.8c**) resulting in a "*closed*

circuit", which is the result of the sum of the intra and intermolecular charge transfers. Despite the fact that values of BEs show an anticooperative effect, this charge delocalization mechanism is cooperative, since there is reinforcement over intramolecular charge transfers upon complexation (see **Table 6**). Furthermore, in the complexes that do not present the side N–H···O interactions, that is the systems: M/(CACl)$_n$ and M/(CABr)$_n$, oxygen atoms still exhibit an increase in the occupation numbers of n_O LP (Δn_O = 0.0081 e in M/(CACl)$_n$, and Δn_O = 0.013 e in M/(CABr)$_n$).

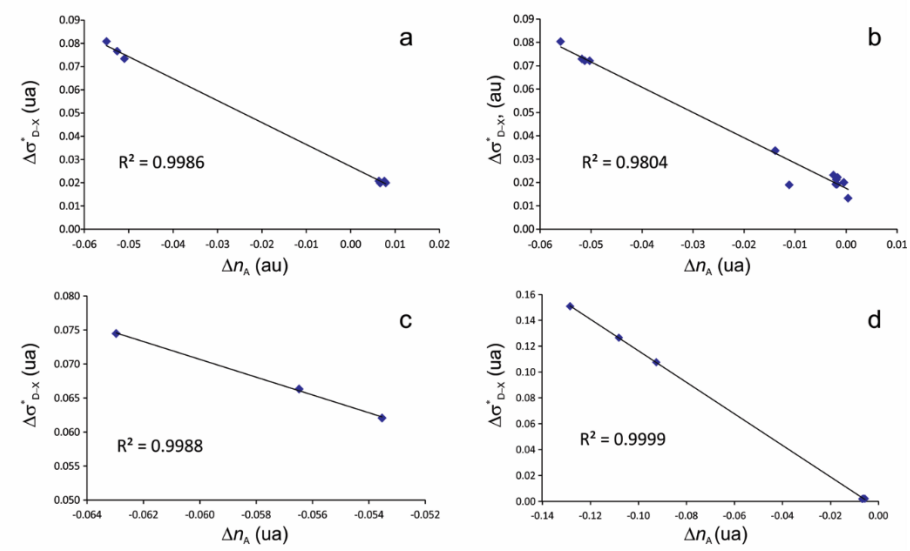

Figure III.7 Linear correlation between Δn and $\Delta\sigma^*_{D-X}$. **(a)** M/(AC)$_n$, **(b)** M/(ATC)$_n$, **(c)** M/(ACCl)$_n$ y **(d)** M/(ACBr)$_n$.

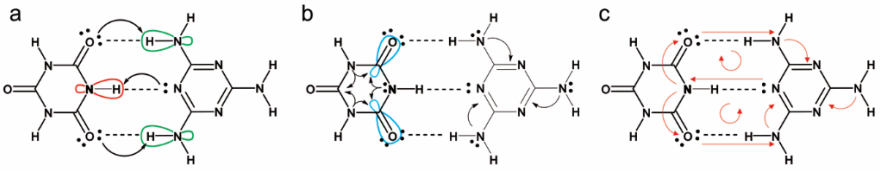

Figure III.8. (a) Schematic representation of $n \rightarrow \sigma^*$ intermolecular charge transfers involving interactions in M/CA adduct. **(b)** Schematic representation $n \rightarrow \sigma^*$ of intramolecular charge transfers within M ($n_N \rightarrow \sigma^*_{C-N}$) and CA ($n_N \rightarrow \sigma^*_{C=O}$). **(c)** Charge delocalization mechanism that defines the interaction between M and CA.

Aromaticity indices

Aromaticity is a fundamental concept of organic chemistry and can give valuable information about the electronic structure of organic compounds[49]. In this way, aromatic indices are suitable for the study of changes in aromaticity due to the intermolecular perturbations like hydrogen bonds[49,50]. This approach was employed in this work as a measure of the intermolecular perturbation over the ring of M in the different complexes.

Table III.6. NBO Analysis of M, CA, and M/CA complex: Second-Order Perturbation Energies $E^{(2)}$ (Donor→Acceptor)[a]

$n \rightarrow \sigma^*$	M	CA	M/CA
Intramolecular			
$n_N \rightarrow \sigma^*_{C=O}$		70.11	81.94
$n_N \rightarrow \sigma^*_{C=O}$			
$n_N \rightarrow \sigma^*_{C=O}$			72.61
$n_N \rightarrow \sigma^*_{C=O}$			
$n_N \rightarrow \sigma^*_{C=O}$			70.28
$n_N \rightarrow \sigma^*_{C=O}$			
$n_N \rightarrow \sigma^*_{C-N}$	75.78		91.35
$n_N \rightarrow \sigma^*_{C-N}$			87.55
$n_N \rightarrow \sigma^*_{C-N}$			78.71
Intermolecular			
$n_N \rightarrow \sigma^*_{N-H}$			41.13
$n_O \rightarrow \sigma^*_{N-H}$			7.76
$n_O \rightarrow \sigma^*_{N-H}$			7.76

[a] Energies in kcal/mol.

Three aromatic indices were taken into account herein. The HOMA index, that senses the energy needed to distort the structure from an idealized set of bond lengths. In this case, it is a six-membered triazine ring. The PDI index weights the number of electron pairs shared between para-related positions in a ring, that is to say, the contributions of: $\delta(1,4)$, $\delta(2,5)$ and $\delta(3,6)$ delocalization indices. Furthermore, the FLU index follows the same philosophy of HOMA, but it takes

into account the delocalization indices. FLU measures the relative electronic deviation of a given ring in a molecule with reference to another molecule.

With regards to the density descriptors, the curvature of electron density perpendicular to ring plane (λ_3) can be taken as the π contribution to the electron density (ρ_π); while the electron density at the RCP can be ascribed to the σ contribution (ρ_σ).

Figure III.9 shows a display of the Aromaticity indices as a function of the monomers added over M. The aromaticity descriptors are shown in **Fig. III.10**. In all cases it can be seen that the aromatic character decreases upon complexes formation. Since there is not a certain method for quantifying the aromatic character of molecules, it cannot be clearly said in which of all systems the aromatic character is more affected. In other words, results show the multidimensional character of aromatic indices. However, correlations of all indices are quite good (cf. **Table S2** in the supplementary material), although some correlations of indices of CABr systems do not show a good linear relationship, considering significant Pearson coefficient values of < 0.05.

By following the rate of change of indices, according to HOMA, the aromaticity of M in the system $M/(CA)_n$ is the most affected (see **Fig. III.9a**); the greater the slope the greater the change of the aromatic character. According to PDI index (**Fig. III.9b**), M is more affected in the $M/(CABr)_n$ system and below it is the $M/(CA)_n$ system. By analyzing FLU indices (see **Fig. III.9c**), it is shown again that the M aromatic character is more affected in the $M/(CABr)_n$ system. Also, charge density descriptors λ_3 and $\rho_{(RCP)}$ of **Figs. III.10a,b** show that M aromatic character decreases to a greater extent in the $M/(CA)_n$ and $M/(CABr)_n$ systems. Thus, we can conclude that M aromatic character is more perturbed in the $M/(CA)_n$ and $M/(CABr)_n$ systems, and less affected in the $M/(CACl)_n$ and $M/(TCA)_n$ systems, but it is not possible to determine a unique trend. This classification is consistent with the strength of the interactions.

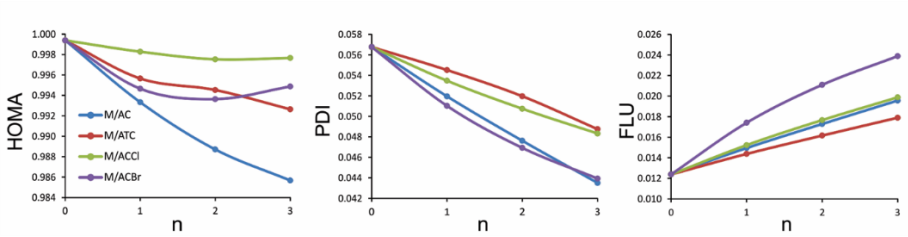

Figure III.9. Aromatic indices of M ring as a function of the monomers around it.

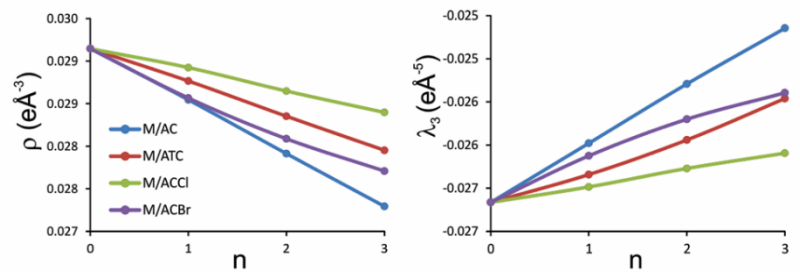

Figure III.10. Aromaticity descriptors of M ring as a function of the monomers around it.

III.4. Conclusions

In this chapter, structural and electronic analyses at ω-B97XD/6-311++G**level of theory were carried out on a series of supramolecular complexes formed by hydrogen and halogen bonds. The AIM theory in conjunction with NBO analysis and a set of aromaticity descriptors were also applied to understand the molecular factors that govern the self-assembly of the compounds studied. Quantitative insights into the electronic structure of M and molecular interactions involved in the self-assembly of this compound were gained. The most important fact is that an anti-cooperative effect is observed in all complexes, against the expected behavior and the general assumption in supramolecular assemblies via hydrogen bonds.

From the QTAIM analysis, as well as the NBO analysis, it is observed that the strongest interactions are those in the $M/(CA)_n$ for hydrogen bonded complexes and in the $M/(CABr)_n$ systems for halogen bonded complexes. These results may be helpful for the future experimental design of new materials, since the design of materials based on halogen bonds is still at an early-stage research.

It could also be seen that TCA molecule is not suitable to form planar structures, despite the fact that the crystalline structure of M/TCA is geometrically the same as M/CA co-crystal.

On the other hand, the complexation of M leads to a great decrease in its aromatic character due to the intermolecular interactions. It can be concluded that the decrease in the aromaticity is higher in complexes in which interactions are stronger, that is in the $M/(CA)_n$ and $M/(CABr)_n$ systems.

III.5. References

(1) Hughes, E. W. The Crystal Structure of Melamine. *J. Am. Chem. Soc.* **1941**, *63* (6), 1737–1752.

(2) Dewar, M. J. S.; Paoloni, L. The Electronic Structure of Melamine. *Trans. Faraday Soc.* **1957**, *53*, 261–271.

(3) Meier, R. J.; Coussens, B. The Molecular Structure of Hydrazine and Melamine: Rotational Barriers and Hybridisation. *J. Mol. Struct. THEOCHEM* **1990**, *209* (3–4), 303–312.

(4) Wang, Y.; Pittman, C. U.; Saebo, S. Investigation of the Structure and Properties of Ammeline, Melamine, and 2,4-Diamino-1,3,5-Triazine by Ab Initio Calculations. *J. Org. Chem.* **1993**, *58* (11), 3085–3090.

(5) Li, Z.; Chen, G.; Xu, Y.; Wang, X.; Wang, Z. Study of the Structural and the Spectral Characteristics of $[C_3N_3(NH_2)_3]_n$ (n =1-4) Clusters. *J. Phys. Chem. A* **2013**, *117*, 12511–12518.

(6) Silly, F.; Shaw, A. Q.; Castell, M. R.; Briggs, G. a. D.; Mura, M.; Martsinovich, N.; Kantorovich, L. Melamine Structures on the Au(111) Surface. *J. Phys. Chem. C* **2008**, *112* (30), 11476–11480.

(7) Chiş, V.; Mile, G.; Ştiufiuc, R.; Leopold, N.; Oltean, M. Vibrational and Electronic Structure of PTCDI and melamine–PTCDI Complexes. *J. Mol. Struct.* **2009**, *924–926*, 47–53.

(8) Atalay, Y.; Avcı, D.; Başoğlu, A.; Okur, İ. Molecular Structure and Vibrational Spectra of Melamine Diborate by Density Functional Theory and Ab Initio Hartree–Fock Calculations. *J. Mol. Struct. THEOCHEM* **2005**, *713* (1–3), 21–26.

(9) Thomas, R.; Kulkarni, G. U. A Hydrogen-Bonded Channel Structure Formed by a Complex of Uracil and Melamine. *Beilstein J. Org. Chem.* **2007**, *3*, 17.

(10) Makowski, S. J.; Lacher, M.; Lermer, C.; Schnick, W. Supramolecular Hydrogen-

Bonded Structures between Melamine and N-Heterocycles. *J. Mol. Struct.* **2012**, *1013*, 19–25.

(11) Xu, J.; Wu, G.; Wang, Z.; Zhang, X. Generation of 2D Organic Microsheets from Protonated Melamine Derivatives: Suppression of the Self Assembly of a Particular Dimension by Introduction of Alkyl Chains. *Chem. Sci.* **2012**, *3* (11), 3227.

(12) Prior, T. J.; Armstrong, J. A.; Benoit, D. M.; Marshall, K. L. The Structure of the Melamine–cyanuric Acid Co-Crystal. *CrystEngComm* **2013**, *15* (29), 5838.

(13) Wang, Y.; Wei, B.; Wang, Q. Crystal Structure of Melamine Cyanuric Acid Complex (1:1) Trihydrochloride, MCA·3HCl. *J. Crystallogr. Spectrosc. Res.* **1990**, *20* (1), 79–84.

(14) Li, S.; Sun, L.; Chung, Y.; Weber, S. G. Artificial Receptor-Facilitated Solid-Phase Microextraction of Barbiturates. *Anal. Chem.* **1999**, *71* (11), 2146–2151.

(15) Bader, R. F. W. *Atoms in Molecules: A Quantum Theory*; Clarendon Press: Oxford, 1994.

(16) Reed, A. E.; Curtiss, L. a; Weinhold, F. Intermolecular Interactions from a Natural Bond Orbital, Donor-Acceptor Viewpoint. *Chem. Rev. (Washington, DC, United States)* **1988**, *88* (6), 899–926.

(17) Krygowski, T. M. Crystallographic Studies of Inter- and Intramolecular Interactions Reflected in Aromatic Character of .pi.-Electron Systems. *J. Chem. Inf. Comput. Sci.* **1993**, *33*, 70–78.

(18) Krygowski, T. M.; Cyranski, M. K. Structural Aspects of Aromaticity. *Chem. Rev.* **2001**, *101*, 1385–1419.

(19) Poater, J.; Fradera, X.; Duran, M.; Solà, M. The Delocalization Index as an Electronic Aromaticity Criterion: Application to a Series of Planar Polycyclic Aromatic Hydrocarbons. *Chem. Eur J.* **2003**, *9*, 400–406.

(20) Matito, M. D.; Solà, M. The Aromatic Fluctuation Index (FLU): A New Aromaticity Index Based on Electron Delocalization. *J. Chem. Phys.* **2005**, *122*, 14109.

(21) Howard, S. T.; Krygowski, T. M. Benzenoid Hydrocarbon Aromaticity in Terms of Charge Density Descriptors. *Can. J. Chem.* **1997**, *75*, 1174–1181.

(22) Frisch, M. J.; Trucks, G. W.; Schlegel, H. B.; Scuseria, G. E.; Robb, M. A.; Cheeseman, J. R.; Montgomery, J. A. J.; Vreven, T.; Kudin, K. N.; Burant, J. C.; et al. Gaussian 03, Revision D.01. Gaussian, Inc.: Wallingford, CT 2004.

(23) Chai, J.-D.; Head-Gordon, M. Long-Range Corrected Hybrid Density Functionals with Damped Atom-Atom Dispersion Corrections. *Phys. Chem. Chem. Phys.* **2008**, *10*, 6615–6620.

(24) Kozuch, S.; Martin, J. M. L. Halogen Bonds: Benchmarks and Theoretical Analysis.

J. Chem. Theory Comput. **2013**, *9* (4), 1918–1931.

(25) Boys, S. F.; Bernardi, F. The Calculation of Small Molecular Interactions by the Differences of Separate Total Energies. Some Procedures with Reduced Errors. *Mol. Phys.* **1970**, *19*, 553–559.

(26) Keith, T. A. AIMAll (Version 11.12.19); TK Gristmill Software, Overland Park KS; Aim.tkgristmill.com. TK Gristmill Software: Overland Park KS 2011.

(27) Glendening, E. D.; Reed, A. E.; Carpenter, J. E.; Weinhold, F. NBO Version 3.1.

(28) Lu, T.; Chen, F. Multiwfn: A Multifunctional Wavefunction Analyzer. *J. Comp. Chem.* **2012**, *33,* 580–592.

(29) Bondi, A. Van Der Waals Volumes and Radii. *J. Phys. Chem.* **1964**, *68*, 441–451.

(30) Song, H. J.; Xiao, H. M.; Dong, H. S.; Zhu, W. H. Cooperative Effects and Strengths of Hydrogen Bonds in Open-Chain Cis-Triaziridine Clusters (N = 2-8): A DFT Investigation. *J. Phys. Chem. A* **2006**, *110* (6), 2225–2230.

(31) Znamenskiy, V. S.; Green, M. E. Quantum Calculations On Hydrogen Bonds In Certain Water Clusters Show Cooperative Effects. *J Chem Theory Comput.* **2007**, *3* (1), 103–114.

(32) Jalili, S.; Aghdastinat, H. Study of Hydrogen Bonding in Dihydroxyacetone and Glyceraldehyde Using Computational Methods. *J. Mol. Struct. THEOCHEM* **2008**, *857* (1–3), 7–12.

(33) Grabowski, S. J.; Bilewicz, E. Cooperativity Halogen Bonding Effect - Ab Initio Calculations on $H_2CO\cdots(ClF)_n$ Complexes. *Chem. Phys. Lett.* **2006**, *427* (1–3), 51–55.

(34) Ranganathan, A.; Pedireddi, V. R.; Rao, C. N. R. Hydrothermal Synthesis of Organic Channel Structures: 1:1 Hydrogen-Bonded Adducts of Melamine with Cyanuric and Trithiocyanuric Acids. *J. Am. Chem. Soc.* **1999**, *121* (8), 1752–1753.

(35) Carroll, M. T.; Bader, R. F. W. An Analysis of the Hydrogen Bond in BASE-HF Complexes Using the Theory of Atoms in Molecules. *Mol. Phys.* **1988**, *65*, 695–722.

(36) Koch, U.; Popelier, P. L. A. Characterization of C-H-O Hydrogen Bonds on the Basis of the Charge Density. *J. Phys. Chem.* **1995**, *99* (24), 9747–9754.

(37) Amezaga, N. J. M.; Pamies, S. C.; Peruchena, N. M.; Sosa, G. L. Halogen Bonding: A Study Based on the Electronic Charge Density. *J. Phys. Chem. A* **2010**, *114* (1), 552–562.

(38) Han, N.; Zeng, Y.; Sun, C.; Li, X.; Sun, Z.; Meng, L. N···I Halogen Bonding Interactions: In Fl Uence of Lewis Bases on Their Strength and Characters. *J. Phys. Chem. A* **2014**, *118*, 7058–7065.

(39) Duarte, D. J. R.; Sosa, G. L.; Peruchena, N. M. Nature of Halogen Bonding. A Study

Based on the Topological Analysis of the Laplacian of the Electron Charge Density and an Energy Decomposition Analysis. *J. Mol. Model.* **2013**, *19* (5), 2035–2041.

(40) Espinosa, E.; Molins, E.; Lecomte, C. Hydrogen Bond Strengths Revealed by Topological Analyses of Experimentally Observed Electron Densities. *Chem. Phys. Lett.* **1998**, *285*, 170–173.

(41) Grabowski, S. J. Ab Initio Calculations on Conventional and Unconventional Hydrogen Bonds Study of the Hydrogen Bond Strength. *J. Phys. Chem. A* **2001**, *105*, 10739–10746.

(42) Szatyłowicz, H.; Sadlej-Sosnowska, N. Characterizing the Strength of Individual Hydrogen Bonds in DNA Base Pairs. *J. Chem. Inf. Model.* **2010**, *50* (12), 2151–2161.

(43) Matta, C. F.; Castillo, N.; Boyd, R. J. Extended Weak Bonding Interactions in DNA: π-Stacking (Base-Base), Base-Backbone, and Backbone-Backbone Interactions. *J. Phys. Chem. B* **2006**, *110*, 563– 578.

(44) Reiher, M.; Sellmann, D.; Hess, B. A. Stabilization of Diazene in Fe(II)–sulfur Model Complexes Relevant for Nitrogenase Activity. I. A New Approach to the Evaluation of Intramolecular Hydrogen Bond Energies. *Theor. Chem. Acc.* **2001**, *106*, 379–392.

(45) Cremer, D.; Kraka, E. Chemical Bonds without Bonding Electron Density – Does the Difference Electron-Density Analysis Suffice for a Description of the Chemical Bond? *Angew. Chem.* **1984**, *23*, 627–628.

(46) Angelina, E. L.; Duarte, D. J. R.; Peruchena, N. M. Is the Decrease of the Total Electron Energy Density a Covalence Indicator in Hydrogen and Halogen Bonds? *J. Mol. Model.* **2013**, *19* (5), 2097–2106.

(47) Angelina, E. L.; Peruchena, N. M. Strength and Nature of Hydrogen Bonding Interactions in Mono- and Di-Hydrated Formamide Complexes. *J. Phys. Chem. A* **2011**, *115* (18), 4701–4710.

(48) Wang, W.; Wong, N. B.; Zheng, W.; Tiang, A. Theoretical Study on the Blueshifting Halogen Bond. *J. Phys. Chem. A* **2004**, *108*, 1799–1805.

(49) Krygowski, T. M.; Szatylowicz, H.; Stasyuk, O. A.; Dominikowska, J.; Palusiak, M. Aromaticity from the Viewpoint of Molecular Geometry: Application to Planar Systems. *Chem. Rev.* **2014**, *114* (12), 6383–6422.

(50) Parreira, R. L. T.; Galembeck, S. E. Computational Study of Pyrylium Cation–water Complexes: Hydrogen Bonds, Resonance Effects, and Aromaticity. *J. Mol. Struct. THEOCHEM* **2006**, *760* (1–3), 59–73.

Supplementary Material

Table S1. Changes in NBO populations of lone pairs (n_A) and antibonds (σ^*_{D-X}) from **(a)** M/(AC)$_n$, **(b)** M/(ATC)$_n$, **(c)** M/(ACCl)$_n$ y **(d)** M/(ACBr)$_n$, and Second-Order Perturbation Energies $E^{(2)}$ ($n_A \rightarrow \sigma^*_{D-X}$).[a]

Complex	D–X···A	Δn	$E^{(2)}$	$\Delta\sigma^*$
(a)				
M/CA	N–H···N	-0,0550	41,1	0,0808
	N–H···O	0,0079	7,8	0,0199
	N–H···O	0,0079	7,8	0,0199
M/(CA)$_2$	N–H···N	-0,0526	38,7	0,0766
	N–H···O	0,0076	8,1	0,0207
	N–H···O	0,0066	7,6	0,0198
M/(CA)$_3$	N–H···N	-0,0510	36,7	0,0734
	N–H···O	0,0064	8,0	0,0207
	N–H···O	0,0064	8,0	0,0207
(b)				
M/TCA	N–H···N	-0,0559	41,2	0,0804
	N–H···S	-0,0004	4,5	0,0200
	N–H···S	-0,0004	4,4	0,0200
M/(TCA)$_2$	N–H···N	-0,0503	36,3	0,0721
	N–H···S	-0,0017	5,0	0,0222
	N–H···S	-0,0020	4,3	0,0193
M/(TCA)$_3$	N–H···N	-0,0512	36,2	0,0721
	N–H···S	-0,0019	4,6	0,0212
	N–H···S	-0,0018	4,1	0,0192
	N–H···N	-0,0518	36,6	0,0729
	N–H···S	-0,0025	5,1	0,0232
	N–H···S	0,0004	2,6	0,0132
	N–H···N	-0,0111	7,0	0,0190
	N–H···S	-0,0139	12,6	0,0336
	N–H···S	-0,0139	12,6	0,0336
(c)				
M/CACl	N–Cl···N	-0,0630	19,1	0,0745
M/(CACl)$_2$	N–Cl···N	-0,0565	17,0	0,0663
M/(CACl)$_3$	N–Cl···N	-0,0535	16,0	0,0621

Complex	D–X···A	Δ*n*	$E^{(2)}$	$\Delta\sigma^{*}$
(d)				
M/CABr	N–Br···N	-0,1284	47,4	0,1508
	N–H···Br	-0,0056	1,3	0,0020
	N–H···Br		1,3	0,0020
$M/(CABr)_2$	N–Br···N	-0,1081	39.0	0,1265
	N–H···Br	-0,0063	1,3	0,0021
	N–H···Br		1,3	0,0017
$M/(CABr)_3$	N–Br···N	-0,0925	32,5	0,1075
	N–H···Br	-0,0067	1,3	0,0018
	N–H···Br		1,3	0,0018

[a] Números de ocupación en e y energías kcal/mol.

Table S2. Pearson coefficients (r^2) and *p*-values for correlation between aromaticity indices for the set of complexes at the ω-B97XD/6-311++G(d,p) level of theory. P values of < 0.05 were considered as significant.

(a) $M/(AC)_n$

Index 1	**Index 2**	**n**	**Pearson**	**p-value**
HOMA	λ_3	4	-1,00	0,0039
HOMA	ρ_{RCP}	4	0,99	0,0059
HOMA	PDI	4	1,00	0,0026
HOMA	FLU	4	-1,00	0,0029
λ_3	ρ_{RCP}	4	-1,00	0,0003
λ_3	PDI	4	-1,00	0,0002
λ_3	FLU	4	1,00	0,0003
ρ_{RCP}	PDI	4	1,00	0,0007
ρ_{RCP}	FLU	4	-1,00	0,0006
PDI	FLU	4	-1,00	< 0,0001

(b) $M/(ATC)_n$

Index 1	Index 2	n	Pearson	p-value
HOMA	λ_3	4	-0,98	0,0176
HOMA	ρ_{RCP}	4	0,99	0,0123
HOMA	PDI	4	0,99	0,0135
HOMA	FLU	4	-1,00	0,0036
λ_3	ρ_{RCP}	4	-1,00	0,0006
λ_3	PDI	4	-1,00	0,0006
λ_3	FLU	4	0,99	0,0057
ρ_{RCP}	PDI	4	1,00	0,0006
ρ_{RCP}	FLU	4	-1,00	0,0028
PDI	FLU	4	-1,00	0,0040

(c) $M/(ACCl)_n$

Index 1	Index 2	n	Pearson	p-value
HOMA	λ_3	4	-0,97	0,0266
HOMA	ρ_{RCP}	4	0,96	0,0381
HOMA	PDI	4	0,98	0,0156
HOMA	FLU	4	-0,98	0,0195
λ_3	ρ_{RCP}	4	-1,00	0,0011
λ_3	PDI	4	-1,00	0,0018
λ_3	FLU	4	1,00	0,0009
ρ_{RCP}	PDI	4	0,99	0,0056
ρ_{RCP}	FLU	4	-1,00	0,0037
PDI	FLU	4	-1,00	0,0002

(d) $M/(ACBr)_n$

Index 1	Index 2	n	Pearson	p-value
HOMA	λ_3	4	-0,92	0,0811
HOMA	ρ_{RCP}	4	0,90	0,0965
HOMA	PDI	4	0,92	0,0769
HOMA	FLU	4	-0,92	0,0807
λ_3	ρ_{RCP}	4	-1,00	0,0007
λ_3	PDI	4	-1,00	0,0001
λ_3	FLU	4	1,00	<0,0001
ρ_{RCP}	PDI	4	1,00	0,0012
ρ_{RCP}	FLU	4	-1,00	0,0007
PDI	FLU	4	-1,00	<0,0001

IV. EVOLUTION OF HYDROGEN BONDS IN MELAMINE/ CYANURIC ACID SUPRAMOLECULAR AGGREGATES.

"Driving a car is one thing, but building it is another; you turn the key and step on the gas pedal, and the car moves – you can use it without any need to know what is happening inside the car. But to truly engineer a better car, you must have knowledge about the properties of its components and how they are put together. The same hold true about DNA as it continues to be used for building these nanostructures, and we are providing a mechanical spec sheet for it through our analysis."

Wonmuk Hwang, about DNA Deformation and Binding

Part of this chapter previously appeared as:

Petelski, A. N.; Peruchena, N. M.; Sosa, G. L. Sosa. Evolution of the hydrogen-bonding motif in the melamine-cyanuric acid co-crystal. A topological study. *J. Mol. Mod.,* **2016***, 22*, 202.

IV.1 Introduction

Supramolecular self-assembly is one of the fundamental concepts of supramolecular chemistry. It can be defined as the spontaneous non-covalent association of two or more molecules from conditions of equilibrium to stable aggregates with well-defined composition and structure.[1,2] This spontaneity implies information that involves the organization of functional structures[3] arranged by multiple binding with positive or negative cooperativity.[4] The interest of current research activity is focused in controlling self-organization at the molecular level[5] and thus, producing a new generation of materials.[6,7] In this way, one of the systems that have monopolized the major interest in this field, and one of the most exploited ones, is the Melamine (M)/Cyanuric Acid (CA) mixture. Many investigations have taken advantage of these compounds in order to obtain structures like polymeric rods,[8] molecular boxes,[1,9] supramolecular membranes,[10,11] and photoresponsive materials.[12] This system has opened a great stream of experimental and theoretical research and applications, and remains the subject of intense scientific activity.

The first crystal structure of M/CA was reported by Wang and coworkers in 1990,[13] although, the structure was obtained from HCl solution (that is CA·M·3HCl) and revealed a one-dimensional linear tape structure. Later on, Ranganathan and

coworkers reported the crystal structure of M/CA adducts obtained by hydrothermal synthesis.[14] This last structure confirmed the expected rosette type structures, which form a hexagonal network arranged through hydrogen bonds (HB's). The molecular structure has also revealed that two additional aggregates can occur: infinite linear tapes or infinite crinkled tapes. However, the M/CA crystal structure was recently more accurately re-determined by Prior et al.[15], displaying precise information on the intermolecular distances and stacking interactions.

Several investigations have been attempted with the purpose of understanding the fundamental process of self-assembly between M and CA. Whitesides and co-workers have extensively studied M/CA structures covalently modified,[16–19] obtaining polymeric structures of high molecular weight and small capsules. Recently, Timmerman group have developed a thermodynamic model that describes the relative stabilities of various hydrogen-bonded species.[20] They have also performed gas-phase calculations on covalently modified trimolecular complexes, which have shown a relationship between the size of the substituents and the coplanarity of the complexes. The study of the M/CA mixture was also performed on a Au(111) surface by Besenbacher and co-workers,[21] in which they found a novel network based on the M_3/CA_1 cluster, besides the well-known lattice. Furthermore, Bong and Ma have studied a M/CA water mixture[22] and also a trivalent derivative system in water[11,22] with the scope of examining recognition and assembly processes in aqueous media, research that is still rare.

With the aim of characterizing the non-covalent interactions in M/CA clusters and thus shed more light on the molecular factors that govern the processes of self-assembly and crystal packing, electronic structure calculations are reported in this chapter on a set of 13 hydrogen-bonded complexes of M_nCA_m (with n, m = 1,2,3) taken from crystallographic data as starting points.

IV.2 Methods

Two well-known motifs of M and CA were explored, the cyclic and the linear hydrogen-bonded assemblies. By following the scheme of aggregation shown in **Fig. IV.1**, geometries of M_n/CA_m clusters (from **I** to **XIII**; with n, m = 1, 2, 3), were taken from the crystallographic structure data obtained by Prior and co-workers.[15]

All geometries were fully optimized without any constraint at the B3LYP/6-311++G(d,p) level of theory using Gaussian 03[23] suit of programs. This functional has shown excellent performance in the calculation of structures[24,25] and topological properties of hydrogen-bonded complexes,[25–28] especially in structures with highly directional interactions.[29,30] The minimum energy nature of the optimized structures was verified using the vibrational frequency analysis.

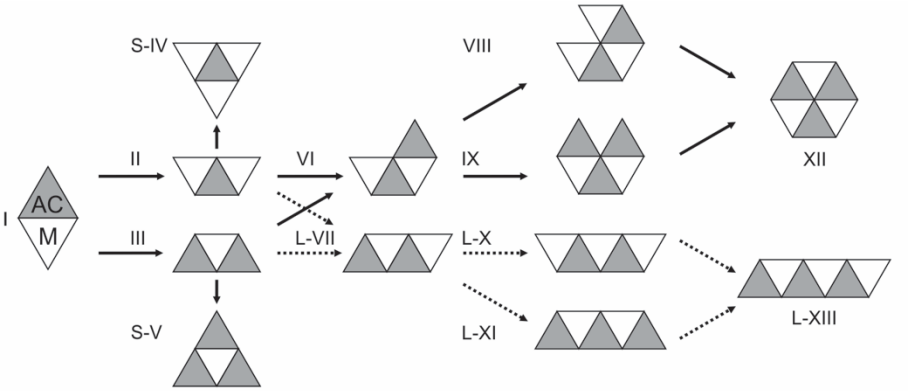

Fig. 1 Schematic representation of different aggregation states. M/CA **I**. M_2/CA **II**. M/CA_2 **III**. M_3/CA star-like structure **S-IV**. M/CA_3 star-like structure **S-V**. M_2/CA_2 **VI**. M_2/CA_2 linear type **L-VII**. M_3/CA_2 **VIII**. M_2/CA_3 **IX**. M_3/CA_2 linear type **L-X**. M_2/CA_3 linear type **L-XI**. M_3/CA_3 **XII**. M_3/CA_3 linear type **L-XIII**.

The bonding energies (ΔE_{bond}) were obtained at the same level of theory using the supermolecular approach, which is calculated as the difference between the total energy of the complex and the sum of total energies of the isolated molecules. Binding energies have also been corrected (ΔE_{bond}^{BSSE}) for the basis set superposition error (BSSE) within the approach of Boys and Bernardi.[31] In order to assess the importance of long range interactions, ω-B97XD[32] single-point energy calculations with the 6-311++G(d,p) basis set were also performed using the B3LYP geometries, since this functional predicts very well the geometrical parameters of the experimental structure. Interactions were quantitatively evaluated by a topological analysis of the electron charge density in the framework of the quantum theory of atoms in molecules[33] (QTAIM). This analysis was carried out with the AIMAll[34]

software, using wave functions generated from the B3LYP/6-311++G(d,p) calculations.

Electrostatic potential surfaces were generated by mapping the electrostatic potential V(r) at the B3LYP/6–311++G(d,p) level of theory. We have considered the electron density isosurface of ρ(r) = 0.001 au. This contour of the molecular electronic density was suggested by Bader et al.[35] and represents the effective molecular volume.

IV.3 Results and Discussion

VI.3.1 Geometries

The optimized geometries of the isolated compounds are shown in **Fig. IV.2**, and the selected optimized geometrical parameters of the isolated molecules are given in **Table IV.1**. As it can be seen in **Figs. IV.2a** and **b**, the isolated geometry of M is quasi planar because of the nitrogen inversion. This result is in accordance with previous experimental and theoretical studies,[36–38] which have shown that M has a structure close in symmetry to D_{3h}. Besides, CA is completely planar (**Fig. IV.2c**). With specific regards to geometrical parameters, one can see that the calculated values are in a significant agreement with the values obtained from X-ray diffraction, with differences less than 1 %.

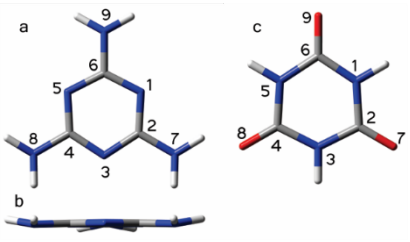

Figure IV.2. Optimized geometries of: **(a)** melamine top view; **(b)** melamine side view; and **(c)** cyanuric acid at B3LYP/6-311++G(d,p) level of theory.

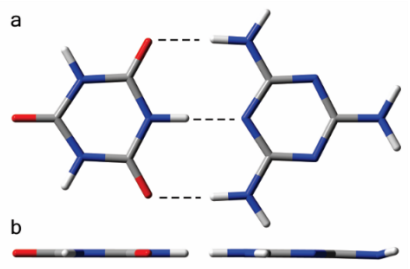

Figure IV.3. Optimized geometry of M/CA complex at B3LYP/6−311++G(d,p) level of theory. **(a)** Top view and **(b)** side view.

Table IV.1. Selected Geometric Parameters of M and CA compounds calculated at B3LYP/6-311++G(d,p) level. X-ray parameters are also given.

Atoms	B3LYP	X-ray[a]	Atoms	B3LYP	X-ray[a]
Melamine			Cyanuric acid		
Distances (Å)					
C2–N7	1.3399	1.3244	C2–O7	1.2254	1.2320
C4–N8	1.3399	1.3300	C4–O8	1.2253	1.2354
C6–N9	1.3399		C6–O9	1.2254	
N5–C6	1.3511	1.3562	N1–C2	1.3771	1.3746
N3–C2	1.3511	1.3600	N3–C4	1.3770	1.3708
N5–C4	1.3511	1.3575	C4–N5	1.3771	1.3746
Angles (°)					
N5–C6–N1	124.51	124.82	N1–C2–N3	115.82	115.92
C6–N1–C2	115.50	115.35	C4–N5–C6	124.19	123.58
C2–N3–C4	115.51	115.69	N5–C6–N1	115.81	116.26
N3–C4–N5	124.50	124.35	C6–N1–C2	124.19	123.97

[a] Experimental values obtained by Prior et al.[15]

All complexes are bound trough a set of three HB's, as shown in **Fig. IV.3a**. That is, a central interaction N–H···N, in which CA acts as a proton donor, and two side interactions, N–H···O, in which M acts as a double proton donor. In **Fig. IV.3b** it can be seen that the two amino groups of M are coplanar with the ring, while the amino group that does not interact with CA keeps its quasi pyramidal form. Nevertheless, upon addition of more CA units, all amino groups become planar, suggesting that conformational changes occur upon hydrogen-bonding formation.

Table IV.2 reports the values of the main parameters that describe the geometry of the M/CA complex (**I**). These parameters are: the H···A intermolecular distance (where A = N, O), the N–H bond length, and the ∠ equilibrium angle N–H···A. Δd_{VdW}(H···A) represents the difference between the sum of A and H Van der Waals radii[39] and the H···A intermolecular distances, and Δd(D–X) represents the variations in the bond donor distance upon complexation, that is, the difference between the distance d(D–X) in the complexes and in the isolated monomers. It is important to note that the calculated values of Tables 1 and 2 are in good agreement with the values obtained from X-ray diffraction; the relative difference between these quantities is less than 2 %. This confirms that the B3LYP/6–311++G(d,p) level of approximation is suitable for the compounds studied here and reflects the environment of the crystal structure.

In all cases, H···A intermolecular distances are substantially shorter than the sum of the van der Waals radii of the H and A atoms. Positive values of Δd_{VdW}(H···A) can be taken as the distance of penetration of electronic densities of atoms H and A. When analyzing the N···N and N···O distances versus the number of molecular units for all complexes (see **Fig. IV.4** and Table S1 in supplementary material), it can be clearly seen that all N···N distances are lengthened from 2.856 Å in complex **I** to a maximum mean elongation of 2.89 Å when going from complex **I** to either the rosette motif (**XII**) or the linear motif (**L-XIII**). Therefore, these results show typical geometrical characteristics of non-cooperative effects.[40,41] It may be noted that all distances are longer than those observed in the crystal except the N···N distance value of complex **I**. With regard to N–H···O interactions, it is evidenced that, some N···O distances shorten and others lengthen, that is, both cooperative and non-cooperative effects could be operating at the same time. However, in the set of tetramolecular complexes only structures **S-IV** and **S-V** do not show shortening of N···O distances.

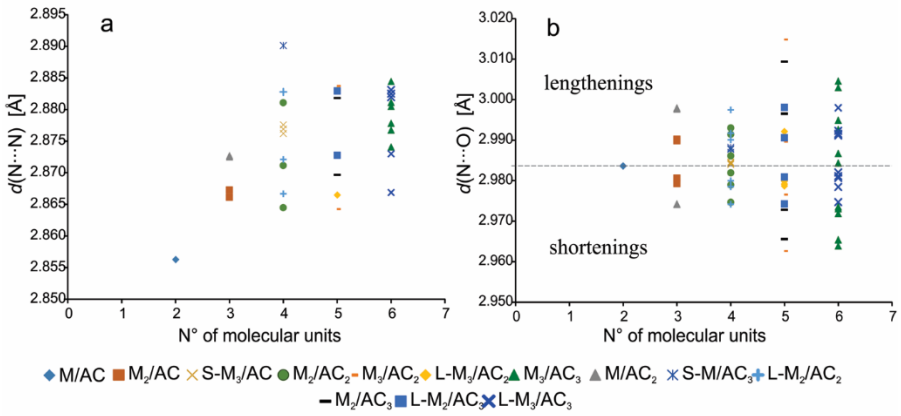

Figure IV.4. (a) $N_M\cdots N_{CA}$ distances vs. number of molecular units. **(b)** $N_M\cdots O_{CA}$ distances vs. number of molecular units. The dashed line represents the $N_M\cdots O_{CA}$ distance of the M/CA adduct.

Table IV.2. Selected Geometric Parameters of complex **I** calculated at B3LYP/6–311++G(d,p) level. Distances are in angstroms and angles are in degrees. Values in parentheses correspond to the structures obtained by X-ray diffraction.

Interaction	*d* (N···A)	*d* (H···A)	Δd_{VdW} (H···A)[a]	*d* (N–H)	Δd (N–H)	∠ N–H···N
N–H···N	2,856 (2.861)[b] (2.850-2.880)[c]	1.798 (1.93)[b]	0.952	1.059 (0.930)[b]	0.048	179.99 (180.00)[b]
N–H···O	2,984 (2.938)[b] (2.940-2.980)[c]	1.970 (2.07)[b]	0.750	1.013 (0.880)[b]	0.008	174.86 (177.70)[b]
N–H···O	2,984 (2.947)[b]	1.970 (2.08)[b]	0.750	1.013 (0.870)[b]	0.008	174.85 (174.80)[b]

[a] Δd_{VdW}(H···A) is the difference between the equilibrium intermolecular distances and the sum of the van der Waals radii of H and A atoms (van der Waals radii, in Å from ref. [39]: H, 1.20; N, 1.55; and O, 1.50).

[b] Experimental values obtained by Prior et al.[15]

[c] Experimental values obtained by Ranganatham et al.[14]

On the other hand, all Δd(N–H) changes are positive; that is, the N–H bond stretched as a result of complexation. However, when going from complex **I** to **L-**

XIII, the magnitude of the N–H bond elongations decrease slightly, contrary, again, to the geometrical features of HB's cooperativity.

Finally, equilibrium angles reflect the collinearity among all the molecules within each complex. N–H···N angles vary from 180° (value of complex **I**), to a mean value of 179°; hence, there is a minor decrease in the coplanarity upon aggregation. The lowest value is observed in complex **L-XIII**, the linear analogue of the rosette type complex. The plane where the molecules are placed is curved, as it is shown in **Fig. IV.5.** With regard to side interactions, being less collinear than the central interaction, N–H···O angles range from 175° to 178°.

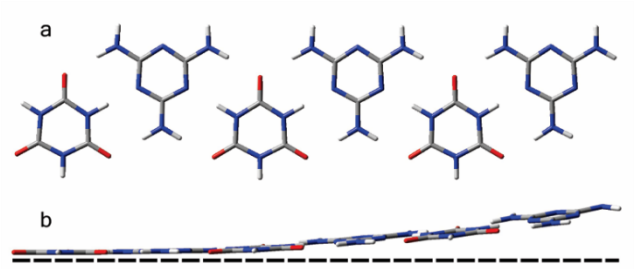

Figure IV.5. Optimized geometry of complex **L-XIII** at B3LYP/6-311++G(d,p) level of theory. **(a)** Top view and **(b)** side view (dash line is depicted as a reference)

IV.3.2 Energetic Analysis

Bonding energies of all clusters are given in Table 3. We also calculated the ΔE_{bond} per molecular unit added (ΔE_{PM}) using **Ecs. IV.1** and **2**.

$$\forall\, m \geq n \;\Delta E_{PM} = E_{M_n/CA_m} - E_{M_{n-1}/CA_m} - E_M \qquad \text{(IV.1)}$$

$$\forall\, n \geq m \;\Delta E_{PM} = E_{M_n/CA_m} - E_{M_n/CA_{m-1}} - E_{CA} \qquad \text{(IV.2)}$$

Where n and m are the numbers of molecular entities, the sub index M refers to melamine and CA refers to cyanuric acid.

As can be seen in **Table IV.3**, the energy differences separating the group of complexes (bi-, tri-, tetra-, and penta-molecular complexes) are very small; the corrected energy differences are even lesser. Therefore, it is hazardous then to address conclusions about relative stabilities and, establishing a progression of

aggregation most energetically stabilized. Nevertheless, the ΔE_{bond} increase in the following order for both functionals: **II** < **III**, **S-IV** < **S-V** < **L-VII** < **VI**, **L-XI** < **IX** < **L-X** < **VIII**, **L-XIII** < **XII**. A clear separation of ΔE_{bond} occurs between complexes XII and L-XIII, with a difference of 14 kcal/mol for B3LYP functional and almost 19 kcal/mol for ω-B97XD functional. This is because completion of the ring in complexes **VIII** and **IX** generates three additional HB's in comparison to the linear hexamer.

Table IV.3. Corrected binding energies[a] calculated at B3LYP/6−311++G(d,p)[b] and ω-B97XD/6-311++G**//B3LYP/6-311++G** level of theory.

Complex		ΔE_{bond}^{BSSE}	ΔE_{PM}		ΔE_{bond}^{BSSE}
		B3LYP	m ≥ n	m ≤ n	ω-B97XD
I	M/CA	-15.26	-	-	-19.33
II	M_2/CA	-30.04	-15.61	-	-38.25
III	M/CA_2	-29.83	-	-15.36	-37.98
S-IV	M_3/CA	-44.34	-15.16	-	-56.92
S-V	M/CA_3	-43.55	-	-14.55	-55.87
VI	M_2/CA_2	-44.82	-15.60	-15.85	-57.14
L-VII	M_2/CA_2	-44.59	-15.60	-15.35	-56.93
VIII	M_3/CA_2	-59.40	-15.45	-	-76.07
IX	M_2/CA_3	-59.24	-	-15.24	-75.72
L-X	L-M_3/CA_2	-59.39	-15.64	-	-75.85
L-XI	L-M_2/CA_3	-59.18	-	-15.39	-75.51
XII	M_3/CA_3	-88.37	-30.95	-30.74	-113.33
L-XIII	L-M_3/CA_3	-73.94	-15.49	-15.29	-94.57

[a] All values in kcal/mol

Despite that some HB's seem to be cooperative, as was seen in section 3.1, it is worth stressing that results obtained by Eqs. IV.1 and IV.2 show that the mean effect is a negative cooperativity in all complexes. That is to say, in all cases, the total interaction energy is lesser than the sum of the ΔE_{bond} of complex **I**, e. g., $\Delta E_{bond\text{-}II} < \Delta E_{bond\text{-}I} \times 2$ and, $\Delta E_{bond\text{-}III} < \Delta E_{bond\text{-}I} \times 2$. In other words, the whole is not greater than the sum of the parts.

IV.3.3 Topology of the Electron Density

The nature of HB's was addressed by analyzing the electron density distribution within the QTAIM.[33] In this work, different bond properties were used to analyze the nature of the interactions that occur in the different complexes: the electron charge density $\rho(r_c)$, that measures the accumulation of charge between the bonded nuclei and reflects the bond strength;[42,43] the Laplacian of the electron density $\nabla^2\rho(r_c)$, that provides information about the local charge concentration ($\nabla^2\rho(r_c) < 0$) or depletion ($\nabla^2\rho(r_c) > 0$); the densities of kinetic energy $G(r_c)$, the densities of potential energy $V(r_c)$, and the total electronic energy density $H(r_c) = V(r_c) + G(r_c)$.

The molecular graphs of all complexes are displayed in **Fig. IV.6**, and the local properties calculated at bond critical points (BCP's) are given in **Table S2** (see the Supplementary Material). The topological properties at each BCP fall within the proposed range used to characterize HB formation.[44] The charge density values lie in the range of 0.02 to 0.05 au. The Laplacian values in all complexes are positive and lie in the range of 0.08 to 0.1 au.

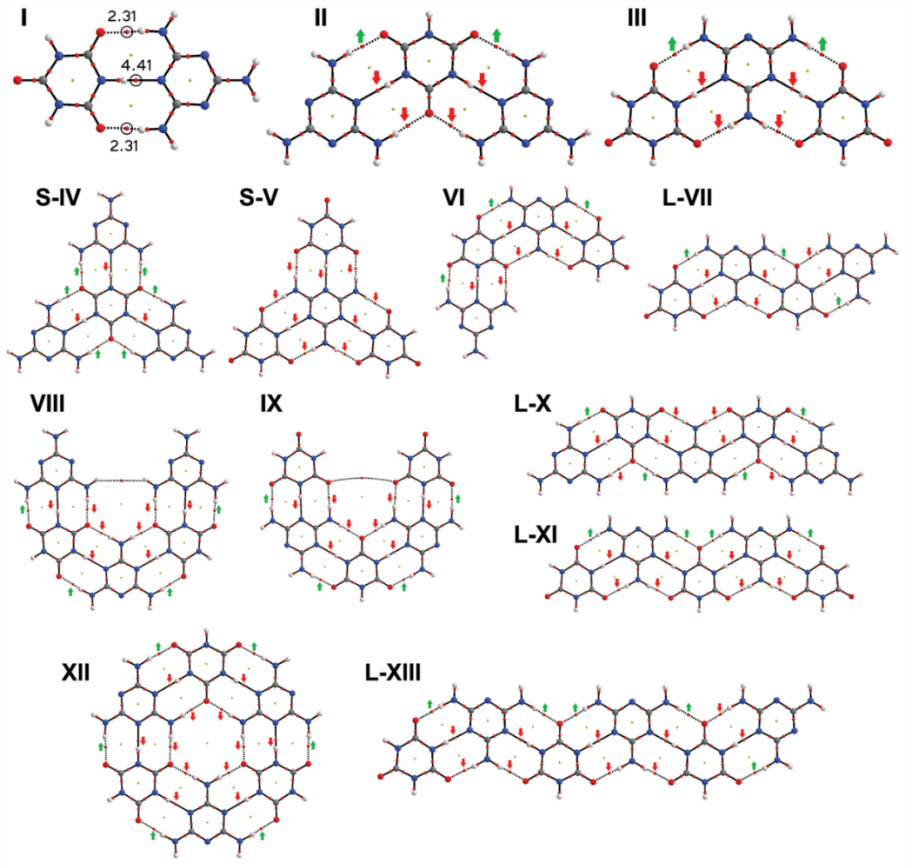

Figure. IV.6 Molecular graphs of complexes. Values of $\rho(r_c)$ at BCP are reported in units of 10^{-3} au. With green and red arrows the increase and decrease of $\rho(r_c)$ at BCP, respectively, is indicated. The lines connecting the nuclei are the bond paths. Small red and yellow dots represent BCPs (3, −1) and ring critical points (RCPs) (3, +1), respectively.

It has been shown that $\rho(r_c)$ is a good indicator of the bond order and the bond strength.[43] Thus, the increase or decrease of this property can be related with the cooperativity or negative cooperativity of HB's, respectively.[45,46] In complex **I** (**Fig. IV.6**), N–H···N is nearly two times stronger than the N–H···O interaction, as values of $\rho(r_c)$ show. **Fig. IV.6** also indicates the increase (green arrows) or decrease (red arrows) of $\rho(r_c)$ at BCP's with respect to complex **I**. In complex **II** and **III**, two N–H···O interactions undergo an increase in the charge density, by 0.95% in complex **II**

and 2.39% in complex **III**. However, complex **III** experiences a greater decrease of density in the remaining interactions (red arrows in **Fig. IV.6**) with respect to complex **II**, which explain a greater ΔE_{bond} in the latter.

In tetramolecular complexes, star-like topologies show different behaviors. With regard to complexes **S-IV**, surprisingly, all N–H···O interactions show an increase of charge density, against geometrical results of section 3.1 which indicate typical characteristics of non-cooperative effects. On the contrary, complex **S-V** exhibits a decrease of charge density in all BCP's. The fact that complex **S-IV** is energetically and topologically favored over complex **S-V** supports previous research of Besenbacher and co-workers.[21] The authors reported a novel phase of M/CA adsorbed on a Au(111) surface with an M:CA ratio of 3:1, which is the equivalent of complex **S-IV**, instead the well-known 1:1 ratio found in the co-crystal. Complex **VI** shows an increase of charge density in N–H···O interactions of the outer edge (see **Fig. IV.5 VI**), while the remaining interactions show a decrease of this property. The linear analogue, complex **L-VII**, shows an increase of $\rho(r_c)$ on one side of the complex (see **Fig. IV.5 L-VII**). A comparison between complexes **VI** and **L-VII** reveals that major decreases of $\rho(r_c)$ occurs in the linear complex, according to a greater ΔE_{bond} in the complex **VI**.

Pentamolecular complexes require a special attention, as interesting topological characteristics arise. With specific respect to cyclic assemblies, an increase of the charge density in N–H···O interactions of the outer edge is observed. Furthermore, in complex **VIII** a so-called dihydrogen bond, H···H, occurs. This interaction was characterized for the first time, within the QTAIM, by Popelier,[47] who has verified the eight criteria used to describe HB's.[44] Our results show deviations from these criteria, since $\rho(r_c)$ at the BCP (0.000106 au) does not fall within the proposed range of 0.002−0.035 au.[44] Therefore, this interaction can be classified as a Van der Waals type since QTAIM parameters fulfill the criteria of closed shell interactions: the value of $\rho(r_c)$ is relatively low; the ratio of the perpendicular contraction of $\rho(\lambda_1)$ to its parallel expansion (λ_3) is $|\lambda_1|/\lambda_3<1$, and $\nabla^2\rho(r_c) > 0$.[33] In concert with complex **IX**, a BCP between two O atoms occurs (O···O) with a density of 0.000028 au, which can be also classified as a Van der Waals interaction. Since complex **VIII** is more stable than complex **IX** by 0.21 kcal/mol, a good indicator of structural

stability is the distance between a BCP and a ring critical point (RCP). If these critical points are joined, the ring tends to open due to a bond rupture.[47] In complex **VIII**, the distance between H···H BCP and the nearest RCP is 1.822 Å, whereas in complex **IX** the distance between O···O BCP to its nearest RCP is 1.528 Å; therefore, the former is more stable in line with the ΔE_{bond}.

Unlike the cyclic pentamolecular complexes, the linear structures (**L-X** and **L-XI**) show different topological patterns as it is shown in **Fig. IIV.6**. In complex **L-X**, the reinforced interactions (green arrows) are alternated from side to side, while in complex **L-XI** they occur in one side of the complex. It is worth stressing that the linear complex **L-X** is more stable than the cyclic one by 0.14 kcal/mol. This small difference could be attributed to the O···O interaction in the complex **IX** that adds a steric stress. As expected, an increase in the stability of the cyclic rosette (**XII**) is produced by the formation of three additional HB's which forms a new RCP. This arrangement is driven by the enhanced interactions (positive cooperativity) that take place in the outer region of the complex; thus, forming a ring of cooperativity.

Besides $\rho(r_c)$, another property that could be considered as an indicator of the strength of interactions is the value and the sign of the total electronic energy density[46,48,49] $H(r_c)$, which has also been associated with the covalent character of a bond when this property takes negative values.[50] All N–H···N interactions show a negative sign in $H(r_c)$, while N–H···O interactions are positive. This fact indicates that the N–H···N interaction is far stronger than N–H···O. **Fig. IV.7** clearly reveals how these two properties vary with the cluster size. The lowest value of $H(r_c)$ and the highest value of $\rho(r_c)$ is reached in the adduct. While $\rho(r_c)$ decreases as the cluster size increases, $H(r_c)$ becomes less negative, a fact that indicates a weakening of N–H···N interactions and, in other words, a negative cooperativity.

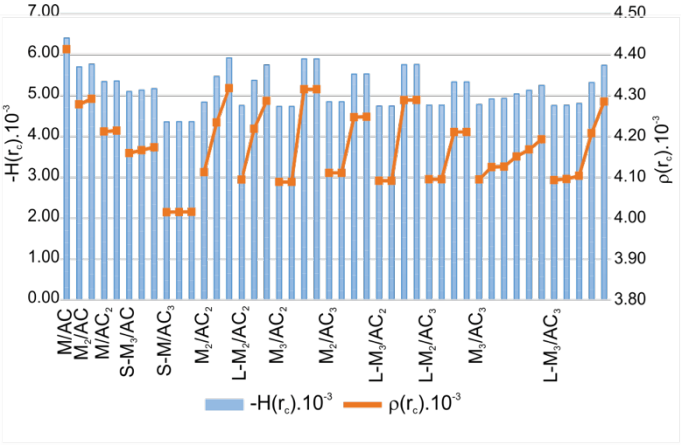

Figure IV.7. $-H(r_c)\cdot 10^{-3}$ and $\rho(r_c)\cdot 10^{-3}$ at N–H···N BCP's. Complexes **I** to **XIII**.

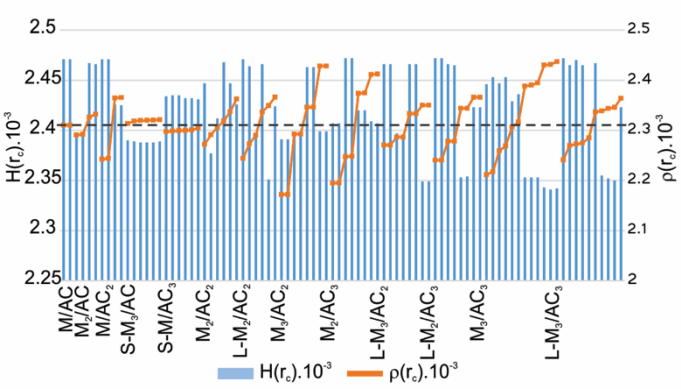

Figure IV.8. $H(r_c)\cdot 10^{-3}$ and $\rho(r_c)\cdot 10^{-3}$ at N–H···O BCP's. Complexes **I** to **XIII**. The dashed line represents $\rho(r_c)$ value of complex **I** as a reference.

Figure IV.8 shows the variations of $H(r_c)$ and $\rho(r_c)$ at N–H···O BCPs. Since $H(r_c)$ accounts both contributions of kinetic and potential energy densities, the most stable complexes are those with lesser $H(r_c)$ values (less positive), that is, complexes with a greater potential energy density, and $V(r_c)$ represents the capacity of concentrating electrons at BCP's. From **Fig. IV.8**, it can be immediately noticed that the electron density increases (above the dashed line) and decreases within each complex, in line with variations of N···O distances. In general, it can be observed that as N···O lengths decrease, $\rho(r_c)$ values increase. Nevertheless, despite that in

M_3CA complex the N···O lengths increase with respect to M/CA complex; the magnitude of $\rho(r_c)$ increases and $H(r_c)$ decreases, a fact that indicates an enhancement of N–H···O interactions.

Finally, the relationship between the local electronic potential energy density, $V(r_c)$, and the ΔE_{bond} was evaluated, since Espinosa and coworkers[51] have shown that $V(r_c)$ is a good parameter that reflects the strength of HB's[52] (involving X–H···O HB's, with X = C, N, O). **Fig. IV.9** shows the linear fitting between $\sum V(r_c)$ at all HB's and ΔE_{bond} for all clusters. These results show an excellent linear correlation, as it is evidenced in the value of the correlation coefficient. Therefore, we consider that this methodology is suitable to quantify the contribution of individual interactions to the total ΔE_{bond}. Considering that $\rho(r_c)$ gives an indication of HB strength, a good linear correlation between this property and ΔE_{bond} was also evidenced, with $R^2 = 0.9999$.

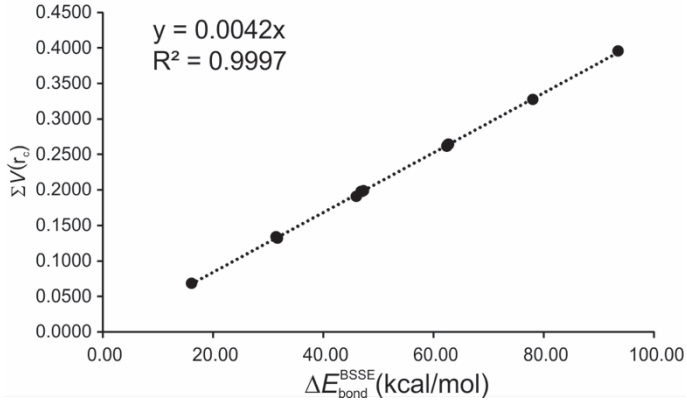

Figure IV.9. Relationship between absolute values of $\sum V(r_c)$ at all HB BCP's and ΔE_{bond}^{BSSE}.

IV.3.4 Molecular Electrostatic Potential Maps

A very useful topographical analysis is the study of the molecular electrostatic potential (MEP). MEP maps allow studying non-covalent interactions, and knowing how the electronic charge is distributed within a complex. The electrostatic behaviors of the M/CA adduct and the isolated molecules were analyzed using this method.

The MEP maps of the CA and M isolated compounds and the corresponding M/CA adduct are shown in **Fig. IV.10**. As it was expected, the most negative electrostatic potentials of CA (**Fig. IV.10a**) lie on the oxygen atoms, associated with its lone pairs. It can also be observed that the central region of the molecule shows a positive electrostatic potential. Concerning M molecule (see **Fig. IV.10b**), since the amino groups have a pyramidal conformation (two up and one down), the molecular plane displays an anisotropic distribution of the electronic charge. Unlike CA, M ring shows a less positive $V(r)$ on the central region, due to the π-electron delocalization on M ring.

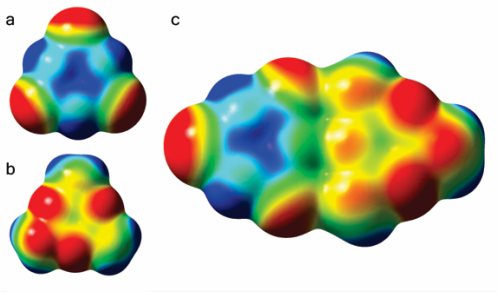

Figure IV.10 Molecular electrostatic potential (MEP) maps of **(a)** CA, **(b)** M, and **(c)** M/CA complex. The values of the MEP vary between −0.027 (red) and +0.044 (blue) au.

When the M/CA adduct is formed, M undergoes a redistribution of the electronic charge. A comparison of **Figs. IV.10b** with **c** shows this fact. As can be seen in **Fig. IV.10c**, all amino groups exhibit a negative region. The $-NH_2$ group that does not interact with CA exhibits a more negative region on one side of the complex, according to the orientation of the nitrogen lone pair. The remaining $-NH_2$ groups display the same $V(r)$ on both sides of the molecular plane. In addition, a look at the contact limit between M and CA shows how the electronic charge is distributed because of the interactions.

Finally, when all $-NH_2$ groups are interacting with at least one CA molecule, they display almost the same charge distribution above and below the molecular plane. This indicates that nitrogen lone pairs delocalized over the entire molecule, and the central region of M takes more positive values.

IV.4 Conclusions

In this chapter, a theoretical study at B3LYP/6-311++G(d,p) level of theory in conjunction with QTAIM and MEP analysis was conducted on a series of melamine-cyanuric acid clusters taken from crystallographic data, in order to characterize the self-assembling interactions and explore the molecular factors that govern the self-assembly process of this system.

The binding energies explain the stability of the different aggregates. The cyclization process is favored over the linear aggregation. In these cyclic motifs, the outer HB's are strengthened, while the inner ones are weakened with respect to the primitive complex, i.e., the M/CA adduct.

The geometrical and topological parameters suggest that the fundamental process of M/CA self-assembly is driven by a hydrogen-bonded network which is governed by a complex combination of cooperative and anticooperative effects. The topological properties at BCP's also give a detailed insight into the strength of intermolecular interactions that conduct the cluster formation. In addition, the N–H···N interaction is far stronger than the N–H···O hydrogen bonds, since the former shows negative values of the total electronic energy density at the BCP, which is associated to a greater stabilization.

It is thought that these findings will serve to complement kinetic and thermodynamic considerations involved in the study of self-assembly systems. Our theoretical results support the experimental finding of a novel M_3/CA (3:1) network, which was found in adsorption experiments, besides the well-known M_3/CA_3 (1:1) hydrogen-bonding network of the co-crystal.

References

(1) Seto, C. T.; Whitesides, G. M. Molecular Self-Assembly through Hydrogen Bonding: Supramolecular Aggregates Based on the Cyanuric Acid-Melamine Lattice. *J. Am. Chem. Soc.* **1993**, *115*, 905–916.

(2) Lindsey, J. S. Self-Assembly in Sinthetic Routes to Molecular Devices. Biological Principles and Chemical Perspectives: A Review. *New J Chem* **1991**, *15*, 153–180.

(3) Lehn, J.-M. Toward Complex Matter: Supramolecular Chemistry and Self-

Organization. *Proc. Natl. Acad. Sci. U. S. A.* **2002**, *99* (8), 4763–4768.

(4) Lehn, J.-M. Supramolecular Chemistry—Scope and Perspectives Molecules, Supermolecules, and Molecular Devices(Nobel Lecture). *Angew. Chemie Int. Ed. English* **1988**, *27* (1), 89–112.

(5) Manzano, B. R.; Jalón, F. A.; Soriano, M. L.; Rodríguez, A. M.; Hoz, A. de la; Sánchez-Migallón, A. Multiple Hydrogen Bonds in the Self-Assembly of Aminotriazine and Glutarimide. Decisive Role of the Triazine Substituents. *Cryst. Growth Des.* **2008**, *8* (5), 1585–1594.

(6) Corradi, E.; Meille, S.; Messina, M.; Metrangolo, P.; Resnati, G. Halogen Bonding versus Hydrogen Bonding in Driving Self-Assembly Processes. *Angew. Chem. Int. Ed. Engl.* **2000**, *39* (10), 1782–1786.

(7) Stupp, S. I.; Palmer, L. C. Supramolecular Chemistry and Self-Assembly in Organic Materials Design. *Chem. Mater.* **2014**, *26*, 507–518.

(8) Choi, I. S.; Li, X.; Simanek, E. E.; Akaba, R.; Whitesides, G. M. Self-Assembly of Hydrogen-Bonded Polymeric Rods Based on the Cyanuric Acid·Melamine Lattice. *Chem. Mater.* **1999**, *11* (3), 684–690.

(9) Kerckhoffs, J. M. C. a; ten Cate, M. G. J.; Mateos-Timoneda, M. a; van Leeuwen, F. W. B.; Snellink-Ruël, B.; Spek, A. L.; Kooijman, H.; Crego-Calama, M.; Reinhoudt, D. N. Selective Self-Organization of Guest Molecules in Self-Assembled Molecular Boxes. *J. Am. Chem. Soc.* **2005**, *127* (36), 12697–12708.

(10) Kimizuka, N.; Kawasaki, T.; Hirata, K.; Kunitake, T. Supramolecular Membranes. Spontaneous Assembly of Aqueous Bilayer Membrane via Formation of Hydrogen Bonded Pairs of Melamine and Cyanuric Acid Derivatives. *J. Am. Chem. Soc.* **1998**, *120*, 4094–4104.

(11) Ma, M.; Gong, Y.; Bong, D. Lipid Membrane Adhesion and Fusion Driven by Designed, Minimally Multivalent Hydrogen-Bonding Lipids. *J. Am. Chem. Soc.* **2009**, *131*, 16919–16926.

(12) Yagai, S.; Nakajima, T.; Karatsu, T.; Saitow, K.; Kitamura, A. Phototriggered Self-Assembly of Hydrogen-Bonded Rosette. *J. Am. Chem. Soc.* **2004**, *126* (37), 11500–11508.

(13) Wang, Y.; Wei, B.; Wang, Q. Crystal Structure of Melamine Cyanuric Acid Complex (1:1) Trihydrochloride, MCA·3HCl. *J. Crystallogr. Spectrosc. Res.* **1990**, *20* (1), 79–84.

(14) Ranganathan, A.; Pedireddi, V. R.; Rao, C. N. R. Hydrothermal Synthesis of Organic Channel Structures: 1:1 Hydrogen-Bonded Adducts of Melamine with Cyanuric and Trithiocyanuric Acids. *J. Am. Chem. Soc.* **1999**, *121* (8), 1752–1753.

(15) Prior, T. J.; Armstrong, J. A.; Benoit, D. M.; Marshall, K. L. The Structure of the Melamine–cyanuric Acid Co-Crystal. *CrystEngComm* **2013**, *15* (29), 5838.

(16) Seto, C. T.; Whitesides, G. M. Self-Assembly Based on the Cyanuric Acid-Melamine Lattice. *J. Am. Chem. Soc.* **1990**, *112* (17), 6409–6411.

(17) Zerkowski, J. A.; Seto, C. T.; Whitesides, G. M. Solid-State Structures of Rosette and Crinkled Tape Motifs Derived from the Cyanuric Acid Melamine Lattice. *J. Am. Chem. Soc.* **1992**, *114* (13), 5473–5475.

(18) Seto, C. T.; Whitesides, G. M. Synthesis, Characterization, and Thermodynamic Analysis of a 1 + 1 Self-Assembling Structure Based on the Cyanuric Acid·melamine Lattice. *J. Am. Chem. Soc.* **1993**, *115* (4), 1330–1340.

(19) Chin, D. N.; Gordon, D. M.; Whitesides, G. M. Computational Simulations of Supramolecular Hydrogen-Bonded Aggregates: HubM3, FlexM3, and Adamantane-Based Hubs in Chloroform. *J. Am. Chem. Soc.* **1994**, *116* (26), 12033–12044.

(20) Bielejewska, A. G.; Marjo, C. E.; Prins, L. J.; Timmerman, P.; Jong, F. De; Reinhoudt, D. N. Thermodynamic Stabilities of Linear and Crinkled Tapes and Cyclic Rosettes in Melamine - Cyanurate Assemblies: A Model Description. *J. Am. Chem. Soc.* **2001**, *123*, 7518–7533.

(21) Xu, W.; Dong, M.; Gersen, H.; Rauls, E.; Vázquez-Campos, S.; Crego-Calama, M.; Reinhoudt, D. N.; Stensgaard, I.; Laegsgaard, E.; Linderoth, T. R.; et al. Cyanuric Acid and Melamine on Au111: Structure and Energetics of Hydrogen-Bonded Networks. *Small* **2007**, *3* (5), 854–858.

(22) Ma, M.; Bong, D. Determinants of Cyanuric Acid and Melamine Assembly in Water. *Langmuir* **2011**, *27* (14), 8841–8853.

(23) Frisch, M. J.; Trucks, G. W.; Schlegel, H. B.; Scuseria, G. E.; Robb, M. A.; Cheeseman, J. R.; Montgomery, J. A. J.; Vreven, T.; Kudin, K. N.; Burant, J. C.; et al. Gaussian 03, Revision D.01. Gaussian, Inc.: Wallingford, CT 2004.

(24) Dey, R.; Bhattacharya, B.; Mondal, P.; Mondal, R.; Ghoshal, D. Fabrication of Two Supramolecular Self-Assemblies of Mn(II)-Dicarboxylates with Trans-4,4′-Azobispyridine: Analysis of H-Bonding Interactions with Hirshfeld Surfaces and DFT Calculations. *J. Mol. Struct.* **2014**, *1067*, 64–73.

(25) Scheiner, S. Dissection of the Factors Affecting Formation of a CH···O H-Bond. A Case Study. *Crystals* **2015**, *5* (3), 327–345.

(26) Duarte, D. J. R.; Sosa, G. L.; Peruchena, N. M. Nature of Halogen Bonding. A Study Based on the Topological Analysis of the Laplacian of the Electron Charge Density and an Energy Decomposition Analysis. *J. Mol. Model.* **2013**, *19* (5), 2035–2041.

(27) Kirsch, P.; Tong, Q.; Untenecker, H. Crystal Design Using Multipolar Electrostatic

Interactions: A Concept Study for Organic Electronics. *Beilstein J. Org. Chem.* **2013**, *9* (1), 2367–2373.

(28) Angelina, E. L.; Andujar, S. A.; Tosso, R. D.; Enriz, R. D.; Peruchena, N. M. Non-Covalent Interactions in Receptor-Ligand Complexes. A Study Based on the Electron Charge Density. *J. Phys. Org. Chem.* **2014**, *27* (2), 128–134.

(29) Elango, M.; Subramanian, V.; Sathyamurthy, N. The Self-Assembly of Metaboric Acid Molecules into Bowls, Balls and Sheets. *J. Phys. Chem. A* **2008**, *112* (35), 8107–8115.

(30) Kannappan, K.; Werblowsky, T. L.; Rim, K. T.; Berne, B. J.; Flynn, G. W. An Experimental and Theoretical Study of the Formation of Nanostructures of Self-Assembled Cyanuric Acid through Hydrogen Bond Networks on Graphite. *J. Phys. Chem. B* **2007**, *111*, 6634–6642.

(31) Boys, S. F.; Bernardi, F. The Calculation of Small Molecular Interactions by the Differences of Separate Total Energies. Some Procedures with Reduced Errors. *Mol. Phys.* **1970**, *19*, 553–559.

(32) Chai, J.-D.; Head-Gordon, M. Long-Range Corrected Hybrid Density Functionals with Damped Atom-Atom Dispersion Corrections. *Phys. Chem. Chem. Phys.* **2008**, *10*, 6615–6620.

(33) Bader, R. F. W. *Atoms in Molecules: A Quantum Theory*; Clarendon Press: Oxford, 1994.

(34) AIMAll Version 12.06.03, Todd A. Keith, TK Gristmill Software, Overland Park KS, USA, 2012 Aim.tkgristmill.com.

(35) Bader, R. F. W.; Caroll, M. T.; Cheeseman, J. R.; Chang, C. Properties of Atoms in Molecules: Atomic Volumes. *J. Am. Chem. Soc.* **1987**, *109*, 7968–7979.

(36) Wang, Y.-L.; Mebel, A. M.; Wu, C.-J.; Chen, Y.-T.; Lin, C.-E.; Jiang, J.-C. IR Spectroscopy and Theoretical Vibrational Calculation of the Melamine Molecule. *J. Chem. Soc. Faraday Trans.* **1997**, *93* (19), 3445–3451.

(37) Drozd, M.; Marchewka, M. K. The Structure, Vibrational Spectra and Nonlinear Optical Properties of Neutral Melamine and Singly, Doubly and Triply Protonated Melaminium Cations—theoretical Studies. *J. Mol. Struct. THEOCHEM* **2005**, *716* (1–3), 175–192.

(38) Li, Z.; Chen, G.; Xu, Y.; Wang, X.; Wang, Z. Study of the Structural and the Spectral Characteristics of $[C_3N_3(NH_2)_3]_n$ (N =1-4) Clusters. *J. Phys. Chem. A* **2013**, *117*, 12511–12518.

(39) Bondi, A. Van Der Waals Volumes and Radii. *J. Phys. Chem.* **1964**, *68*, 441–451.

(40) Lee, H. M.; Singh, N. J.; Kim, K. S. Weak to Strong Hydrogen Bond. In *Hydrogen*

Bonding—New Insights; Grabowski, S., Ed.; Springer: Netherlands, 2006; pp 149–192.

(41) Karpfen, A. Cooperative Effects in Hydrogen Bonding. In *Advances in Chemical Physics*; John Wiley & Sons, Inc., 2003; pp 469–510.

(42) Bader, R. F. W.; Beddall, P. M. Virial Field Relationship for Molecular Charge Distributions and the Spatial Partitioning of Molecular Properties. *J. Chem. Phys.* **1972**, *56* (7), 3320.

(43) Ramírez, F.; Hadad, C. Z.; Guerra, D.; David, J.; Restrepo, A. Structural Studies of the Water Pentamer. *Chem. Phys. Lett.* **2011**, *507* (4–6), 229–233.

(44) Koch, U.; Popelier, P. L. A. Characterization of C-H-O Hydrogen Bonds on the Basis of the Charge Density. *J. Phys. Chem.* **1995**, *99* (24), 9747–9754.

(45) Vallejos, M. M.; Peruchena, N. M. Preferential Formation of the Different Hydrogen Bonds and Their Effects in Tetrahydrofuran and Tetrahydropyran Microhydrated Complexes. *J. Phys. Chem. A* **2012**, *116* (16), 4199–4210.

(46) Angelina, E. L.; Peruchena, N. M. Strength and Nature of Hydrogen Bonding Interactions in Mono- and Di-Hydrated Formamide Complexes. *J. Phys. Chem. A* **2011**, *115* (18), 4701–4710.

(47) Popelier, P. L. A. Characterization of a Dihydrogen Bond on the Basis of the Electron Density. *J. Phys. Chem. A* **1998**, *102*, 1873–1878.

(48) Angelina, E. L.; Duarte, D. J. R.; Peruchena, N. M. Is the Decrease of the Total Electron Energy Density a Covalence Indicator in Hydrogen and Halogen Bonds? *J. Mol. Model.* **2013**, *19* (5), 2097–2106.

(49) Duarte, D. J. R.; Angelina, E. L.; Peruchena, N. M. Physical Meaning of the QTAIM Topological Parameters in Hydrogen Bonding. *J. Mol. Model.* **2014**, *20* (11), 2510.

(50) Cremer, D.; Kraka, E. Chemical Bonds without Bonding Electron Density? Does the Difference Electron-Density Analysis Suffice for a Description of the Chemical Bond? *Angew. Chemie Int. Ed. English* **1984**, *23* (8), 627–628.

(51) Espinosa, E.; Molins, E.; Lecomte, C. Hydrogen Bond Strengths Revealed by Topological Analyses of Experimentally Observed Electron Densities. *Chem. Phys. Lett.* **1998**, *285*, 170–173.

(52) Ofori, A.; Suvanto, S.; Jääskeläinen, S.; Koskinen, L.; Koshevoy, I. O.; Hirva, P. Versatile Coordination Modes in Silver-Imidazolecarbaldehyde Oxime Complexes: Structural and Computational Analysis. *Cryst. Growth. & Des.* **2016**, *16* (1), 255–264.

Supplementary Material

Table S1. Selected Geometric Parameters of complex **I** to **XIII** calculated at B3LYP/6–311++G(d,p) level. Distances (*d*) are in angstroms and angles (∠) are in degrees.

Complex	D–H···A	*d* (H···A)	Δd_{VdW} (N···X)	*d* (D–H)	Δ*d* (D–H)	∠ (D–H···A)	*d* (D···A)
M/CA	N–H···N	1.7976	0.9524	1.0587	0.0475	179.99	2.8563
	N–H···O	1.9702	0.7498	1.0134	0.0077	174.86	2.9836
	N–H···O	1.9702	0.7498	1.0134	0.0077	174.85	2.9836
M_2/CA	N–H···N	1.8106	0.9394	1.0566	0.0455	179.16	2.8673
	N–H···O	1.9658	0.7543	1.0135	0.0079	174.78	2.9793
	N–H···O	1.9770	0.7430	1.0132	0.0076	175.45	2.9902
	N–H···N	1.8093	0.9407	1.0568	0.0457	179.15	2.8661
	N–H···O	1.9670	0.7530	1.0136	0.0080	175.37	2.9806
	N–H···O	1.9767	0.7434	1.0132	0.0076	174.77	2.9899
M/CA_2	N–H···N	1.8168	0.9332	1.0557	0.0446	179.98	2.8725
	N–H···O	1.9606	0.7594	1.0135	0.0079	175.69	2.9741
	N–H···O	1.9839	0.7361	1.0137	0.0081	177.49	2.9977
	N–H···N	1.8171	0.9329	1.0556	0.0445	179.96	2.8727
	N–H···O	1.9607	0.7593	1.0135	0.0079	175.69	2.9743
	N–H···O	1.9842	0.7358	1.0137	0.0081	177.50	2.9979
M_3/CA	N–H···N	1.8210	0.9290	1.0552	0.0441	179.95	2.8762
	N–H···O	1.9724	0.7476	1.0134	0.0077	175.35	2.9858
	N–H···O	1.9710	0.7490	1.0133	0.0077	175.32	2.9844
	N–H···N	1.8218	0.9282	1.0551	0.0440	179.86	2.8769
	N–H···O	1.9707	0.7493	1.0133	0.0077	175.35	2.9840
	N–H···O	1.9710	0.7490	1.0134	0.0077	175.44	2.9843
	N–H···N	1.8225	0.9275	1.0551	0.0439	179.79	2.8776
	N–H···O	1.9713	0.7487	1.0133	0.0077	175.44	2.9846
	N–H···O	1.9709	0.7491	1.0133	0.0076	175.41	2.9842
M/CA_3	N–H···N	1.8373	0.9128	1.0529	0.0417	179.98	2.8901
	N–H···O	1.9731	0.7469	1.0139	0.0082	178.61	2.9870
	N–H···O	1.9744	0.7456	1.0138	0.0082	178.54	2.9882
	N–H···N	1.8373	0.9127	1.0528	0.0417	179.98	2.8901
	N–H···O	1.9738	0.7462	1.0139	0.0082	178.50	2.9877
	N–H···O	1.9740	0.7460	1.0139	0.0082	178.53	2.9879
	N–H···N	1.8373	0.9127	1.0528	0.0417	179.96	2.8902
	N–H···O	1.9741	0.7459	1.0138	0.0082	178.51	2.9879

	N–H···O	1.9740	0.7460	1.0139	0.0082	178.61	2.9879
M_2/CA_2	N–H···N	1.8069	0.9431	1.0575	0.0464	179.30	2.8645
	N–H···O	1.9730	0.7470	1.0131	0.0074	175.19	2.9861
	N–H···O	1.9685	0.7515	1.0134	0.0078	174.85	2.9819
	N–H···N	1.8271	0.9229	1.0540	0.0428	179.17	2.8811
	N–H···O	1.9780	0.7420	1.0134	0.0078	177.52	2.9914
	N–H···O	1.9607	0.7593	1.0139	0.0083	175.55	2.9747
	N–H···N	1.8150	0.9350	1.0561	0.0450	179.70	2.8712
	N–H···O	1.9797	0.7403	1.0133	0.0077	177.03	2.9930
	N–H···O	1.9653	0.7547	1.0136	0.0080	175.35	2.9789
M_2/CA_2 linear	N–H···N	1.8164	0.9336	1.0557	0.0446	179.80	2.8721
	N–H···O	1.9604	0.7596	1.0138	0.0081	175.66	2.9742
	N–H···O	1.9840	0.7361	1.0135	0.0079	177.47	2.9974
	N–H···N	1.8289	0.9211	1.0539	0.0428	179.13	2.8828
	N–H···O	1.9780	0.7421	1.0138	0.0081	177.45	2.9917
	N–H···O	1.9664	0.7536	1.0135	0.0079	176.29	2.9800
	N–H···N	1.8098	0.9402	1.0569	0.0457	179.05	2.8667
	N–H···O	1.9770	0.7430	1.0131	0.0074	175.41	2.9900
	N–H···O	1.9650	0.7551	1.0136	0.0079	174.83	2.9785
M_3/CA_2	N–H···N	1.8071	0.9429	1.0572	0.0461	179.13	2.8643
	N–H···O	1.9764	0.7436	1.0133	0.0076	175.36	2.9896
	N–H···O	1.9630	0.7570	1.0135	0.0079	174.76	2.9765
	N–H···N	1.8296	0.9204	1.0541	0.0430	178.99	2.8837
	N–H···O	2.0017	0.7183	1.0132	0.0075	177.75	3.0149
	N–H···O	1.9487	0.7713	1.0139	0.0083	175.73	2.9626
	N–H···N	1.8296	0.9204	1.0541	0.0430	178.99	2.8837
	N–H···O	2.0017	0.7183	1.0132	0.0075	177.75	3.0149
	N–H···O	1.9487	0.7713	1.0139	0.0083	175.73	2.9626
	N–H···N	1.8071	0.9429	1.0572	0.0461	179.14	2.8643
	N–H···O	1.9764	0.7436	1.0133	0.0076	175.36	2.9896
	N–H···O	1.9630	0.7570	1.0135	0.0079	174.76	2.9765
M_2/CA_3	N–H···N	1.8135	0.9365	1.0562	0.0450	179.99	2.8696
	N–H···O	1.9828	0.7372	1.0136	0.0080	177.22	2.9964
	N–H···O	1.9591	0.7609	1.0137	0.0081	175.68	2.9728
	N–H···N	1.8274	0.9226	1.0544	0.0433	179.09	2.8818
	N–H···O	1.9962	0.7238	1.0133	0.0076	177.87	3.0094
	N–H···O	1.9516	0.7684	1.0139	0.0082	175.67	2.9655
	N–H···N	1.8274	0.9226	1.0544	0.0433	179.09	2.8818
	N–H···O	1.9961	0.7239	1.0133	0.0076	177.87	3.0093
	N–H···O	1.9518	0.7682	1.0139	0.0082	175.67	2.9657
	N–H···N	1.8136	0.9364	1.0561	0.0450	179.97	2.8697

	N–H···O	1.9830	0.7370	1.0136	0.0079	177.20	2.9966
	N–H···O	1.9590	0.7610	1.0137	0.0081	175.68	2.9728
M_3/CA_2 linear	N–H···N	1.8096	0.9404	1.0569	0.0457	179.16	2.8665
	N–H···O	1.9656	0.7544	1.0136	0.0079	174.78	2.9792
	N–H···O	1.9656	0.7544	1.0131	0.0074	175.37	2.9787
	N–H···N	1.8292	0.9208	1.0539	0.0427	179.15	2.8831
	N–H···O	1.9663	0.7537	1.0136	0.0079	176.27	2.9798
	N–H···O	1.9784	0.7416	1.0137	0.0081	177.40	2.9921
	N–H···N	1.8292	0.9208	1.0539	0.0427	179.15	2.8831
	N–H···O	1.9784	0.7416	1.0137	0.0081	177.40	2.9921
	N–H···O	1.9663	0.7537	1.0136	0.0079	176.27	2.9798
	N–H···N	1.8096	0.9404	1.0569	0.0457	179.16	2.8665
	N–H···O	1.9778	0.7423	1.0131	0.0074	175.37	2.9908
	N–H···O	1.9656	0.7544	1.0136	0.0079	174.78	2.9792
M_2/CA_3 linear	N–H···N	1.8172	0.9328	1.0556	0.0445	179.97	2.8728
	N–H···O	1.9605	0.7595	1.0138	0.0081	175.69	2.9742
	N–H···O	1.9846	0.7354	1.0135	0.0079	177.44	2.9981
	N–H···N	1.8289	0.9211	1.0540	0.0429	179.16	2.8829
	N–H···O	1.9769	0.7431	1.0137	0.0081	177.47	2.9906
	N–H···O	1.9674	0.7526	1.0135	0.0078	176.25	2.9809
	N–H···N	1.8289	0.9211	1.0540	0.0429	179.16	2.8829
	N–H···O	1.9674	0.7526	1.0135	0.0078	176.25	2.9809
	N–H···O	1.9769	0.7431	1.0137	0.0081	177.47	2.9906
	N–H···N	1.8172	0.9328	1.0556	0.0445	179.97	2.8728
	N–H···O	1.9846	0.7354	1.0135	0.0079	177.44	2.9981
	N–H···O	1.9605	0.7595	1.0138	0.0081	175.69	2.9742
M_3/CA_3	N–H···N	1.8190	0.9310	1.0551	0.0439	179.80	2.8741
	N–H···O	1.9515	0.7685	1.0139	0.0083	177.95	2.9654
	N–H···O	1.9717	0.7483	1.0149	0.0093	175.75	2.9867
	N–H···N	1.8216	0.9284	1.0552	0.0440	179.44	2.8768
	N–H···O	1.9596	0.7604	1.0139	0.0083	178.07	2.9736
	N–H···O	1.9694	0.7506	1.0150	0.0093	175.56	2.9843
	N–H···N	1.8260	0.9240	1.0552	0.0441	179.90	2.8811
	N–H···O	1.9500	0.7700	1.0139	0.0083	178.31	2.9639
	N–H···O	1.9904	0.7296	1.0142	0.0086	175.53	3.0046
	N–H···N	1.8233	0.9267	1.0545	0.0434	179.72	2.8778
	N–H···O	1.9512	0.7688	1.0141	0.0085	178.35	2.9653
	N–H···O	1.9809	0.7391	1.0140	0.0083	175.51	2.9949
	N–H···N	1.8260	0.9240	1.0545	0.0434	179.47	2.8805
	N–H···O	1.9589	0.7611	1.0141	0.0085	178.42	2.9731
	N–H···O	1.9787	0.7413	1.0140	0.0083	175.39	2.9926
	N–H···N	1.8293	0.9207	1.0552	0.0441	179.66	2.8845

	N–H···O	1.9580	0.7620	1.0139	0.0083	178.44	2.9719
	N–H···O	1.9888	0.7312	1.0142	0.0086	175.41	3.0030
M_3/CA_3 linear	N–H···N	1.8175	0.9325	1.0555	0.0444	179.69	2.8730
	N–H···O	1.9609	0.7591	1.0138	0.0081	175.72	2.9747
	N–H···O	1.9845	0.7356	1.0135	0.0079	177.40	2.9980
	N–H···N	1.8280	0.9221	1.0540	0.0429	179.16	2.8820
	N–H···O	1.9776	0.7424	1.0138	0.0081	177.42	2.9913
	N–H···O	1.9685	0.7515	1.0135	0.0079	176.19	2.9820
	N–H···N	1.8291	0.9209	1.0540	0.0429	178.83	2.8831
	N–H···O	1.9672	0.7528	1.0135	0.0078	176.31	2.9807
	N–H···O	1.9779	0.7422	1.0137	0.0081	177.20	2.9915
	N–H···N	1.8287	0.9213	1.0538	0.0427	179.16	2.8825
	N–H···O	1.9786	0.7414	1.0137	0.0081	177.38	2.9923
	N–H···O	1.9675	0.7525	1.0136	0.0080	176.19	2.9811
	N–H···N	1.8100	0.9400	1.0569	0.0457	178.98	2.8669
	N–H···O	1.9781	0.7419	1.0131	0.0074	175.44	2.9911
	N–H···O	1.9649	0.7551	1.0136	0.0079	174.78	2.9784

Table S2. Local Properties at D–X···A bond critical points in M_n/CA_m complexes.

Complex	Interaction	$\rho(r_c)$	$\nabla^2\rho(r_c)$	$V(r_c)$	$G(r_c)$	$H(r_c)$
M/CA	N–H···O	0.0231	0.0859	-0.0165	0.0190	0.0025
	N–H···O	0.0231	0.0859	-0.0165	0.0190	0.0025
	N–H···N	0.0441	0.0900	-0.0353	0.0289	-0.0064
M_2/CA	N–H···O	0.0229	0.0849	-0.0164	0.0188	0.0024
	N–H···O	0.0229	0.0850	-0.0165	0.0189	0.0024
	N–H···O	0.0233	0.0865	-0.0167	0.0192	0.0025
	N–H···O	0.0233	0.0868	-0.0168	0.0192	0.0025
	N–H···N	0.0428	0.0895	-0.0338	0.0281	-0.0057
	N–H···N	0.0429	0.0896	-0.0339	0.0282	-0.0058
M/CA_2	N–H···O	0.0224	0.0831	-0.0158	0.0183	0.0025
	N–H···O	0.0224	0.0832	-0.0158	0.0183	0.0025
	N–H···O	0.0236	0.0876	-0.0170	0.0195	0.0024
	N–H···O	0.0237	0.0876	-0.0171	0.0195	0.0024
	N–H···N	0.0421	0.0893	-0.0330	0.0277	-0.0053
	N–H···N	0.0421	0.0893	-0.0330	0.0277	-0.0054
M_3/CA	N–H···O	0.0231	0.0859	-0.0167	0.0191	0.0024
	N–H···O	0.0232	0.0861	-0.0167	0.0191	0.0024
	N–H···O	0.0232	0.0861	-0.0168	0.0191	0.0024
	N–H···O	0.0232	0.0861	-0.0168	0.0191	0.0024
	N–H···O	0.0232	0.0861	-0.0168	0.0191	0.0024

	N–H···O	0.0232	0.0862	-0.0168	0.0192	0.0024
	N–H···N	0.0416	0.0889	-0.0324	0.0273	-0.0051
	N–H···N	0.0417	0.0890	-0.0325	0.0274	-0.0051
	N–H···N	0.0417	0.0890	-0.0326	0.0274	-0.0052
M/CA_3	N–H···O	0.0230	0.0849	-0.0164	0.0188	0.0024
	N–H···O	0.0230	0.0850	-0.0164	0.0188	0.0024
	N–H···O	0.0230	0.0850	-0.0164	0.0188	0.0024
	N–H···O	0.0230	0.0850	-0.0164	0.0188	0.0024
	N–H···O	0.0230	0.0850	-0.0164	0.0188	0.0024
	N–H···O	0.0230	0.0852	-0.0164	0.0189	0.0024
	N–H···N	0.0401	0.0883	-0.0308	0.0264	-0.0044
	N–H···N	0.0402	0.0883	-0.0308	0.0264	-0.0044
	N–H···N	0.0402	0.0883	-0.0308	0.0264	-0.0044
M_2CA_2	N–H···O	0.0227	0.0840	-0.0161	0.0186	0.0024
	N–H···O	0.0229	0.0847	-0.0164	0.0188	0.0024
	N–H···O	0.0231	0.0858	-0.0166	0.0190	0.0024
	N–H···O	0.0232	0.0862	-0.0166	0.0191	0.0025
	N–H···O	0.0234	0.0867	-0.0168	0.0192	0.0024
	N–H···O	0.0236	0.0876	-0.0170	0.0195	0.0024
	N–H···N	0.0411	0.0889	-0.0319	0.0271	-0.0048
	N–H···N	0.0423	0.0893	-0.0332	0.0278	-0.0055
	N–H···N	0.0432	0.0895	-0.0342	0.0283	-0.0059
M_2CA_2 linear	N–H···O	0.0224	0.0832	-0.0159	0.0183	0.0025
	N–H···O	0.0227	0.0843	-0.0162	0.0186	0.0025
	N–H···O	0.0229	0.0850	-0.0164	0.0188	0.0024
	N–H···O	0.0234	0.0870	-0.0168	0.0193	0.0025
	N–H···O	0.0235	0.0868	-0.0170	0.0194	0.0024
	N–H···O	0.0237	0.0877	-0.0171	0.0195	0.0024
	N–H···N	0.0409	0.0888	-0.0317	0.0270	-0.0048
	N–H···N	0.0422	0.0894	-0.0331	0.0277	-0.0054
	N–H···N	0.0429	0.0895	-0.0339	0.0281	-0.0057
M_3/CA_2	N–H···O	0.0001	0.0006	0.0000	0.0001	0.0001
	N–H···O	0.0217	0.0801	-0.0152	0.0176	0.0024
	N–H···O	0.0217	0.0801	-0.0152	0.0176	0.0024
	N–H···O	0.0229	0.0850	-0.0165	0.0189	0.0024
	N–H···O	0.0229	0.0850	-0.0165	0.0189	0.0024
	N–H···O	0.0235	0.0874	-0.0169	0.0194	0.0025
	N–H···O	0.0235	0.0874	-0.0169	0.0194	0.0025
	N–H···O	0.0243	0.0901	-0.0177	0.0201	0.0024
	N–H···O	0.0243	0.0901	-0.0177	0.0201	0.0024
	N–H···N	0.0409	0.0886	-0.0316	0.0269	-0.0047

	N–H···N	0.0409	0.0886	-0.0316	0.0269	-0.0047
	N–H···N	0.0432	0.0896	-0.0342	0.0283	-0.0059
	N–H···N	0.0432	0.0896	-0.0342	0.0283	-0.0059
M_2/CA_3	N–H···O	0.0000	0.0001	0.0000	0.0000	0.0000
	N–H···O	0.0219	0.0812	-0.0155	0.0179	0.0024
	N–H···O	0.0220	0.0812	-0.0155	0.0179	0.0024
	N–H···O	0.0225	0.0833	-0.0159	0.0184	0.0025
	N–H···O	0.0225	0.0834	-0.0159	0.0184	0.0025
	N–H···O	0.0237	0.0879	-0.0171	0.0196	0.0024
	N–H···O	0.0237	0.0880	-0.0172	0.0196	0.0024
	N–H···O	0.0241	0.0895	-0.0176	0.0200	0.0024
	N–H···O	0.0241	0.0895	-0.0176	0.0200	0.0024
	N–H···N	0.0411	0.0887	-0.0319	0.0270	-0.0048
	N–H···N	0.0411	0.0887	-0.0319	0.0270	-0.0048
	N–H···N	0.0425	0.0895	-0.0334	0.0279	-0.0055
	N–H···N	0.0425	0.0895	-0.0334	0.0279	-0.0055
M_3/CA_2 linear	N–H···O	0.0227	0.0843	-0.0161	0.0186	0.0025
	N–H···O	0.0227	0.0843	-0.0161	0.0186	0.0025
	N–H···O	0.0229	0.0848	-0.0164	0.0188	0.0024
	N–H···O	0.0229	0.0848	-0.0164	0.0188	0.0024
	N–H···O	0.0233	0.0868	-0.0168	0.0192	0.0025
	N–H···O	0.0233	0.0868	-0.0168	0.0192	0.0025
	N–H···O	0.0235	0.0869	-0.0170	0.0194	0.0023
	N–H···O	0.0235	0.0869	-0.0170	0.0194	0.0023
	N–H···N	0.0409	0.0888	-0.0317	0.0269	-0.0047
	N–H···N	0.0409	0.0888	-0.0317	0.0269	-0.0047
	N–H···N	0.0429	0.0895	-0.0339	0.0281	-0.0058
	N–H···N	0.0429	0.0895	-0.0339	0.0281	-0.0058
M_2/CA_3 linear	N–H···O	0.0224	0.0830	-0.0158	0.0183	0.0025
	N–H···O	0.0224	0.0830	-0.0158	0.0183	0.0025
	N–H···O	0.0228	0.0846	-0.0162	0.0187	0.0025
	N–H···O	0.0228	0.0846	-0.0162	0.0187	0.0025
	N–H···O	0.0234	0.0867	-0.0170	0.0193	0.0024
	N–H···O	0.0234	0.0867	-0.0170	0.0193	0.0024
	N–H···O	0.0237	0.0876	-0.0171	0.0195	0.0024
	N–H···O	0.0237	0.0876	-0.0171	0.0195	0.0024
	N–H···N	0.0410	0.0887	-0.0317	0.0269	-0.0048
	N–H···N	0.0410	0.0887	-0.0317	0.0269	-0.0048
	N–H···N	0.0421	0.0893	-0.0330	0.0277	-0.0053
	N–H···N	0.0421	0.0893	-0.0330	0.0277	-0.0053
M_3/CA_3	N–H···O	0.0221	0.0816	-0.0155	0.0179	0.0024
	N–H···O	0.0222	0.0819	-0.0156	0.0180	0.0025

	N–H···O	0.0226	0.0835	-0.0160	0.0184	0.0024
	N–H···O	0.0227	0.0840	-0.0161	0.0185	0.0025
	N–H···O	0.0231	0.0852	-0.0164	0.0189	0.0024
	N–H···O	0.0232	0.0857	-0.0166	0.0190	0.0024
	N–H···O	0.0239	0.0886	-0.0174	0.0198	0.0024
	N–H···O	0.0239	0.0887	-0.0175	0.0198	0.0024
	N–H···O	0.0239	0.0889	-0.0175	0.0199	0.0024
	N–H···O	0.0243	0.0903	-0.0179	0.0202	0.0023
	N–H···O	0.0243	0.0904	-0.0179	0.0203	0.0023
	N–H···O	0.0244	0.0906	-0.0180	0.0203	0.0023
	N–H···N	0.0409	0.0883	-0.0316	0.0269	-0.0048
	N–H···N	0.0413	0.0888	-0.0320	0.0271	-0.0049
	N–H···N	0.0413	0.0886	-0.0320	0.0271	-0.0049
	N–H···N	0.0415	0.0890	-0.0323	0.0273	-0.0050
	N–H···N	0.0417	0.0890	-0.0325	0.0274	-0.0051
	N–H···N	0.0419	0.0893	-0.0328	0.0276	-0.0052
M_3/CA_3 linear	N–H···O	0.0224	0.0831	-0.0158	0.0183	0.0025
	N–H···O	0.0227	0.0842	-0.0161	0.0186	0.0025
	N–H···O	0.0227	0.0844	-0.0162	0.0186	0.0025
	N–H···O	0.0227	0.0844	-0.0162	0.0186	0.0025
	N–H···O	0.0229	0.0847	-0.0164	0.0188	0.0024
	N–H···O	0.0234	0.0870	-0.0168	0.0193	0.0025
	N–H···O	0.0234	0.0865	-0.0169	0.0193	0.0024
	N–H···O	0.0234	0.0866	-0.0170	0.0193	0.0024
	N–H···O	0.0235	0.0867	-0.0170	0.0193	0.0024
	N–H···O	0.0236	0.0875	-0.0170	0.0195	0.0024
	N–H···N	0.0409	0.0887	-0.0317	0.0269	-0.0048
	N–H···N	0.0410	0.0888	-0.0317	0.0270	-0.0048
	N–H···N	0.0410	0.0888	-0.0318	0.0270	-0.0048
	N–H···N	0.0421	0.0893	-0.0330	0.0277	-0.0053
	N–H···N	0.0429	0.0895	-0.0338	0.0281	-0.0057

V. COOPERATIVITY IN CYANURIC ACID SUPRAMOLECULES: FROM DIMERS TO ROSETTE LIKE MOTIFS

"Chemists are still fascinated by hydrogen bonding interactions almost 100 years after Latimer and Rodebush first proposed the now classic concept. (...)"

Scott Cockroft.

Part of this chapter previously appeared as:

Petelski, Andre N.; Peruchena, Nélida M.; Pamies, Silvana C.; Sosa, Gladis L. Sosa. Insights into the self-assembly steps of Cyanuric Acid toward rosette motifs. A DFT Study. *J. Mol. Mod.,* **2016**, *23*, 263 (Topical Collection QUITEL 2016).

V.1. Introduction

The chemistry of non-covalent interactions, or supramolecular chemistry, is of enormous interest in material science research, in crystal engineering as well as in nanochemistry. It is accepted that this field constitutes a promising way to technological applications, covering areas of supramolecular polymers, smart materials and molecular devices.[1] Much of the exploration in this field involves the use of 1,3,5-triazinane-2,4,6-trione or cyanuric acid (CA). This triazine-derivative has been most commonly known for their uses in swimming pools as a stabilizer,[2,3] since it combines with the free available chlorine to form trichloroisocyanuric acid, which acts as a sanitizer and is more stable against UV rays than free chlorine. Furthermore, due to its high structural similarity with RNA and DNA base pairs, such as uracil and thymine respectively, CA has also become an excellent candidate to be used in the research of supramolecular assemblies, with potential applications in the field of biology[4,5] and materials science.[6,7]

It is known that CA can occur as two tautomer forms: the imidate-like triazine-triol and the amide-like tautomer (See **Figs. V.1a,b**), which is more stable than the former.[8–10] Its singular features are due to their three hydrogen bond (H-Bond) donor and three acceptor sites with the ability to form nine H-Bonds at the same time e. g. with Melamine (M),[11] and six H-Bond with itself.[12,13] In the field of crystalline materials and crystal engineering, there has been a marked research of CA co-

crystals with a great variety of compounds like M,[14,15] 4,4'-bipyridyl,[16] dimethylsulfoxide, dimethylamine and dimethilformamide,[17] and some phenantrolines.[18] One of the co-founder of the bases of supramolecular chemistry and co-workers: Jean-Marie Lehn, et al.[19] have synthetized a supramolecular helical structure based on a linear oligo-isophtalamide strand using CA as a template that directs the assembly process of the helix. Therefore, it is worthwhile to go on in this direction, since this topic still triggers a great scientific activity for the development of new materials.

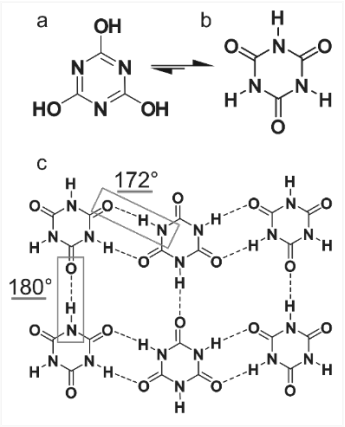

Figure V.1 (a) Structure of 1,3,5-triazine-2,4,6-triol, **(b)** Structure of 1,3,5-triazinane-2,4,6-trione, **(c)** H-Bond Pattern of the CA crystal structure.[12]

The crystal structure of pure CA has been well studied since its resolution.[12] In the 3D structure the molecules are arranged by N−H···O H-Bonds having two geometrical features, that is, N−H···O bond angles of 180° and 172.4°[12] (See **Fig. V.1c**). Besides, if water is used as a crystallization solvent the CA hydrate is obtained,[20] in which water molecules are placed coplanar with CA by interacting with three units via N−H···O (water as acceptor) and O−H···O (water as donor) H-Bonds. The water molecules disrupt those N−H···O H-Bonds of 172.4° between CA units, and just those ones of 180° remain. However, unlike the pure crystal, in the crystal hydrate the CA molecules are placed in the same position whereas in the dehydrated one, the molecules are inverted relative to one another (See **Fig. V.1c**). Furthermore, Flynn et al.[13] have successfully obtained CA self-assembled monolayers on graphite. In this study, they have shown the coexistence of three new

H-Bond patterns beside the well-known arrangement of the 3D crystal structure. This behavior is partially explained by two energetic components: the electrostatic and the Lennard-Jones energy. They also suggest that the three domains are metastable configurations. However, the nucleation process that originates these domains and their coexistence is not fully understood. Hence, knowing how to master the intermolecular forces involved in self-assembly strategies, it requires further examination into the nature of the interactions between CA units. In addition, exploring the diversity of possible supramolecular arrangements is of great importance for structure prediction and design of new programmed structures.

In order to gain a deeper insight about how systems are reorganized by the possible combinations of H-Bonds until they reach the most stable structures, we discuss different hydrogen bonding arrangements of CA supramolecules by analyzing complexes taken from literature and, as far as we know, molecular aggregates that have not been considered yet. In this work, we have performed a topological study via the quantum theory of atoms in molecules (QTAIM) and a Natural Bond Orbital analysis (NBO) on several CA molecular assemblies.

V.2. Computational Methods

The set of complexes studied here were chosen as follows: three dimers (**D1**, **D2** and **D3**), four trimers (**T1**, **T2**, **T3** and **T4**), two rosette type structures taken from Flynn's et al. work[13] (**R1** and **R2**) and a rosette type structure based on five CA units (**R3**). Finally, a molecular aggregate with the H-Bond pattern of the pure crystal (**Fig. V.1c**) was also studied. This last structure was taken from the crystallographic structure data obtained by Coppens and Vos.[12] According to the H-Bond types, linear or double, the set of complexes can be arranged in an aggregation path which is shown in **Fig. V.2**.

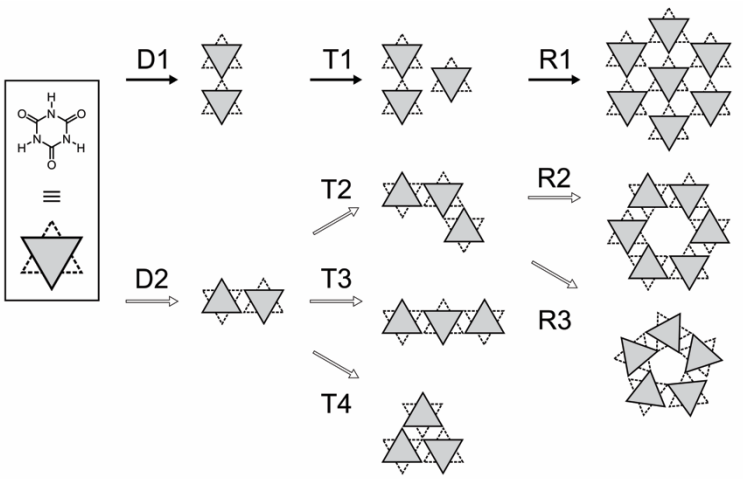

Figure V.2 Schematic representation of a hypothetical aggregation path.

Geometries of CA_n clusters (with n = 1, 2, 3, 5, 6, 7) were manually assembled and fully optimized without any constraint using the GAMESS[21] quantum chemistry package. The optimizations were done using three levels of theory with the 6-311++G(d,p) basis set: the B3LYP hybrid functional;[22,23] the B3LYP-D3 functional, which accounts for Grimme dispersion corrections;[24] and the ω-B97XD hybrid functional from Head-Gordon et al.[25] which also includes empirical dispersion and correction designed for long-range interactions. The minimum energy nature of the optimized structures was verified using the vibrational frequency analysis. The binding energies ΔE_{Bond} (BE) were obtained at the same level of theory using the approach of Fonseca Guerra et al.,[26–28] which is calculated as the sum between the interaction energy of the complex ΔE_{Int} and the preparation energy ΔE_{Prep} (**Equation V.1**).

$$\Delta E_{\text{Bond}} = \Delta E_{\text{Int}} + \sum \Delta E_{\text{Prep}} \qquad \text{(V.1)}$$

In this equation, the interaction energy ΔE_{Int} is the difference between the energy of the complex and the sum of energies of the monomers within the structure of the complex. The preparation energy ΔE_{Prep} is the difference between the energy of the

monomer in the complex and the energy of its isolated structure, or in other words, is the deformation energy of each monomer upon complexation. The ΔE_{Bond} have also been corrected for the basis set superposition error (BSSE) within the approach of Boys and Bernardi.[29]

The cooperativity (ΔE_{coop}) was calculated by **Equation V.2**.[30,31]

$$\Delta E_{coop} = \Delta E_{Int}(CA_{n>2}) - \sum \Delta E_{Int}(CA_2) \quad (V.2)$$

where ΔE_{Int} ($CA_{n>2}$) is the total interaction energy of either trimers or rosettes and $\sum\Delta E_{Int}$ (CA_2) is the sum of the interaction energies of the corresponding dimers (either **D1** or **D2**).

The synergy effect was also evaluated by equation 3 within the procedure of Fonseca Guerra et al.[27,32]

$$\Delta E_{Syn} = \Delta E_{Int} - (\sum\Delta E_{Pair} + \sum\Delta E_{Diag}) \quad (V.3)$$

where ΔE_{Pair} is the interaction between two molecules connected by H-Bonds, ΔE_{Diag} is the interaction between two non-H-bonded molecules in the complex, and ΔE_{Syn} is the interaction synergy (cooperative effect) that takes place in the complex. Thus, if $\Delta E_{Syn} < 0$ a positive cooperative effect is present, whereas if $\Delta E_{Syn} > 0$ the cooperativity is negative.

For the topological analysis, total electron densities were calculated at the B3LYP/6−311++G(d,p), level of theory. The local properties at bond critical points (BCP) were calculated using the AIMALL[33] program. The QTAIM of Bader[34] provides a rigorous definition of the chemical concepts of atom, bond, and structure. This theory has been used successfully for the characterization of H-Bond interactions through a set of local topological properties calculated at BCP of electron charge density. In this work, the electron charge density at the BCP, ρ_b, which measures the accumulation of charge between the bonded nuclei and reflects the bond strength;[35,36] the Laplacian of the electron density $\nabla^2\rho_b$ that provides information about the local charge concentration ($\nabla^2\rho_b < 0$) or depletion ($\nabla^2\rho_b > 0$);

the densities of kinetic energy G_b, the densities of potential energy V_b, and the total electronic energy density $H_b = V_b + G_b$ were used to analyze the nature of the interactions that occur in the different complexes. Another parameter that describes a chemical bond is the delocalization index (DI(A,B)), which measures the average number of electrons delocalized between two atomic basins, A and B.

Finally, the optimized geometries computed at B3LYP/6–311++G(d,p) level of theory were used to perform a NBO analysis[37] from NBO 3.1 program[38] as implemented in Gaussian 03.[39] This analysis was conducted to quantitatively evaluate the interactions of charge transfer (CT) involved in the formation of H-Bonds and the cooperative effects.

V.3. Results and Discussion

V.3.1. Geometric, Energetic, and Electron Charge Density Analysis

Table S1 reports relevant optimized geometrical parameters of N–H···O interactions, such as H-Bond lengths $d_{H\cdots O}$, $\theta_{N-H\cdots O}$ H-Bonds angles, and the d_{N-H} proton-donor bond lengths. Due to the geometrical features of trimers and rosette complexes, the interactions are classified as *inner* and *outer*. **Table V.1** shows corrected BEs by BSSE obtained with the B3LYP, B3LYP-D3 and ω-B97XD functionals. Optimization results slightly diverge for the three theoretical methods evaluated. In general, it is identified that the B3LYP-D3 and the ω-B97XD functionals show longer d_{N-H} and shorter $d_{H\cdots O}$ distances compared with B3LYP calculations. It is also verified in all complexes that N–H distances are elongated as a consequence of complex formation, which is consistent to the formation of a conventional H-Bond. In addition, as expected, BEs with dispersion correction are more negative than B3LYP calculations.

The following discussion is organized as follows: *dimers*, *trimers* and *rosette*-like structures are discussed separately. Finally, *cooperative effects* are examined among all set of complexes.

Table 1 Corrected binding energies ΔE_{Bond} by BSSE

Complexes	B3LYP	B3LYP-D3	ω-B97XD
D1	-5.67	-7.00[a]	-6.75[b]
D2	-11.37	-14.29	-13.73
D3	-6.12	-9.68	-9.32
T1	-18.40	-22.63[a]	-21.88[b]
T2	-22.87	-28.77	-27.66
T3	-22.63	-28.47	-27.30
T4	-21.61	-28.46	-27.34
R1	-71.87	-88.90[a]	-85.81[b]
R2	-69.12	-86.98	-83.56
R3	-53.52	-68.65	-66.05

All values in kcal/mol. [a]B3LYP-D3/6-311++G**//B3LYP/6-311++G** single point results for comparison. [b]ω-B97XD/6-311++G**//B3LYP/6-311++G** single point results for comparison.

Dimers

Figure V.3 shows the molecular graphs of the dimers obtained. The values of charge density at the H-Bond BCPs, ρ_b, are also included. Three different configurations of H-Bonded complexes can be seen in this figure. In **D1**, the N−H···O H-Bond with an angle of 180° is verified; in **D2**, both CA units play a dual role as a proton acceptor and as a proton donor, with $\theta_{N-H\cdots O}$ values of 167.2° (close to the experimental value: θ = 172.4°[12]). Finally, in **D3**, the N−H···O H-Bond shows an angle of 156.6°, which is less collinear than the previous ones. When considering optimizations, in the case of the functionals with dispersion correction, they do not predict a structure of **D1** complex, but it tends to adopt the conformation of **D2** complex. Moreover, the proposed T-shaped and parallel stacked arrangements have not been observed. Instead, the optimization of both structures unambiguously gives the **D3** structure, with either of the functionals. In this structure it can be seen that the carbonylic oxygen interacts with the positive region of the ring, as expected, which is confirmed by the presence of a C···O BCP.

Observation of the energetic analysis reported in **Table V.1** shows that BEs decrease in the following order: **D2** > **D3** > **D1**. It is important to note that ΔE_{Bond} (B3LYP) of complex **D2** is almost twice the ΔE_{Bond} (B3LYP) of complex **D1**; thus it is difficult to establish what the primitive structure of **R1** is, and also to explain the energetic stabilities of **R1** and **R2** structures, since both arrangements were found to coexist.[13] Then, an interesting question arise what is the mechanism by which H-Bond arrangement of 180° is formed? The following sections intend to answer this question.

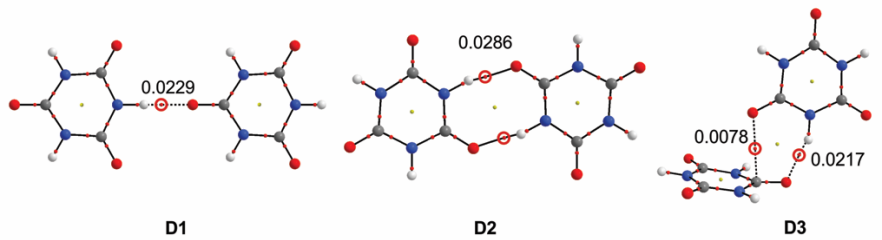

Figure IV.3 Molecular graphs of optimized dimers. The lines connecting the nuclei are the bond paths. *Red circles* are the BCPs or (3, −1) critical points, and *yellow circles* represent ring critical points or (3, +1) critical points. Values of ρ_b at BCPs, which were obtained at B3LYP level, are given in atomic units.

Detailed information of H-Bonds, as well as other interactions, is obtained by the QTAIM analysis reported in **Table IV.2.** In all the complexes studied, values of ρ_b and $\nabla^2\rho_b$ at the H-Bond BCPs fall within the proposed range for closed shell interactions.[40] In addition, V_b and G_b are of the same order of magnitude, and H_b is positive and close to cero. On the basis of the local energy density parameters derived from the QTAIM scheme, H_b has been used as a descriptor of covalent character when this property is negative.[41,42]

Furthermore, taking into account the values of ρ_b and DI(H,O), which are good indicators of the bond strength and bond order respectively, and, being them also strongly correlated;[41,42] the strongest interactions observed are those in the **D2** dimer, in line with the shortest $d_{H\cdots O}$ distance and a highest binding energy. When topological parameters of **D1** and **D3** complexes are compared, the N−H···O H-Bond

of the **D1** complex is stronger than in the **D3** complex. However the later shows a second interaction between the carbonylic oxygen and the endocyclic carbon. This additional C···O interaction may favor the complex **D3** over **D1**.

Trimers

As it was seen in dimers, the optimized structure of **T1** trimer obtained at B3LYP level is notably different from those obtained at B3LYP-D3 and ω-B97XD levels. This is a consequence of dispersion corrections terms. The optimization with B3LYP-D3 and ω-B97XD functionals tends to impose conformations that increase the number of intermolecular interactions. **Fig. V.4a** shows the molecular graph of the optimized **T1** complex using the B3LYP/6-311++G(d,p) level of theory. From this figure, one can infer that the complex keeps the $\theta_{N-H\cdots O}$ angle close to 180° (**see Table S1**). In addition, when going from **D1** to **T1** geometry $d_{H\cdots O}$ distances are shortened and, the charge density at the BCPs, ρ_b, and DI(H,O) also increase (See **Table S1** and **Table V.2**). Since the increase or decrease of ρ_b can be related to the cooperativity or negative cooperativity of H-Bonds,[31,43] respectively, the observed changes indicate an enhancement of the H-Bonds strength, and consequently a positive cooperativity. **Figures V.4b-c** show the molecular graphs of the optimized **T1** complex using the B3LYP-D3/6-311++G(d,p) and the ω-B97XD/6-311++G(d,p) levels of theory. Again, by comparison of these figures, they do not predict the expected arrangement. It can be seen that both functionals predict almost the same complexes and they just differ by the presence of an interaction of the type O···O (**Fig. V.4c**).

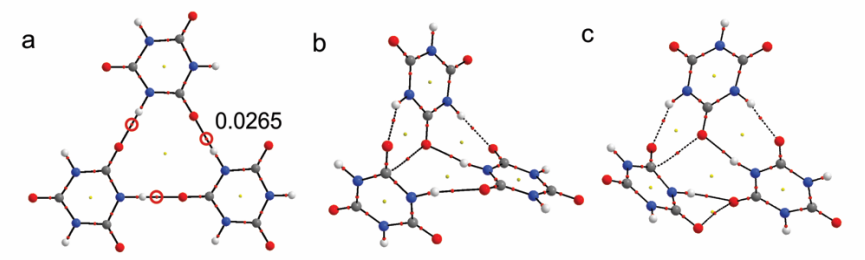

Figure V.4. Molecular graphs of **T1** complexes **(a)** B3LYP/6−311++G(d,p) structure. The electron density at bond critical points is given in atomic units, all interactions are equivalent. **(b)** B3LYP-D3/6−311++G(d,p) geometry, **(c)** ω-B97XD/6−311++G(d,p) geometry.

What is more, both B3LYP-D3 and ω-B97XD functionals predict an H-Bond pattern with the same arrangement of the **D3** complex. At this point, it is important to highlight that although B3LYP is characterized by a lacking of London dispersion energy, it has shown an excellent performance in the calculation of geometries,[44,45] even with weak interactions like C–H···O HBs.[46] On the contrary, with regards to energy and thermochemistry calculations, it is widely known that dispersion corrected functionals give better results than non-corrected ones.[44,47] In addition, it is known that corrected functionals tend to overestimate the binding.[48] For instance, in a study of the dimethylamine−trimethylphosphine complex, Kjaergaard et al.[49] have found that the B3LYP functional favors a structure with an N–H···P HB, while both B3LYP-D3 and ω-B97XD functionals favor almost the same structure with both an N–H···P HB and C–H···N secondary interactions. In this work, the B3LYP functional is the best choice since it gives a reasonable reproduction of the experimental structure; and it is evident that the dispersion correction does not imply a better description of the systems because the long-range interactions seem to be less important. Finally, it is worth stressing that the **R1** rosette motif was obtained as a monolayer on both graphite[13] and Au(111)[50] surfaces, which also may affect the formation of the rosette.

Table V.2 Local Topological Properties at N−H···O BCPs.

Complex	Interaction	ρ_b	$\nabla^2\rho_b$	$-V_b$	G_b	H_b	DI(H,O)
D1	N−H···O	0.0229	0.1017	0.0179	0.0217	0.0037	0.0678
D2	N−H···O	0.0286	0.1047	0.0225	0.0243	0.0019	0.0849
	N−H···O	0.0287	0.1048	0.0225	0.0244	0.0018	0.0850
D3	N−H···O	0.0217	0.0854	0.0156	0.0185	0.0029	0.0656
	O···C	0.0078	0.0299	0.0052	0.0063	0.0011	0.0187
T1	N−H···O	0.0266	0.1141	0.0220	0.0253	0.0032	0.0765
T2	$N-H\cdots O_{outer}$	0.0285	0.1043	0.0223	0.0242	0.0019	0.0847
	$N-H\cdots O_{inner}$	0.0291	0.1062	0.0230	0.0248	0.0018	0.0859
T3	N−H···O	0.0283	0.1038	0.0221	0.0240	0.0019	0.0841

T4	N−H···O_{outer}	0.0282	0.1014	0.0217	0.0235	0.0018	0.0848
	N−H···O_{inner}	0.0283	0.1029	0.0222	0.0239	0.0018	0.0841
	O···O	0.0010	0.0046	0.0004	0.0008	0.0004	0.0076
R1	N−H···O_{outer}	0.0247	0.1061	0.0197	0.0231	0.0034	0.0721
	N−H···O_{inner}	0.0283	0.1183	0.0239	0.0268	0.0028	0.0805
R2	N−H···O_{outer}	0.0287	0.1051	0.0226	0.0244	0.0018	0.0849
	N−H···O_{inner}	0.0286	0.1044	0.0224	0.0243	0.0018	0.0849
R3	N−H···O_{outer}	0.0218	0.0811	0.0153	0.0178	0.0025	0.0685
	N−H···O_{inner}	0.0334	0.1195	0.0281	0.0290	0.0009	0.0940
R4	N−H···O_{outer}	0.0247	0.1061	0.0197	0.0231	0.0034	0.0721
	N−H···O_{inner}	0.0283	0.1183	0.0239	0.0268	0.0028	0.0805

All values are in atomic units.

Figure V.5 shows the molecular graph of the optimized **T2** and **T3** complexes using the B3LYP/6-311++G(d,p) level of theory. By following the scheme of aggregation of Fig. 2, if more CA units are added to **T2** complex, a rosette-like structure (either **R2** or **R3**) is obtained. Besides, if more CA units are added to **T3** complex it will give an infinite linear arrangement. When going from **D2** to **T2** complex, $d_{H\cdots O}$ distances of inner interactions are shortened and, likewise ρ_b and DI(H,O) increase (See Table S1 and 2), which indicates a strengthening of these interactions. On the contrary, in the transition **D2→T3** all the interactions are weakened.

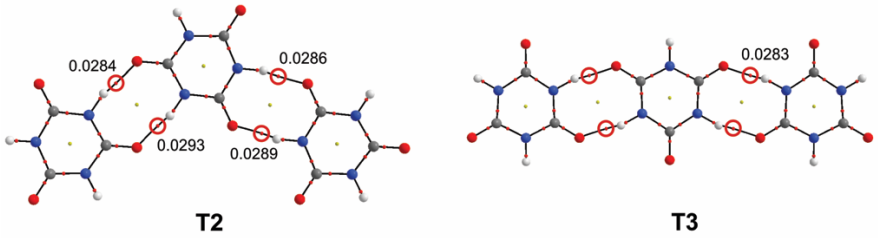

Figure V.5. Molecular graphs of complexes **T2** and **T3**. Values of ρ_b at BCPs, which were obtained at B3LYP level, are given in atomic units.

Finally, **Fig. V.6** shows the molecular graph of the optimized **T4** complex using the B3LYP/6-311++G(d,p) level of theory. In this case, either of the functionals employed predict the same geometry, with slight differences. This structure was not

previously reported, and we consider that it constitutes an important part of the combinatorial library of CA complexes. In **Fig. V.6** the presence of a bifurcated H-Bond can also be verified, in which an oxygen atom acts as a double proton acceptor. Topological values of these H-Bonds do fall within the proposed range of Popelier.[51] In this arrangement can also be seen an interaction of the type O···O which can be classified as a van der Waals interaction.[41]

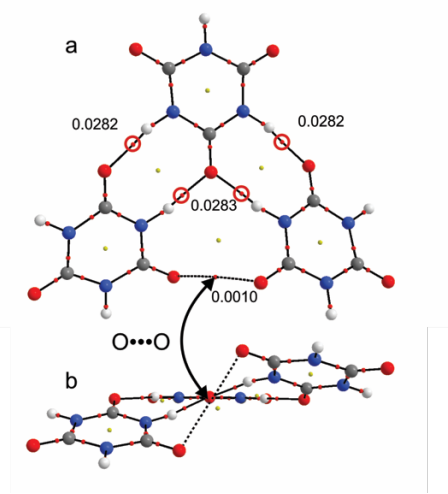

Figure V.6. Molecular graph of the **T4** complex. **(a)** Top view. **(b)** Side view. Values of ρ_b at BCPs, which were obtained at the B3LYP level, are given in atomic units.

Trends in BEs slightly differ between the functionals. For B3LYP and B3LYP-D3, BEs decrease in the following order: **T2** > **T3** > **T4** > **T1**, while for ω-B97XD the trend is: **T2** > **T4** > **T3** > **T1**. The most stable structure is **T2**, however, the energy differences separating the group of complexes range from -0.2 kcal/mol to -4.5 kcal/mol. The largest difference is of ~ -4.5 kcal/mol between **T1** and **T2**.

Rosettes

Figure V.7 shows the molecular graph of the optimized **R1**, **R2** and **R3** rosettes. Observation of this geometries shows that the most coplanar structure is **R2**, while **R1** complex shows some coplanarity but it seems to be unstable. Regarding **R3** complex, it shows a bowl-like structure alike the pentamer of metaboric acid.[52] Since **R2** and **R3** rosettes exhibit holes in their center with different sizes (4,3 Å and

3 Å respectively, for an isosurface density of $\rho(r)$ = 0.001 au), they are good candidates to host ions with different sizes, just like quintets of uracil and thymine found by Qiu et al.[53]

When considering the **D1**→**T1**→**R1** evolution, the primitive N−H···O H-Bond is enhanced in every step. That is, when going from **D1** to **R1**, $d_{H\cdots O}$ distances are shortened and ρ_b and DI(H,O) values increase in magnitude. In addition, the inner interactions are more strengthened than the outer ones.

On the contrary, when considering the **D2**→**T2**→**R2** evolution, in general the inner N−H···O H-Bonds are enhanced and the outer ones are weakened. For example, when going from **D2** to **T2**, the inner interactions are enhanced (from ρ_{D2} = 0.0286 to ρ_{T4} = 0.0289 ~ 0.0293). However, when going from **T2** to **R2**, this trend is not so clear in terms of the charge density analysis. When looking at the **T2**→**R3** transition, there is a clear enhancement of the inner interactions and the outer ones are weakened.

Despite that **R1** and **R2** complexes are geometrically different, they share the same number of interactions, which is twelve H-Bonds. By comparing **R1** with **R2** complexes of Fig. 7, the H-Bonds of **R2** complex are far stronger than interactions of **R1** complex (according ρ_b values). The sum of densities at H-Bond BCPs is: 0.3175 au for **R1** complex and 0.3438 au for **R2** complex. This trend is in line with the interaction energies ΔE_{Int}. However, when looking ΔE_{Bond} values, **R1** is almost 2,75 kcal/mol stronger than **R2** (for B3LYP, and ~2 kcal/mol for B3LYP-D3 and ω-B97XD). Consequently, the positive cooperativity gains an enormous importance in these systems.

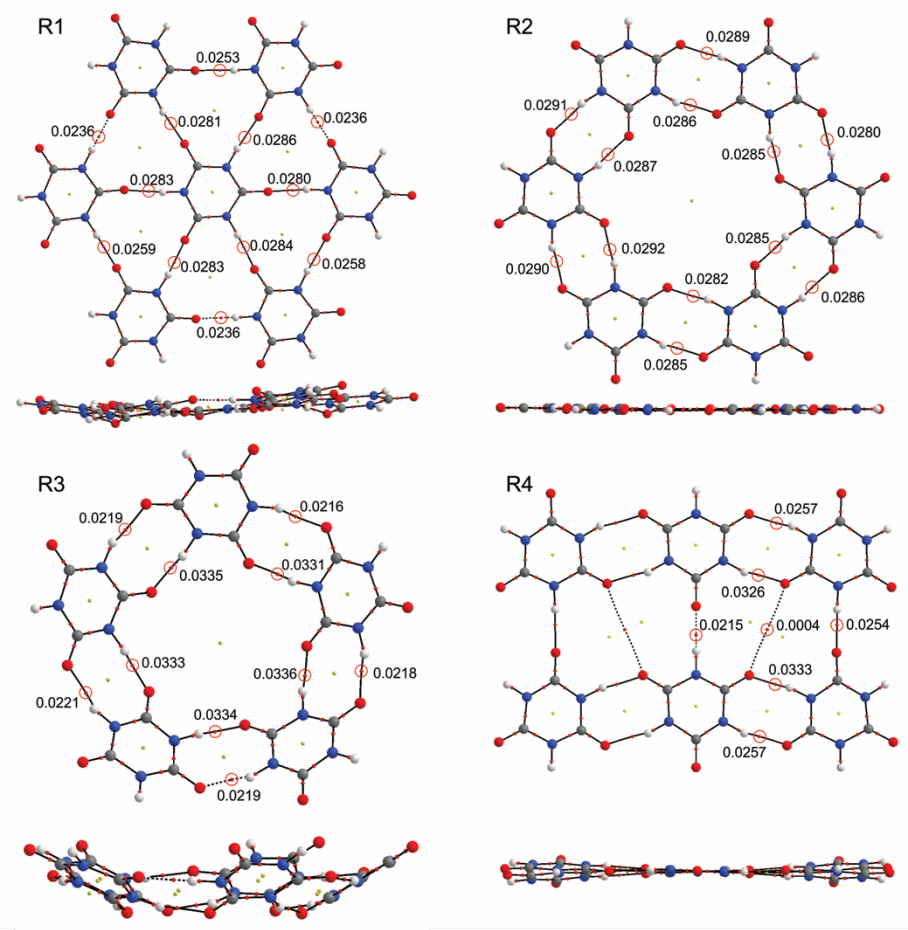

Figure V.7. Top and side view of Molecular graphs of **R1**, **R2**, **R3** and **R4** complexes. Values of ρ_b at BCPs, which were at the B3LYP level, are given in atomic units.

It is also interesting to examine the H-Bond arrangement of the CA crystal structure (**Fig. V.7**, **R4**). This H-Bond pattern shows components of both rosettes **R1** and **R2**. That is, the H-Bond pattern shows the presence of H-Bonds with $\theta_{N-H\cdots O}$ close to 180° and 172°. It is interesting to note that neither of the functionals predict the coplanar structure of the crystal, not even the B3LYP functional which is widely known to predict good geometries.[43] With regards to intermolecular interactions within the crystal, a BCP is evidenced between O atoms, as well as in previous complexes (**T1**/ω-B97XD and **T4**). However, topological values (ρ_b, $\nabla^2\rho_b$, H_b)

indicate that this interaction is a van der Waals bonding. It should also be noted, that the closed-shell O···O interaction has been observed in several environments, going from ligand-receptor systems,[54] silicates,[55] the $Mn_2(CO)_{10}$ complex,[56] and in several derivatives of cis-β-diketone.[57] Therefore, within the QTAIM methodology, this interaction is receiving increasing attention either in biological systems or in materials chemistry.

Cooperative effects

In order to evaluate the cooperativity from an energetic point of view, we compared the H-Bond interactions in the trimers and rosettes with their similar counterparts in dimer complexes. **Table V.3** shows the energetic contribution due to cooperativity ΔE_{coop}, as well as the synergy effect ΔE_{Syn}.

The greatest gain of energy is observed in the series **D1→T1** and **T1→R1**. It is worst stressing that the three functionals predict almost the same trends of ΔE_{coop} and ΔE_{Syn}. On the contrary, the series of complexes **D2→T2** and **T2→R2** exhibit a lesser cooperative effect, which can be neglected. By comparing **T1** and **T2** structures, **T1** has three N−H···O H-Bonds while **T2** has four ones. Also, **T2** is 4 kcal/mol greater than **T1** but, the later shows a greater cooperative effect. Therefore, these structures can compete with each other during the self-assembly process.

Finally, the cooperative effect of **R3** rosette is fundamentally zero, which may explain the fact that it was not observed as a self-assembled monolayer. However, this structure could exist as a stable aggregate in solution since similar quintets have been observed between uracil molecules.[53]

Table V.3 Energetic Contributions due to the Cooperativity

Complex	ΔE_{Coop}			ΔE_{Syn}		
	B3LYP	B3LYP-D3	ω-B97XD	B3LYP	B3LYP-D3	ω-B97XD
T1	-1.88	-2.09	-2.02	-1.52	-1.52	-1.43
T2	-0.09	-0.17	-0.11	0.02	0.01	0.03
T3	0.12	0.08	0.11	0.13	0.15	0.14
T4	0.97	-0.18	-0.06	-0.32	-0.30	-0.29
R1	-4.59	-5.76	-5.45	-4.73	-4.73	-4.43
R2	-0.38	-0.92	-0.75	0.20	0.15	0.19
R3	3.65	3.09	3.27	-0.08	-0.06	0.00

All values in kcal/mol

3.2 Critical points of $-\nabla^2\rho(r)$

The Laplacian of the electron density distribution, $\nabla^2\rho(\mathrm{r})$, is a powerful tool in the interpretation of molecular interactions. The topology of $\nabla^2\rho(\mathrm{r})$, can also show in a molecular graph the localization of basic and acidic regions.[34,58] According to the $L(\mathrm{r}) = -¼\nabla^2\rho(\mathbf{r})$ function, a (3, -3) critical point (CP) corresponds to a local maximum, and indicates a local electronic charge concentration. It has been shown that the maxima in $L(\mathrm{r})$ are associated to electron pair domains of Lewis model.[58] Besides, a (3, +3) CP corresponds to a local minimum and indicates a local depletion of the electronic charge.

Figure V.8 displays the (3, -3) and (3, +3) CPs in $L(\mathrm{r})$, superimposed on the molecular graph of **D1** and **D2** complexes. It can be immediately seen that in **D1** complex the molecules are oriented so that the minima in $L(\mathrm{r})$ (*pink circles*), that corresponds to regions of charge depletion, are aligned, which explains why this arrangement is unstable. With regards to **D2** complex, Fig. 8 shows that this arrangement is stabilized by the well-known hole−lump interaction: a maxima of charge concentration is aligned with a minima of charge depletion. The latter case is the most energetically favored.

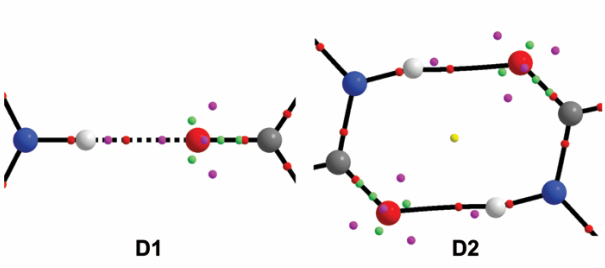

Figure V.8. Critical points of the $L(r)$ function superimposed on molecular graph of **D1** and **D2** complexes. Lines connecting the nuclei are the bond paths. *Red circles* are BCPs or (3, −1) critical points in $\rho(\mathbf{r})$ function, *yellow circles* are ring critical points or (3, +1) critical points in $\rho(\mathbf{r})$ function, *green circles* are (3, −3) critical points in $L(r)$ function, and pink circles are (3, +3) critical points in $L(r)$ function.

3.3 Natural Bond Orbital Analysis

The cooperativity of H-Bonds can also be analyzed from the viewpoint of hyperconjugative energies of charge transfer (CT) between NBOs. The results of NBO analysis conducted on CA complexes are given in Table 4. The values reported in this table are the second-order perturbation energies ($E^{(2)}$) (donor→acceptor) that involve the oxygen lone pairs (LP) 1 and 2 and the N–H σ* antibonds ($n_O \rightarrow \sigma^*_{N-H}$). By analyzing these results the cooperativity can be clearly seen. In the **D1→T1→R1** transition, an augmentation of $E^{(2)}$ values is evidenced. The inner interactions undergo a strong enhancement. Since the N−H···O is strongly directional, it is observed that the LP2 does not participate in the CT interaction.

On the other hand, when looking at both **D2→T3** and **D2→T4** transitions, no increase is observed in $E^{(2)}$ energies, but, **T2** structure exhibits an enhancement of inner interactions, as well as the **R2** rosette. Finally, when looking at the **D2→T2→R3** transition, the **R3** rosette displays a strong increment of $E^{(2)}$ energies on inner interactions, while the outer ones display the opposite effect. Thus, these cooperative and anti-cooperative effects compensate each other and the total binding energy results being lesser than the sum of the parts, that is, a negative cooperativity.

Table 4 Average Second-Order Perturbation Energies $E^{(2)}$ (Donor→Acceptor) involving contributions of lone pairs (LP) 1 and 2 to σ* antibonds: $LP1_O \rightarrow \sigma^*_{(N-H)}$ and $LP2_O \rightarrow \sigma^*_{(N-H)}$ interactions

Complex	Interaction	$E^{(2)}$	
		LP1	LP2
D1	N−H···O	9.13	0.00
T1	N−H···O	11.78	0.00
R1	$N-H\cdots O_{inner}$	12.90	< 0.1
	$N-H\cdots O_{outer}$	9.87	< 0.1
D2	N−H···O	6.93	7.52
	N−H···O	6.91	7.50
T2	$N-H\cdots O_{inner}$	6.79	5.31
	$N-H\cdots O_{outer}$	6.27	7.76
T3	$N-H\cdots O_{inner}$	7.21	7.68
	$N-H\cdots O_{outer}$	6.87	7.46
T4	N−H···O	6.81	7.33
R2	$N-H\cdots O_{inner}$	7.17	7.44
	$N-H\cdots O_{outer}$	6.97	7.45
R3	$N-H\cdots O_{inner}$	8.97	8.32
	$N-H\cdots O_{outer}$	4.33	4.59

All values in kcal/mol

The origin of the cooperativity

In our previous study on M/CA complexes,[59] we showed that the $n_N \rightarrow \sigma^*_{(C=O)}$ intramolecular CTs experience an increase of $E^{(2)}$ energies upon complex formation. The charge flows through both inter and intramolecular interactions like in a "circuit". This effect is also present in CA supramolecules, as it can be visualized in **Fig. V.9**. This figure outlines the intra and intermolecular CTs between NBOs: $n_N \rightarrow \sigma^*_{C=O}$ and $n_0 \rightarrow \sigma^*_{N-H}$. It can be seen that in **T1** complex, the H-Bonds point in one direction and there is a direct path that connects the three molecules involving $n_N \rightarrow \sigma^*_{C=O}$ and $n_0 \rightarrow \sigma^*_{N-H}$ CTs. Contrarily, when looking **T2**, **T3** and **T4** complexes there is no such direct path that connects the molecular units. Besides, the H-Bonds point in opposite directions.

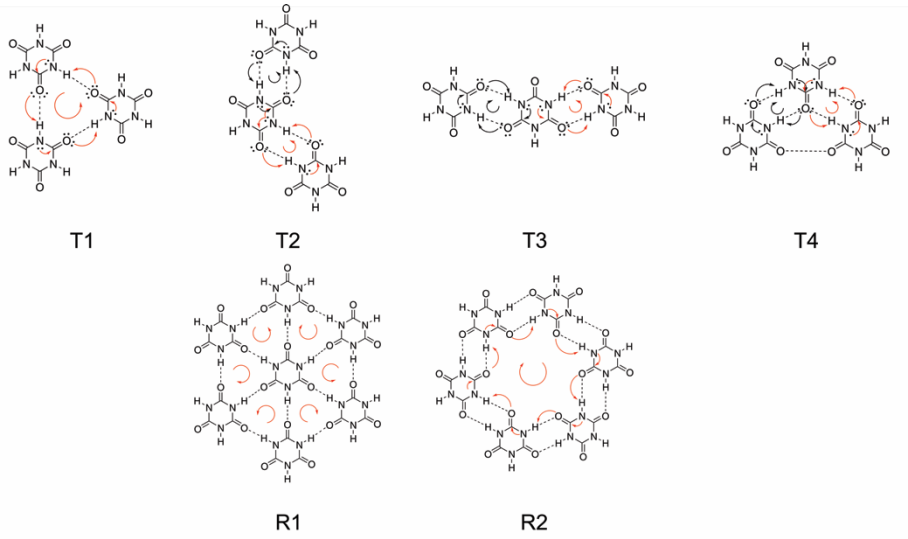

Figure V.9. Schematic representation of $n \rightarrow \sigma^*$ inter ($n_O \rightarrow \sigma^*_{N-H}$) and intramolecular ($n_N \rightarrow \sigma^*_{C=O}$) charge transfers involving interactions in CA trimers and rosettes. Circular arrows indicate the net charge flow as a consequence of $n_O \rightarrow \sigma^*_{N-H}$ and $n_N \rightarrow \sigma^*_{C=O}$ charge transfers.

When going from **T1** to **R1**, the inner interactions are reinforced because each C=O bond from the central unit receives charge from two nitrogen LPs. Moreover, the interactions of the outer periphery are weaker than the inner ones because there is not a direct path that connects them, in fact the H-Bonds are in opposite directions.

With regard to the **T2** → **R2** transition, a direct path that connects $n_N \rightarrow \sigma^*_{C=O}$ and $n_O \rightarrow \sigma^*_{N-H}$ CTs is manifested with the completion of the rosette, which explains why the inner interactions are stronger than the outer ones (either in **R2** or **R3** complexes).

These results are in good accordance with an earlier work of Fonseca Guerra et al.,[27] in which they showed that supramolecules of Guanine display a cooperativity effect that is absent in xanthine ones. This effect originates in the σ-electron system. The charge goes from one unit to the other in one direction. They have also argued that their model is expected to apply to other hydrogen-bonded supramolecules.

V.4. Conclusions

In this chapter, a structural and an electronic analyses at B3LYP, B3LYP-D3 and ω-B97XD/6-311++G(d,p) levels of theory were carried out on a series of supramolecular complexes formed by hydrogen bonds. It has been shown a variety of possibilities in which CA can be arranged through H-Bonds, that is, a combinatorial library of complexes. It is evident, that the formation of complex structures of CA involves an intricate path of supramolecular arrangements since the beginning of the self-assembly process. The B3LYP functional has shown the best performance to describe the interactions.

CA is a very versatile building block because it can form at least four rosette-like structures with different degrees of cooperativity. Since different organizations of the same building block show special energetic and topological features, it is a fact that they would lead to different functionalities and thus different macroscopic properties. For instance, **R2** and **R3** supramolecules could hold different cations with different ionic radii.

The energetic, topological and NBO results demonstrate that the structures with $\theta_{N-H\cdots O}$ = 180° (**T1** and **R1**) display the highest cooperative effect. However, some structures with double H-Bonds show greater binding energies but very low or zero cooperative effects. Therefore, they may compete with each other during the self-assembly steps, which may explain why all of these structures coexist in the same monolayer. The next ultimate challenge will be to obtain pure arrangements as self-assembled monolayers. It is also interesting to highlight that a greater cooperative effect is not always associated with a greater binding energy. The intramolecular charge transfers play a key role in the cooperative effect.

Finally, it is suggested that the nucleation process of **R1** rosette motif (with all $\theta_{N-H\cdots O}$ close to 180°) cannot be originated from **D1** dimer ($\theta_{N-H\cdots O}$ = 180°), since it is a very unstable structure and its cyclic analogue (**D2**), which has two H-Bonds, is twice more stable. Therefore, the **T1** structure could be originated as a concerted assembly process, and, the **R1** rosette is originated form the **T1** structure.

V.5. References

(1) Ariga, K.; Hill, J. P.; Lee, M. V; Vinu, A.; Charvet, R.; Acharya, S. Challenges and Breakthroughs in Recent Research on Self-Assembly. *Sci. Technol. Adv. Mater.* **2008**, *9* (1), 14109.

(2) Downes, C. J.; Mitchell, J. W.; Viotto, E. S.; Eggers, N. J. Determination of Cyanuric Acid Levels in Swimming Pool Waters by U.v. Absorbance, HPLC and Melamine Cyanurate Precipitation. *Water Res.* **1984**, *18* (3), 277–280.

(3) Cantú, R.; Evans, O.; Kawahara, F. K.; Wymer, L. J.; Dufour, A. P. HPLC Determination of Cyanuric Acid in Swimming Pool Waters Using Phenyl and Confirmatory Porous Graphitic Carbon Columns. *Anal. Chem.* **2001**, *73* (14), 3358–3364.

(4) Ma, M.; Gong, Y.; Bong, D. Lipid Membrane Adhesion and Fusion Driven by Designed, Minimally Multivalent Hydrogen-Bonding Lipids. *J. Am. Chem. Soc.* **2009**, *131*, 16919–16926.

(5) Avakyan, N.; Greschner, A. A.; Aldaye, F.; Serpell, C. J.; Toader, V.; Petitjean, A.; Sleiman, H. F. Reprogramming the Assembly of Unmodified DNA with a Small Molecule. *Nat. Chem.* **2016**, No. February, 1–9.

(6) Yagai, S.; Nakajima, T.; Karatsu, T.; Saitow, K.; Kitamura, A. Phototriggered Self-Assembly of Hydrogen-Bonded Rosette. *J. Am. Chem. Soc.* **2004**, *126* (37), 11500–11508.

(7) Liu, Y.; Wang, Q. Melamine Cyanurate-Microencapsulated Red Phosphorus Flame Retardant Unreinforced and Glass Fiber Reinforced Polyamide 66. *Polym. Degrad. Stab.* **2006**, *91* (12), 3103–3109.

(8) Mukherjee, S.; Ren, J. Gas-Phase Acid-Base Properties of Melamine and Cyanuric Acid. *J. Am. Soc. Mass Spectrom.* **2010**, *21* (10), 1720–1729.

(9) Pérez-Manríquez, L.; Cabrera, A.; Sansores, L. E.; Salcedo, R. Aromaticity in Cyanuric Acid. *J. Mol. Model.* **2011**, *17* (6), 1311–1315.

(10) Klotz, I. M.; Askounis, T. J. Absorption Spectra and Tautomerism of Cyanuric Acid, Melamine and Some Related Compounds. *J. Am. Chem. Soc.* **1947**, *69*, 801.

(11) Ranganathan, A.; Pedireddi, V. R.; Rao, C. N. R. Hydrothermal Synthesis of Organic Channel Structures: 1:1 Hydrogen-Bonded Adducts of Melamine with Cyanuric and Trithiocyanuric Acids. *J. Am. Chem. Soc.* **1999**, *121* (8), 1752–1753.

(12) Coppens, P.; Vos, A. Electron Density Distribution in Cyanuric Acid. II. Neutron Diffraction Study at Liquid Nitrogen Temperature and Comparison of X-Ray Neutron

Diffraction Results. *Acta Crystallogr. Sect. B Struct. Crystallogr. Cryst. Chem.* **1971**, *27* (1), 146–158.

(13) Kannappan, K.; Werblowsky, T. L.; Rim, K. T.; Berne, B. J.; Flynn, G. W. An Experimental and Theoretical Study of the Formation of Nanostructures of Self-Assembled Cyanuric Acid through Hydrogen Bond Networks on Graphite. *J. Phys. Chem. B* **2007**, *111*, 6634–6642.

(14) Choi, I. S.; Li, X.; Simanek, E. E.; Akaba, R.; Whitesides, G. M. Self-Assembly of Hydrogen-Bonded Polymeric Rods Based on the Cyanuric Acid·Melamine Lattice. *Chem. Mater.* **1999**, *11* (3), 684–690.

(15) Prior, T. J.; Armstrong, J. A.; Benoit, D. M.; Marshall, K. L. The Structure of the Melamine–cyanuric Acid Co-Crystal. *CrystEngComm* **2013**, *15* (29), 5838.

(16) Ranganathan, A.; Pedireddi, V. R.; Sanjayan, G.; Ganesh, K. N.; Rao, C. N. R. Sensitive Dependence of the Hydrogen-Bonded Assemblies in Cyanuric acid–4,4'-bipyridyl Adducts on the Solvent and the Structure of the Parent Acid. *J. Mol. Struct.* **2000**, *522*, 87–94.

(17) Pedireddi, V. R.; Belhekar, D. Investigation of Some Layered Structures of Cyanuric Acid. *Tetrahedron* **2002**, *58*, 2937–2941.

(18) Marivel, S.; Suresh, E.; Pedireddi, V. R. Molecules to Supermolecules and Self Assembly: A Study of Some Cocrystals of Cyanuric Acid. *Tetrahedron Lett.* **2008**, *49*, 3666–3671.

(19) Berl, V. V; Krische, M. J.; Huc, I.; Lehn, J. M.; Schmutz, M. Template-Induced and Molecular Recognition Directed Hierarchical Generation of Supramolecular Assemblies from Molecular Strands. *Chem. Eur. J.* **2000**, *6* (11), 1938–1946.

(20) Lewis, T. C.; Tocher, D. A.; Price, S. L. Investigating Unused Hydrogen Bond Acceptors Using Known and Hypothetical Crystal Polymorphism. *Cryst. Growth Des.* **2005**, *5* (3), 983–993.

(21) Schmidt, M. W.; Baldridge, K. K.; Boatz, J. A.; Elbert, S. T.; Gordon, M. S.; Jensen, J. H.; Koseki, S.; Matsunaga, N.; Nguyen, K. A.; Su, S.; et al. General Atomic and Molecular Electronic Structure System. *J. Comput. Chem.* **1993**, *14*, 1347–1363.

(22) Becke, A. D. Density-Functional Thermochemistry. III. The Role of Exact Exchange. *J. Chem. Phys.* **1993**, *98*, 5648–5652.

(23) Lee, C.; Yang, W.; Parr, R. G. Development of the Colle-Salvetti Correlation-Energy Formula into a Functional of the Electron Density. *Phys. Rev. B* **1988**, *37*, 785–789.

(24) Grimme, S.; Antony, J.; Ehrlich, S.; Krieg, H. A Consistent and Accurate Ab Initio Parametrization of Density Functional Dispersion Correction (DFT-D) for the 94 Elements H-Pu. *J. Chem. Phys.* **2010**, *132* (15), 154104.

(25) Chai, J.-D.; Head-Gordon, M. Long-Range Corrected Hybrid Density Functionals with Damped Atom-Atom Dispersion Corrections. *Phys. Chem. Chem. Phys.* **2008**, *10*, 6615–6620.

(26) Fonseca Guerra, C.; van der Wijst, T.; Bickelhaupt, F. M. Substituent Effects on Hydrogen Bonding in Watson–Crick Base Pairs. A Theoretical Study. *Struct. Chem.* **2005**, *16* (3), 211–221.

(27) Fonseca Guerra, C.; Zijlstra, H.; Paragi, G.; Bickelhaupt, F. M. Telomere Structure and Stability: Covalency in Hydrogen Bonds, Not Resonance Assistance, Causes Cooperativity in Guanine Quartets. *Chem. - A Eur. J.* **2011**, *17* (45), 12612–12622.

(28) Paragi, G.; Kupihár, Z.; Guerra, C.; Bickelhaupt, F.; Kovács, L. Supramolecular Ring Structures of 7-Methylguanine: A Computational Study of Its Self-Assembly and Anion Binding. *Molecules* **2012**, *18* (1), 225–235.

(29) Boys, S. F.; Bernardi, F. The Calculation of Small Molecular Interactions by the Differences of Separate Total Energies. Some Procedures with Reduced Errors. *Mol. Phys.* **1970**, *19*, 553–559.

(30) Dannenberg, J. J. Enthalpies of Hydration of N-Methylacetamide by One, Two, and Three Waters and the Effect upon the C=O Stretching Frequency. An Ab Initio DFT Study. *J. Phys. Chem. A* **2006**, *110* (17), 5798–5802.

(31) Angelina, E. L.; Peruchena, N. M. Strength and Nature of Hydrogen Bonding Interactions in Mono- and Di-Hydrated Formamide Complexes. *J. Phys. Chem. A* **2011**, *115* (18), 4701–4710.

(32) Dominikowska, J.; Bickelhaupt, F. M.; Palusiak, M.; Fonseca Guerra, C. Source of Cooperativity in Halogen-Bonded Haloamine Tetramers. *ChemPhysChem* **2016**, *17*, 474–480.

(33) AIMAll Version 12.06.03, Todd A. Keith, TK Gristmill Software, Overland Park KS, USA, 2012 Aim.tkgristmill.com.

(34) Bader, R. F. W. *Atoms in Molecules: A Quantum Theory*; Clarendon Press: Oxford, 1994.

(35) Boyd, R. J.; Choi, S. C. Hydrogen Bonding between Nitriles and Hydrogen Halides and the Topological Properties of Molecular Charge Distributions. *Chem. Phys. Lett.* **1986**, *129* (1), 62–65.

(36) Carroll, M. T.; Bader, R. F. W. An Analysis of the Hydrogen Bond in BASE-HF Complexes Using the Theory of Atoms in Molecules. *Mol. Phys.* **1988**, *65*, 695–722.

(37) Reed, E. A.; Curtis, A. L.; Weinhold, F. Intermolecular Interactions from a Natural Bond Orbital, Donor-Acceptor Viewpoint. *Chem. ReV.* **1988**, *88*, 899–926.

(38) Glendening, E. D.; Reed, A. E.; Carpenter, J. E.; Weinhold, F. NBO Version 3.1.

(39) Frisch, M. J.; Trucks, G. W.; Schlegel, H. B.; Scuseria, G. E.; Robb, M. A.; Cheeseman, J. R.; Montgomery, J. A. J.; Vreven, T.; Kudin, K. N.; Burant, J. C.; et al. Gaussian 03, Revision D.01. Gaussian, Inc.: Wallingford, CT 2004.

(40) Koch, U.; Popelier, P. L. A. Characterization of C-H-O Hydrogen Bonds on the Basis of the Charge Density. *J. Phys. Chem.* **1995**, *99* (24), 9747–9754.

(41) Matta, C. F.; Boyd, R. J. *The Quantum Theory of Atoms in Molecules: From Solid State to DNA and Drug Design*; Wiley-VCH: Weinheim, 2007.

(42) Matta, C. F. Modeling Biophysical and Biological Properties from the Characteristics of the Molecular Electron Density, Electron Localization and Delocalization Matrices, and the Electrostatic Potential. *J. Comput. Chem.* **2014**, *35*, 1165–1198.

(43) Petelski, A. N.; Peruchena, N. M.; Sosa, G. L. Evolution of the Hydrogen-Bonding Motif in the Melamine–cyanuric Acid Co-Crystal: A Topological Study. *J. Mol. Model.* **2016**, *22* (9), 202.

(44) Filipe, S. S.; Fernandes, P. A.; Ramos, M. J. General Performance of Density Functionals. *J. Phys. Chem. A* **2007**, *111*, 10439–10452.

(45) Tsipis, A. C. DFT Flavor of Coordination Chemistry. *Coord. Chem. Rev.* **2014**, *272*, 1–29.

(46) Scheiner, S. Dissection of the Factors Affecting Formation of a CH···O H-Bond. A Case Study. *Crystals* **2015**, *5* (3), 327–345.

(47) Fonseca Guerra, C.; van der Wijst, T.; Poater, J.; Swart, M.; Bickelhaupt, F. M. Adenine versus Guanine Quartets in Aqueous Solution: Dispersion-Corrected DFT Study on the Differences in π-Stacking and Hydrogen-Bonding Behavior. *Theor. Chem. Acc.* **2010**, *125*, 245–252.

(48) Thanthiriwatte, K. S.; Hohenstein, E. G.; Burns, L. A.; Sherrill, C. D. Assessment of the Performance of DFT and DFT-D Methods for Describing Distance Dependence of Hydrogen-Bonded Interactions. *J. Chem. Theory Comput.* **2011**, *7*, 88–96.

(49) Møller, K. H.; Hansen, A. S.; Kjaergaard, H. G. Gas Phase Detection of the NH−P Hydrogen Bond and Importance of Secondary Interactions. *J. Phys. Chem. A* **2015**, *119*, 10988−10998.

(50) Staniec, P. A.; Perdigão, L. M. A.; Rogers, B. L.; Champness, N. R.; Beton, P. H. Honeycomb Networks and Chiral Superstructures Formed by Cyanuric Acid and Melamine on Au(111). *J. Phys. Chem. C* **2007**, *111* (2), 886–893.

(51) Popelier, P. L. A. Characterization of a Dihydrogen Bond on the Basis of the Electron Density. *J. Phys. Chem. A* **1998**, *102*, 1873–1878.

(52) Elango, M.; Subramanian, V.; Sathyamurthy, N. The Self-Assembly of Metaboric Acid Molecules into Bowls, Balls and Sheets. *J. Phys. Chem. A* **2008**, *112* (35), 8107–

8115.

(53) Qiu, B.; Liu, J.; Qin, Z.; Wang, G.; Luo, H. Quintets of Uracil and Thymine: A Novel Structure of Nucleobase Self-Assembly Studied by Electrospray Ionization Mass Spectrometry. *Chem. Commun.* **2009**, 2863–2865.

(54) Andujar, S. A.; Tosso, R. D.; Suvire, F. D.; Angelina, E.; Peruchena, N.; Cabedo, N.; Cortes, D.; Enriz, R. D. Searching The "biologically Relevant"conformation of Dopamine: A Computational Approach. *J. Chem. Inf. Model.* **2012**, *52* (1), 99–112.

(55) Gibbs, G. V.; Downs, R. T.; Cox, D. F.; Ross, N. L.; Boisen, M. B.; Rosso, K. M. Shared and Closed-Shell O-O Interactions in Silicates. *J. Phys. Chem. A* **2008**, *112* (16), 3693–3699.

(56) Bianchi, R.; Gervasio, G.; Marabello., D. Experimental Electron Density Analysis of Mn2(CO)10: Metal–metal and Metal–ligand Bond Characterization. *Inorg. Chem.* **2000**, *39*, 2360–2366.

(57) Pakiari, A. H.; Eskandari, K. Closed Shell Oxygen-Oxygen Bonding Interaction Based on Electron Density Analysis. *J. Mol. Struct. THEOCHEM* **2007**, *806* (1–3), 1–7.

(58) Bader, R. F. W.; Johnson, S.; Tang, T.-H. The Electron Pair. *J. Phys. Chem.* **1996**, *100*, 15398–15415.

(59) Petelski, A. N.; Duarte, D. J. R.; Pamies, S. C.; Peruchena, N. M.; Sosa, G. L. Intermolecular Perturbation in the Self-Assembly of Melamine. *Theor. Chem. Acc.* **2016**, *135* (3), 65.

Supplementary Material

Table S1. Selected geometric parameters[a] of CA, dimers, trimers and rosettes calculated at B3LYP/6-311++G(d,p)

System	Interaction	d_{N-H}	$d_{H\cdots O}$	$\theta_{N-H\cdots O}$
CA		1.0111	-	-
D1	N–H···O	1.0196	2.9171	180.0
D2	N–H···O	1.0273	1.8655	167.2
	N–H···O	1.0273	1.8647	167.2
D3	N–H···O	1.0213	1.9654	156.6
T1[b]	N–H···O	1.0239	1.8405	178.9
T2[b]	N–H···O_{outer}	1.0279	1.8553	167.3
	N–H···O_{inner}	1.0272	1.8693	167.0
T3[b]	N–H···O	1.0271	1.8693	167.1
	N–H···O	1.0271	1.8701	166.8
T4[b]	N–H···O_{outer}	1.0279	1.8761	168.0
	N–H···O_{inner}	1.0252	1.8764	167.6
R1[c]	N–H···O_{outer}	1.0262	1.8192	177.18
	N–H···O_{inner}	1.0217	1.8735	178.51
R2[c]	N–H···O_{outer}	1.0282	1.8648	166.51
	N–H···O_{inner}	1.0270	1.8641	167.40
R3[c]	N–H···O_{outer}	1.0294	1.7999	166.15
	N–H···O_{inner}	1.0238	1.9832	160.85

[a] Distances in Å and angles in degrees. [b] All other interactions are essentially equal due to symmetry reasons. [c] Mean values

VI. DESIGNING SELF-ASSEMBLED ROSETTES: WHY AMMELINE IS A SUPERIOR BUILDING BLOCK TO MELAMINE

"If you know where you're going, you're not gonna find anything really interesting"

Michel Levitt,

Nobel Prize in Chemistry 2013, on the importance of basic research, and how unexpected the future is.

Part of this chapter previously appeared as:

Petelski, Andre N.; Fonseca Guerra, Célia. Designing self-assembled rosettes: Why ammeline is a superior building block to melamine. *ChemistryOpen,* **2019**, *8*, 135–142. (Front Cover and Cover Profile)

VI.1. Introduction

Due to their promising applications as self-assembling materials, the use hydrogen-bonded rosettes as building blocks for large nanostructures has attracted much attention during the last years.[1] These supramolecules are cyclic complexes of small organic compounds, which are associated by hydrogen bonds. They play a fundamental role in biology, as in the case of the naturally occurring guanine quartets;[2] but they may also have potent applications in materials science research[3] and nanoelectronics.[4]

Beyond its industrial importance,[5] melamine (M, see Scheme VI.1, black structure with R=NH_2) has been considered a very versatile building block for producing a great diversity of sophisticated functional materials.[6] For instance, melamine rosettes can be deposited as self-assembled monolayers (SAMs) over gold[7] or graphite.[8] This molecule is usually covalently modified, by replacing one amino group by long alkylic chains with aromatic rings, in order to add van der Waals interactions and therefore improve the binding of the supramolecule. The assembled rosettes of these

new species are able to form not only SAMs with new functionalities,[9] but they can also stack on top of each other to obtain pillar arrays or long nanowires.[10] In addition, it has been found that these wires can fold itself to form toroidal nanostructures.[11] The flexibility of this system reflects how important they can be for bottom-up applications in nanotechnology.

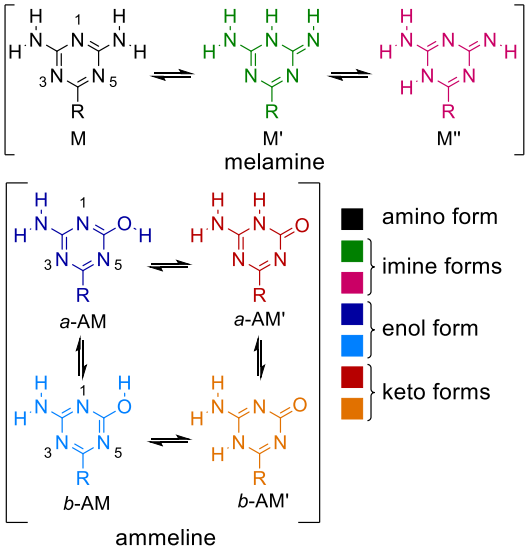

Scheme VI.1. Molecular structures of isomers that can form rosettes: 1,3,5-triazine-2,4,6-triamine or melamine (M); and 4,6-Diamino-1,3,5-triazin-2(1H)-one or ammeline (AM).

On the other hand, it is known that the sequential hydrolysis of melamine leads to the obtainment of three related triazine by-products: namely ammeline (AM, see also Scheme VI.1, blue structures with R = NH_2), ammelide, and cyanuric acid. Among these compounds, rosettes of melamine and cyanuric acid (1:1) are widely known. However, to the best of our knowledge, there is no actual report of hydrogen-bonded rosettes of AM.

With that in mind, computational experiments were assessed by us on hydrogen-bonded rosettes of melamine (M) and ammeline (AM). Since they can undergo amino-imine and amide-imidate tautomerisms,[12] respectively, our studies consider all

the tautomers of these species (see Scheme VI.1) that could form rosettes, as shown in Schemes VI.2 and 3 (R = H). In the present work we show that AM could be a more appropriate compound to synthesis hydrogen-bonded supramolecular systems. Our investigations are based on dispersion-corrected density functional theory (DFT-D) in the framework of Kohn–Sham molecular orbital (MO) theory[13] and supported by the corresponding energy decomposition analysis[14] (EDA) and Voronoi deformation density (VDD) analysis of the charge distribution.[15] We cover the situations of rosettes in the gas phase and in aqueous solution.

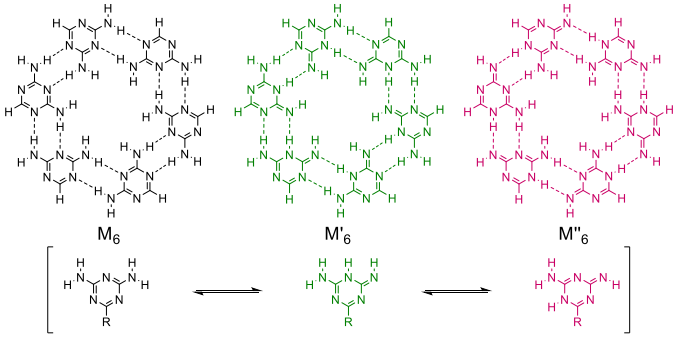

Scheme VI.2. Molecular structures of M rosettes and monomeric units.

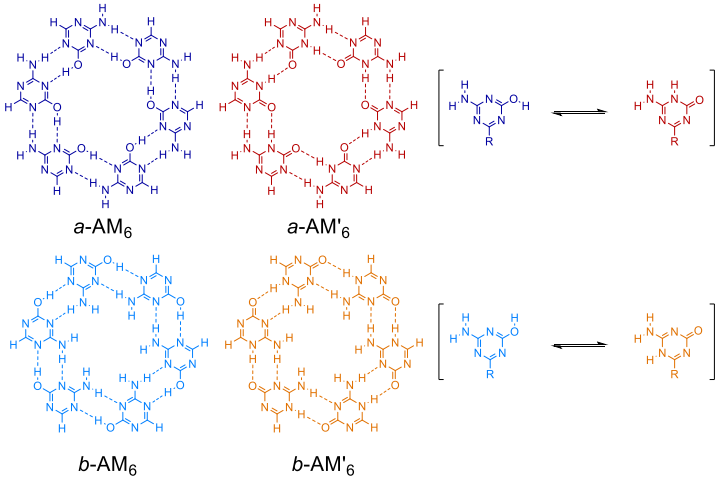

Scheme VI.3. Molecular structures of AM rosettes and monomeric units.

VI.2. Computational Methods

All calculations were performed using the Amsterdam Density Functional (ADF) program developed by Baerends *et al.*,[16] based on dispersion-corrected relativistic density functional theory at the ZORA-BLYP-D3(BJ)/TZ2P level for geometry optimizations and energies,[17] which was shown to accurately reproduce hydrogen bond strengths and structures.[18] The basis set superposition error (BSSE) was not computed because the functional has been developed such that it is essentially free of this effect.[17b] In order to mimic either a surface environment or a stacking arrangement, a planar symmetry (C_s) to all the rosettes was imposed. This approach provides also a clear σ–π separation, which is more informative.

It is known that the solvents can affect the tautomeric equilibrium.[19] In addition, since recognition and assembly processes in aqueous media are still challenging issues for chemists, and water is considered a green solvent by excellence,[20] solvent effects in this medium have been estimated using the conductor-like screening model[21] (COSMO), as implemented in the ADF program.

Bonding energy analysis

The energy of formation of the rosette is defined according to [Eqs. (1 and 2)]:

$$\Delta E_f = E_{\mathrm{R}} - 6\times E_{\mathrm{m}} \tag{1}$$

$$\Delta E_f = \left(E_{\mathrm{R}} - 6\times E_{\mathrm{m}}^{*}\right) + \left[6\times\left(E_{\mathrm{m}}^{*} - E_{\mathrm{m}}\right)\right] = \Delta E_{\mathrm{bond}} + \Delta E_{\mathrm{taut}} \tag{2}$$

where E_{R} is the energy of the rosette with C_1 symmetry and E_{m} the energy of the most stable tautomer conformation of the isolated monomer (see Scheme VI.4). ΔE_{taut} is the energy required for the tautomerization: $E_{\mathrm{m}}^{*} - E_{\mathrm{m}}$.

The bonding energy of the planar system with C_s symmetry is defined as:

$$\Delta E_{\mathrm{bond}}^{C_S} = \Delta E_{\mathrm{bond}} + \Delta E_{C_1 \rightarrow C_S} \tag{3}$$

where $\Delta E_{C_1 \rightarrow C_S}$ is the planarization energy (that is, $E_R^{C_S} - E_R$), that is, the energy needed to go from the global minimum of the rosette to the planar, C_S-symmetric structure.

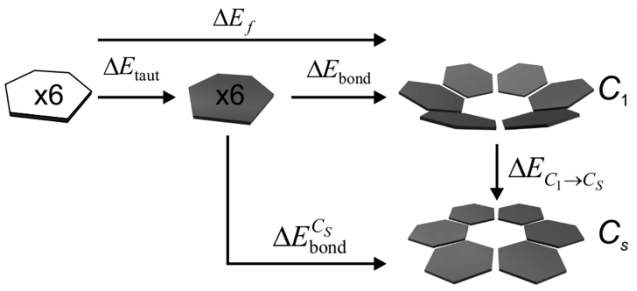

Scheme VI.4. Partition of the bond energy of rosettes (monomers are indicated by hexagons).

The overall planar bond energy is made up of two major components:

$$\Delta E_{bond}^{C_S} = \Delta E_{prep} + \Delta E_{int} \quad (4)$$

In this equation, the preparation energy ΔE_{prep} is the amount of energy required to deform the separate tautomers from their equilibrium structure to the geometry that they acquire in the planar rosette. The interaction energy ΔE_{int} corresponds to the actual energy change when the prepared units are combined to form the rosettes.

All the interaction energy terms were examined in the framework of the Kohn–Sham Molecular Orbital model using a quantitative EDA[14] into electrostatic interaction, Pauli-repulsive orbital interactions, and attractive orbital interactions [Eq. (5)].

$$\Delta E_{int} = \Delta V_{elstat} + \Delta E_{Pauli} + \Delta E_{oi} + \Delta E_{disp} \quad (5)$$

The term ΔV_{elstat} corresponds to the classical electrostatic interaction between the unperturbed charge distributions of the prepared (that is, deformed) units and is usually attractive. The Pauli repulsion ΔE_{Pauli} comprises the destabilizing interactions

between occupied orbitals and is responsible for any steric repulsion. The orbital interaction ΔE_{oi} accounts for charge transfer (that is, donor–acceptor interactions between occupied orbitals on one moiety with unoccupied orbitals of the other, including the HOMO–LUMO interactions) and polarization (empty/occupied orbital mixing on one fragment due to the presence of another fragment). The term ΔE_{disp} accounts for the dispersion corrections. The orbital interaction energy can be further decomposed into the contributions from each irreducible representation Γ of the interacting system [Eq. (6)].

$$\Delta E_{oi} = \Delta E_{\sigma} + \Delta E_{\pi} \tag{6}$$

The cooperativity of the hydrogen-bonded rosettes is quantified by comparing ΔE_{int} (that is, formation of the rosettes from their prepared units) with the sum ΔE_{sum} of the individual pairwise interactions for all possible pairs of units in the rosette (see Scheme VI.5), defined as:

$$\Delta E_{sum} = 6\times\Delta E_{pair} + 6\times\Delta E_{diag} + 3\times\Delta E_{front} \tag{7}$$

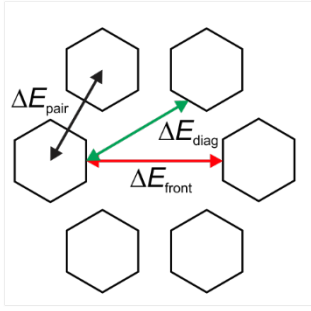

Scheme VI.5. Definition of interaction-energy terms (arrows) in the empty rosette.

Here ΔE_{pair} is the interaction between two hydrogen-bonded molecules in the geometry of the rosette, ΔE_{diag} is the interaction between two mutually diagonally oriented molecules, and ΔE_{front} is the interaction between two frontal molecules.

The synergy ΔE_{syn} that occurs in the rosette motifs is then defined as the difference:

$$\Delta E_{syn} = \Delta E_{int} - \Delta E_{sum} \quad (8)$$

Thus, a negative value of ΔE_{syn} corresponds to a constructive cooperative effect, in other words, the whole is greater than the sum of the parts.

VI.3. Results and Discussion

Structure and relative stability

As was seen in Scheme VI.2 and 3, there are different tautomeric forms of M and AM that can form rosettes, and two conformers in the case of AM (*a*-AM and *b*-AM). Each isomeric form determines a unique hydrogen-bonding motif, so we first studied the relative energies of the isolated tautomers in the gas phase and in water, and then the geometries and stabilities of the single rosettes in both media. Because the outer amino groups do not participate in hydrogen bonds, and thus are not needed for assembly, we simplified our systems by replacing them with hydrogen atoms. In addition, to produce rosettes or nanowires exclusively, it is a current experimental procedure to replace them with long alkylic chains.[1,10] Therefore, one may wonder if this change could affect the relative stabilities. Our results show the same trend whether there is a hydrogen atom or an NH_2 group (see Table 1). The energy differences between the amino-imine tautomers are significant, both in gas phase and in water: up to 27 and 15 kcal mol^{-1}, respectively. This is consistent with experimental findings that the imino-like tautomers of some related compounds have to be obtained by a considerable amount of energy like UV radiation.[22, 23]

In the case of AM, our results are in line with previous computations in gas phase.[12a,c] However, the energetic preference of its hydroxy or carbonyl tautomers has been under debate since the 1950s[24] due to the lack of data in the solid state. It has been shown that the preference for a specific tautomer will depend whether they

are found in the solid state or in solution.[25] Our computations show that the energy difference between the *a*-AM (imidate form) and *a*-AM' (first amide form, protonated at position 1 as shown in Scheme VI.1) is very small, and this is consistent with the fact they may coexist in solution.[12a] The next amide form (*b*-AM'), is 13.1 kcal mol^{-1} and 3.7 kcal mol^{-1} less stable in gas phase and in water, respectively. However, in water, the relative stabilities of AM tautomers are surprisingly reversed. In aqueous media *a*-AM' is now the most stable tautomer, and *a*-AM or *b*-AM are the less stable ones. There are some experimental evidences of ammeline tautomers in the solid state,[24a,b] however, the tautomeric equilibrium of this compound in solution is still unknown.

Table 1. Relative energies (in kcal mol^{-1}) of tautomers

Monomer	Gas phase		Water	
	R = H	R = NH_2	R = H	R = NH_2
M	0.0	0.0	0.0	0.0
M'	24.0	23.1	13.2	12.7
M''	27.6	31.5	15.2	17.6
a-AM	0.0	0.0	7.5	8.2
a-AM'	2.3	0.8	0.0	0.0
b-AM	0.6	0.0	7.4	8.2
b-AM'	13.1	18.7	3.7	6.9

Now we address the situation in the rosettes. The molecular structures without symmetry restrictions are shown in Figure VI.1 and 2, and the bonding energy analysis in gas phase is presented in Table 2 (geometrical parameters are shown in Table S1). It is interesting to note that two molecules could give rise to seven different rosettes with different electronic structures. If we consider the H atoms of the inner and outer hydrogen bond donors, it can be noticed that the structures with primed

labels are the results of moving a proton from one atom to another (see Schemes VI.2 and 3), that is, an intermolecular proton transfer from amine to imine forms (M → M' or M'') and from imidate to amide forms (*a*-AM → *a*-AM', or *b*-AM → *b*-AM'). More interestingly, AM could form two different rosettes depending on the orientation of the –OH group, which could lead to two different functionalities with the same molecule. From Figure VI.1 and 2, one can notice that neither of the global minima are completely planar. They adopt a C_2-symmetric structure, except *a*-AM_6 which assumes a S_6-symmetric one. For instance, there are three general shapes: saddle like shapes (M_6, *a*-AM_6 and *a*-AM'_6), bowl like shapes (*b*-AM_6 and *b*-AM'_6) and irregular or almost planar structures (M'_6 and M''_6). The energy needed to make them planar ($\Delta E_{C_1 \rightarrow C_S}$) is very low, as shown in Table 2; so it could be easily compensated in a stacking environment, due to π-π interactions, or over a surface due to adsorption effects. These results also justify all the analysis of the planar systems.

Table 2. Analysis of the bonding energies (in kcal mol^{-1}) of rosettes in gas phase (ZORA-BLYP-D3(BJ)/TZ2P level of theory).

Rosette	ΔG_f[a]	ΔE_f[b]	ΔE_{taut}[c]	ΔE_{bond}[d]	$\Delta E_{bond}^{C_S}$[e]	$\Delta E_{C_1 \rightarrow C_S}$[f]
M_6	-2.8	-80.3	0.0	-80.3	-79.3	1.0
M'_6	40.4	-36.3	143.8	-180.1	-180.1	0.0
M''_6	58.8	-16.6	165.5	-182.1	-178.9	3.2
a-AM_6	-30.9	-102.5	0.0	-102.5	-101.5	1.0
a-AM'_6	-57.1	-128.4	13.7	-142.2	-141.8	0.3
b-AM_6	-14.6	-86.3	0.0	-90.0	-85.5	4.5
b-AM'_6	-21.1	-90.9	78.5	-169.4	-163.1	6.3

[a] Gibbs free energy of formation of non-symmetric minima. [b] Formation energy. [c] Tautomerization energy. [d] Bonding energy. [e] Planar bond energy. [f] Planarization energy. [Eqs. (1–4)]

Although the bonding energies are much larger for the primed systems, the relative stability of the rosettes is defined by the formation energy. For M'_6 and M''_6, we see

that the tautomerization energy required to get the imine-like structures is very large (see Tables 1 and 2). Thus, M_6 is the most energetically favored, because there is no energetic cost for tautomerization. Although the most stable structure of AM is either *a*-AM or *b*-AM in gas phase, the formation energy indicates that the most stable rosette is *a*-AM'$_6$. Even the rosette of the least stable tautomer *b*-AM'$_6$ is more strongly bound than *b*-AM$_6$ and *a*-AM'$_6$, but again, the tautomerization energy counterbalances the overall energy. In the following section we will show the interplay of the cooperativity.

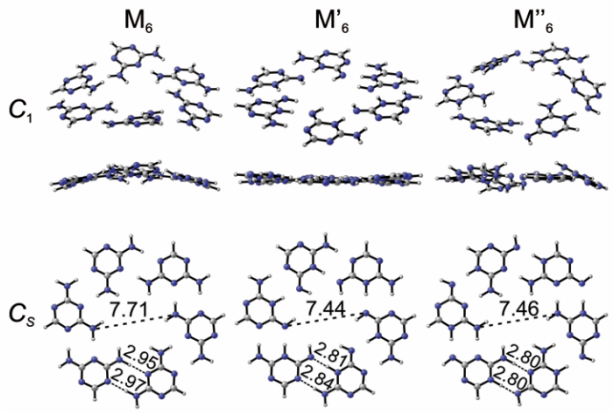

Figure VI.1. Global minima of M rosette-like structures and C_s structures with hydrogen bond lengths [Å]. ZORA-BLYP-D3(BJ)/TZ2P.

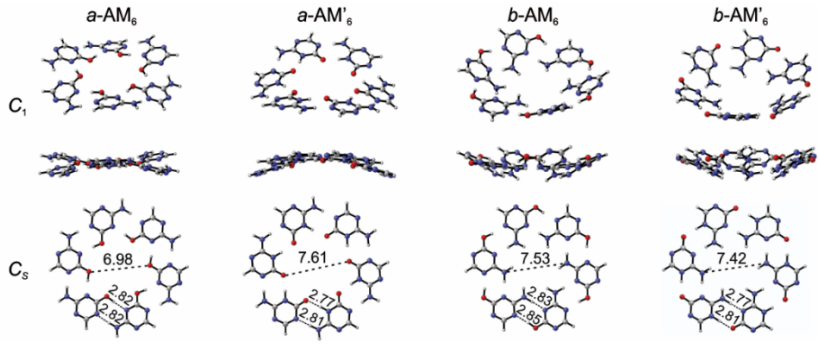

Figure VI.2. Global minima of AM rosette-like structures and C_s structures with hydrogen bond lengths [Å]. ZORA-BLYP-D3(BJ)/TZ2P.

Finally, when we put the systems in water the differences are stressed. The formation energies in water (see Table 3) suggest that only two systems will prevail in solution: M_6 and *a*-AM'$_6$, although *b*-AM'$_6$ could coexist or compete with the later. Despite that ΔE_f^w values for M'$_6$ and M''$_6$ are positive, we have to bear in mind that the bonding energies indicate that they are stable systems. Therefore, unless we provide them the energy needed to overcome the tautomerization barrier, the imine-like rosettes are not accessible.

Table 3. Analysis of the formation energies (in kcal mol^{-1}) of rosettes with C_{2h} symmetry in water. (ZORA-BLYP-D3(BJ)/TZ2P level of theory).

Rosette	ΔE_f^w	ΔE_{taut}^w	ΔE_{bond}^w
M_6	-44.3	0.0	-44.3
M'$_6$	1.6	78.9	-77.3
M''$_6$	16.6	91.3	-74.7
a-AM$_6$	-23.3	44.6	-67.9
a-AM'$_6$	-63.8	0.0	-63.8
b-AM$_6$	-15.3	44.7	-60.0
b-AM'$_6$	-40.5	22.0	-62.6

Cooperativity in gas phase

In previous works on guanine[26] and cyanuric acid[27] cyclic complexes, we showed that when all the H-bonds point in the same direction they experience a large synergetic effect. The origin of this cooperativity is the charge separation occurring due to donor–acceptor interactions in the σ-electron system from monomer to monomer.[26] Herein, when considering the proton transfer in the transitions amino→imine (M → M' or M'') and imidate→amide (*a*-AM → *a*-AM', or *b*-AM → *b*-AM') tautomerisms, cooperativity shows up. Consequently, the primed systems show a larger bonding energy than their amino (M) and imidate counterparts (*a*-AM$_6$

and *b*-AM$_6$), as shown in Table 4. However, there are two energy penalties that will have an impact on the formation energy. Firstly, the most stable monomers have to overcome the tautomerization energy, as was shown in Table 2. The second penalty is the energy needed to deform the isolated tautomers to the geometry they will acquire in the rosette. From Table 4 it can be seen that the preparation energy (deformation) is also larger for imine tautomers, and much lower for the amide forms of AM.

Table 4. Analysis of the bonding energies (in kcal mol^{-1}) of rosettes in gas phase (ZORA-BLYP-D3(BJ)/TZ2P level of theory).

Rosette	$\Delta E_{\text{bond}}^{CS}$	ΔE_{prep}	ΔE_{int}	ΔE_{pair}	ΔE_{diag}	ΔE_{front}	ΔE_{syn}
M$_6$	-79.3	7.4	-86.8	-14.3	0.0	0.1	-1.8
M'$_6$	-180.1	24.6	-204.7	-21.5	-2.4	-1.2	-57.8
M''$_6$	-178.9	33.5	-212.4	-22.2	-1.8	-0.8	-66.2
a-AM$_6$	-101.5	19.2	-120.7	-19.7	-0.1	0.0	-1.9
a-AM'$_6$	-141.8	19.3	-161.1	-17.4	-1.7	-0.8	-44.6
b-AM$_6$	-85.5	15.6	-101.1	-16.8	0.4	0.4	-3.7
b-AM'$_6$	-163.1	25.7	-188.8	-19.5	-1.7	-0.7	-59.8

The interplay between cooperativity, tautomerization and preparation energy determine the final outcome. Therefore, ammeline is the only case in which the tautomerization energy of the first amide form (*a*-AM'$_6$) is sufficiently low to be overcome by the large synergy. For example, the synergy of *b*-AM'$_6$ is 15 kcal mol^{-1} greater than that of *a*-AM'$_6$, but again, the former has to pull against big tautomerization and preparation energies. Since *a*-AM'$_6$ is the most stable rosette in gas phase and in water, which also has the additional factor of a large cooperativity effect, AM seems to be a better candidate than M for designing self-assembling rosettes.

Energy decomposition analysis

Ammeline is the first hydrolysis product of melamine. Thus, the main difference between M_6 and *a*-AM_6/*b*-AM_6 is just one functional group, $-NH_2$ in the former and –OH in the later. While there is almost zero cooperativity in *a*-AM_6 and *b*-AM_6, these rosettes are more strongly bound than M_6. For instance, the bonding energy difference between *a*-AM_6 and M_6 is 22.2 kcal mol^{-1}, between *b*-AM_6 and M_6 the difference is 6.2 kcal mol^{-1} (see Table 4). The ΔE_{int} of the dimers is also larger for AM (see also Table 4). Because cooperativity is not such an important factor as it is in guanine and xanthine quartets,[26] this difference can only be explained on the basis of the pair interaction energies and their individual energy contributions.

As we saw that the energy of formation of the dimers is important for determining the stabilization of the rosette, we have computed the interaction energy profiles for the most stable dimers in gas phase (M_2, *a*-AM_2 and *b*-AM_2), which contain benzenoid-type rings and are comparable electronically. A potential energy surface scan was performed over the hydrogen bond distances according to the procedure presented in ref [28]. Then we have decomposed the ΔE_{int} in every step into physically meaningful energy terms that contributes to the hydrogen bond energy: electrostatic, steric interactions and covalence. The results are plotted in Figure VI.3.

Both AM dimers show stronger pair interaction energies than M for the same distances. Although the differences among attractive terms is almost negligible, M_2 shows a stronger electrostatic contribution but *a*-AM_2 shows a greater orbital component. Nevertheless, the decisive factor is the Pauli repulsion. Despite some small variations, these findings are in line with previous results for similar systems,[28] in which Pauli repulsion determines the hydrogen bond strength.

Source and mechanism of cooperativity

Finally, to explore the basis of the cooperativity mechanism of M and AM rosettes, we used the same approach as for the four-membered rosettes of guanine[26] and N-

halo-guanine.[29] The method consists in the construction of the rosette starting from the monomer, and stepwise adding more monomers till complete the cycle, as shown in Scheme VI.6. This also allows us to investigate whether the source of cooperativity in these rosettes is similar as that in the guanine quartets.

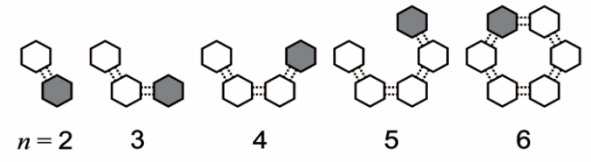

Scheme VI.6. Formation of the rosette in five steps by a stepwise addition of monomers (*m*) in one-way direction: $m_n + m$ (with n = 1, 2, 3, 4, 5). The grey-shaded hexagons represent the incoming *m*.

We decomposed therefore the interaction energy in every step, and then we computed the synergy in each energy component by applying [Eqns. (6) and (7), see Computational Methods]. To illustrate this, the synergy in the electrostatic component of *a*-AM'$_6$ is computed as follow:

$$\Delta E_{\text{syn, elstat}} = \left[\sum_{n=1}^{5} \Delta V_{\text{elstat}}(a\text{-AM}'_{n+1})\right] - \left(6\times\Delta V_{\text{elstat, pair}} + 6\times\Delta V_{\text{elstat, diag}} + 6\times\Delta V_{\text{elstat, front}}\right)$$

Results for *a*-AM'$_{n+1}$, the rosette with the largest formation energy, are presented in Table 5. The values for M'$_{n+1}$, M''$_{n+1}$ and *b*-AM'$_{n+1}$ are collected in Tables S2-S4. From Table 5 we can infer that every component increases progressively with the addition of monomers due to the cooperativity phenomenon. The interaction energy per monomer added increases from –17.4 to –30.5 kcal mol^{-1}, a strengthening of 13.1 kcal mol^{-1}. The addition of the last monomer leads to the formation of two pairs of hydrogen bonds, which correspond to an ΔEint per molecular unit of –31.4 kcal mol^{-1}.

The energy decomposition analysis shows that the synergy in these rosettes is made up of 52% electrostatic, and 36 and 12% of orbital interactions in the σ and π-

electron systems, respectively. The same behavior is observed in M'$_6$, M''$_6$ and *b*-AM'$_6$ (see Tables S2-S4). However, their synergy in the σ-electron system is even greater: –21.9, –26.5 and –22.1 kcal mol^{-1} respectively.

Table 5. Energy decomposition (kcal mol^{-1}) for the formation of *a*-AM'$_{n+1}$ from *a*-AM'$_n$ + *a*-AM' in stepwise one-way direction (n = 1, 2, 3, 4, 5).

n + 1	ΔE_{int}	ΔV_{elstat}	ΔE_{Pauli}	ΔE_{oi}		ΔE_{disp}
				ΔE_σ	ΔE_π	
1 + 1	-17.4	-30.6	36.6	-17.3	-1.8	-4.4
2 + 1	-23.9	-35.7	37.5	-19.1	-2.2	-4.5
3 + 1	-26.8	-37.9	37.8	-19.8	-2.4	-4.5
4 + 1	-30.5	-40.7	37.9	-20.4	-2.7	-4.5
5 + 1	-62.7	-75.1	73.4	-44.8	-7.3	-8.9
ΔE_{syn}	-44.6	-24.9	3.5	-17.5	-5.7	0.0

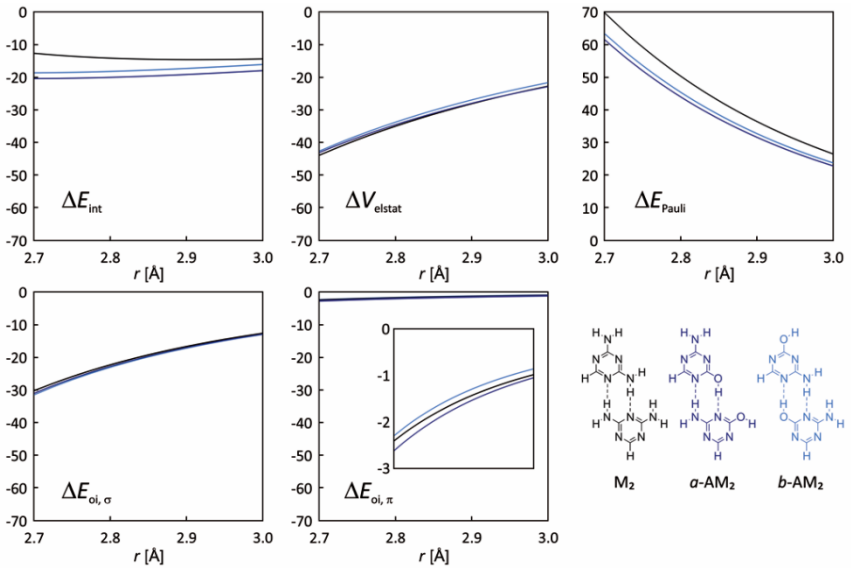

Figure VI.3. Decomposed energy terms [kcal mol^{-1}] as a function of the hydrogen-bond distance r [Å] for M_2, a-AM_2, and b-AM_2. The dimers were optimized along the constrained hydrogen bond distances at the BLYP-D3(BJ)/TZ2P level of theory.

The mechanism of the cooperativity is reexamined and explained by analyzing the charge redistribution within the construction shown in Scheme VI.6. The pair formation leads to donor-acceptor orbital interactions between lone-pair (LP) orbitals and N–H antibonding acceptor orbitals: $\sigma_{LP} \rightarrow \sigma^*_{N-H}$. Throughout the stepwise addition of monomers, the charge separation is gradually and monotonically increased, as shown in Figure VI.4 with the VDD atomic charges of the front atoms and the total VDD charge of the monomers. The net charge of the frontier protons experiences an average increment of 17%, whilst the net charge of the hydrogen bond acceptor atoms decreases ~14%. Furthermore, the monomers with the hydrogen bond acceptors becomes gradually more negatively charged and the monomers with the hydrogen bond donors more positively charged. This has two consequences: 1) it improves the electrostatic attraction with additional monomers, and 2) the LP orbital σ_{HOMO} of the hydrogen bond acceptor is destabilized and goes up in energy and, contrarily, the antibonding orbital σ_{LUMO} of the hydrogen bond donor is stabilized; as shown in Figure VI.5. As a consequence, the σ_{HOMO} and σ_{LUMO} orbitals become better partners for donor-acceptor interactions every time a monomer is added to the cycle.

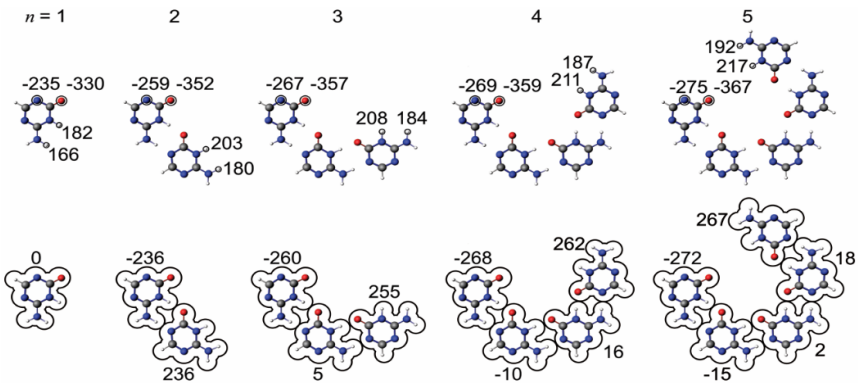

Figure VI.4. Top: VDD atomic charges [milli-atomic units] of the front atoms of a-AM'$_n$, in the geometry they adopt in the C_{2h}-symmetric orbitals. Down: Total VDD charges of a-AM'$_n$.

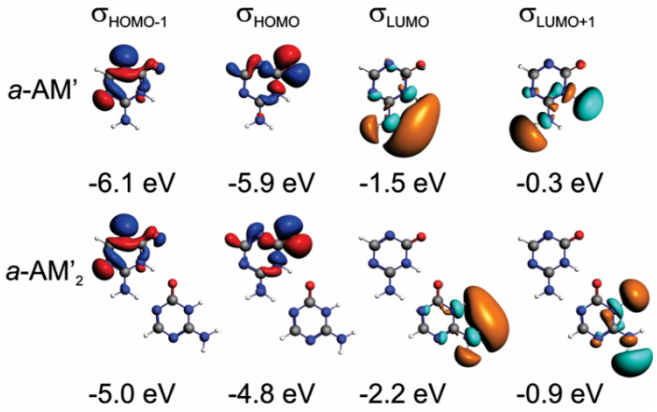

Figure VI.5. Oxygen (σ_{HOMO}), Nitrogen lone-pair orbitals (σ_{HOMO-1}) and N–H unoccupied orbitals (σ_{LUMO} and σ_{LUMO+1}), and their energies [eV] of the front atoms of *a*-AM' and *a*-AM'$_2$. ZORA-BLYP-D3(BJ)/TZ2P level of theory. (See also Figures S1 and S2 in supporting information).

VI.4. Conclusions

In this contribution we have given a theoretical background for design principles of supramolecular systems. Through our DFT-D calculations we have pinpointed the factors that make ammeline a more robust building block against melamine for constructing self-assembling rosettes. Our results show that the most stable structures, in gas phase and in water solution, are those of melamine in its amino-like form (M_6) and ammeline in its amide-like form (protonated at position 1, *a*-AM'). Unlike M, the most stable rosettes of AM show great synergy effects and thus strong binding energies. Besides that, AM also display larger pair interactions. Therefore, these positive factors can be exploited by chemists in non-covalent synthesis approaches. Furthermore, if it would be experimentally possible to control the selectivity of both amide forms of AM rosettes, our results show that it would be possible to get two materials with different properties.

The mechanism of the cooperativity phenomenon was proven to be the same as that in guanine and N-halo-guanine quartets: namely, the charge separation in the s electronic system caused by the donor-acceptor interactions between the lone pairs on

the proton acceptor and the unoccupied orbitals on the proton donor groups. This charge separation is the mechanism for the enhancement of the electrostatic interaction as well as the s orbital interactions. In the rosettes studied herein, the electrostatic component represents an average contribution of 50% of the total synergy, while the σ and π orbital interactions contribute with 40% and 10% to the synergy, respectively. Our findings prove synergy can be used as a tool to improve self-assembly in supramolecular chemistry.

VI.5. References

(1) a) S. I. Stupp, L. C. Palmer, *Chem. Mater.* **2014**, *26*, 507–518. b) M. J. Mayoral, N. Bilbao, D. González-Rodríguez, *ChemistryOpen* **2016**, *5*, 10–32. c) R. L. Beingessner, Y. Fan, H. Fenniri, *RSC Adv.* **2016**, *6*, 75820–75838. d) B. Adhikari, X. Lin, M. Yamauchi, H. Ouchi, K. Aratsu, S. Yagai, *Chem. Commun.* **2017**, *53*, 9663–9683.

(2) Guanine Quartets: Structure and Application, (Eds.: W. Fritzsche, L. Spindler), RSC Publishing, Cambridge, 2012.

(3) a) A. Kohlmeier, L. Vogel, D. Janietz, *Soft Matter* **2013**, *9*, 9476–9486. b) L. Niu, J. Song, J. Li, N. Tao, M. Lu, K. Fan, *Soft Matter* **2013**, *9*, 7780. c) V. Venkatesh, N. K. Mishra, I. Romero-Canelón, R. R. Vernooij, H. Shi, J. P. C. Coverdale, A. Habtemariam, S. Verma, P. J. Sadler, *J. Am. Chem. Soc.* **2017**, *139*, 5656–5659.

(4) A. P. H. J. Schenning, P. Jonkheijm, F. J. M. Hoeben, J. Van Herrikhuyzen, S. C. J. Meskers, E. W. Meijer, L. M. Herz, C. Daniel, C. Silva, R. T. Phillips, R.H. Friend, D. Beljonne, A. Miura, S. De Feyter, M. Zdanowska, H. Uji-i, F.C. De Schryver, Z. Chen, F.Würthner, M. Mas-Torrent, D. den Boer, M. Durkut, P. Hadley, *Synth. Met.* **2004**, *147*, 43–48.

(5) H. Diem, G. Matthias, R. A. Wagner in *Amino Resins. Ullmann's Encyclopedia of Industrial Chemistry*, Wiley-VCH Verlag GmbH & Co. KGaA, Weinheim, Germany, **2010**.

(6) B. Roy, P. Bairi, A. K. Nandi, *RSC Adv.* **2014**, *4*, 1708.

(7) a) P. A. Staniec, L. M. A. Perdigão, B. L. Rogers, N. R. Champness, P. H. Beton, *J. Phys. Chem. C* **2007**, *111*, 886–893. b) W. Xu, M. Dong, H. Gersen, E. Rauls, S. Vázquez-Campos, M. Crego-Calama, D. N. Reinhoudt, I. Stensgaard, E. Laegsgaard, T. R. Linderoth, F. Besenbacher, *Small* **2007**, *3*, 854–8. c) F. Silly, A. Q. Shaw, M. R. Castell, G. a. D. Briggs, M. Mura, N. Martsinovich, L. Kantorovich, *J. Phys. Chem. C* **2008**, *112*, 11476–11480. d) M. Mura, N. Martsinovich, L. Kantorovich, *Nanotechnology* **2008**, *19*, 465704. e) H. Zhang, Z. Xie, L. Long, H. Zhong, W. Zhao, B.-W. Mao, X. Xu, L.-S. Zheng, *J. Phys. Chem. C* **2008**, *111*, 4209–4218.

(8) a) H. -M. Zhang, Z. -K. Pei, Z. -X. Xie, L.-S. Long, B.-W. Mao, X. Xu, L. -S. Zheng. *J. Phys. Chem. C* **2009**, *113,* 13940–13946. b) A. Ciesielski, S. Haar, G. Paragi, Z. Kupihár, Z. Kele, S. Masiero, C. Fonseca Guerra, F. M. Bickelhaupt, G. P. Spada, L. Kovács, P. Samorì, *Phys. Chem. Chem. Phys.* **2013**, *15*, 12442.

(9) a) N. Katsonis, H. Xu, R. M. Haak, T. Kudernac, Ž. Tomović, S. George, M. Van Der Auweraer, A. P. H. J. Schenning, E. W. Meijer, B. L. Feringa, S. De Feyter, *Angew. Chemie - Int. Ed.* **2008**, *47*, 4997–5001. b) A. Minoia, Z. Guo, H. Xu, S. J. George, A. P. H. J. Schenning, S. De Feyter, R. Lazzaroni, *Chem. Commun.* **2011**, *47*, 10924–10926

(10) a) P. Jonkheijm, A. Miura, M. Zdanowska, F. J. M. Hoeben, S. De Feyter, A. P. H. J. Schenning, F. C. De Schryver, E. W. Meijer, *Angew. Chemie - Int. Ed.* **2004**, *43*, 74–78. b) K. E. Maly, C. Dauphin, J. D. Wuest, *J. Mater. Chem.* **2006**, *16*, 4695.

(11) S. Yagai, S. Mahesh, Y. Kikkawa, K. Unoike, T. Karatsu, A. Kitamura, A. Ajayaghosh, *Angew. Chem.* **2008**, *120*, 4769 –4772.

(12) a) Y. Wang, C. U. Pittman, Jr., S. Saebo, *J. Org. Chem.* **1993**, *58*, 3085–3090. b) Y. H. Jang, S. Hwang, S. B. Chang, J. Ku, D. S. Chung, *J. Phys. Chem. A* **2009**, *113*, 13036–13040. c) M. Hatanaka, *J. Phys. Chem. A* **2015**, *119*, 1074−1086.

(13) a) F. M. Bickelhaupt and E. J. Baerends, in *Reviews in Computational Chemistry*, *Vol. 15* (Eds.: K. B. Lipkowitz, D. B. Boyd), Wiley-VCH, New York, **2000**, pp. 1–86. b) R. Stowasser, R. Hoffmann, *J. Am. Chem. Soc.* **1999**, *121*, 3414–3420; c) E. J. Baerends, O. V. Gritsenko and R. Van Meer, *Phys. Chem. Chem. Phys.* **2013**, *15*, 16408–16425.

(14) T. Ziegler, A. Rauk, *Inorg. Chem.* **1979**, *18*, 1558–1565.

(15) C. Fonseca Guerra, J.-W. Handgraaf, E. J. Baerends and F. M. Bickelhaupt, *J. Comput. Chem.* **2004**, *25*, 189–210.

(16) a) G. te Velde, F. M. Bickelhaupt, E. J. Baerends, S. J. A. van Gisbergen, C. Fonseca Guerra, J. G. Snijders and T. Ziegler, *J. Comput. Chem.* **2001**, *22*, 931–967. b) E. J. Baerends, T. Ziegler, J. Autschbach, D. Bashford, A. Bérces, F. M. Bickelhaupt, C. Bo, P. M. Boerrigter, L. Cavallo, D. P. Chong, L. Deng, R. M. Dickson, D. E. Ellis, M. van Faassen, L. Fan, T. H. Fischer, C. Fonseca Guerra, A. Ghysels, A. Giammona, S. J. A. van Gisbergen, A. W. Gçtz, J. A. Groeneveld, O. V. Gritsenko, M. Grüning, S. Gusarov, F. E. Harris, P. van den Hoek, C. R. Jacob, H. Jacobsen, L. Jensen, J. W. Kaminski, G. van Kessel, F. Kootstra, A. Kovalenko, M. V. Krykunov, E. van Lenthe, D. A. McCormack, A. Michalak, M. Mitoraj, J. Neugebauer, V. P. Nicu, L. Noodleman, V. P. Osinga, S. Patchkovskii, P. H. T. Philipsen, D. Post, C. C. Pye, W. Ravenek, J. I. Rodríguez, P. Ros, P. R. T. Schipper, G. Schreckenbach, J. S. Seldenthuis, M. Seth, J. G. Snijders, M. Solà, M. Swart, D. Swerhone, G. te Velde, P. Vernooijs, L. Versluis, L. Visscher, O. Visser, F. Wang, T. A. Wesolowski, E. M. van Wezenbeek, G. Wiesenekker, S. K. Wolff, T. K. Woo, A. L. Yakovlev, ADF2014.01, SCM, Theoretical Chemistry, Vrije Universiteit, Amsterdam, The Netherlands, http://www.scm.com.

(17) a) S. Grimme, J. Antony, S. Ehrlich, H. Krieg, *J. Chem. Phys.* **2010**, *132*, 154104. b) S. Grimme, S. Ehrlich, L. Goerigk, *J. Comput. Chem.* **2011**, *32*, 1456–1465. c) S. Grimme, *J. Comput. Chem.* **2004**, *25*, 1463–1473. d) S. Grimme, *J. Comput. Chem.* **2006**, *27*, 1787–1799.

(18) a) C. Fonseca Guerra, T. van der Wijst, J. Poater, M. Swart, F. M. Bickelhaupt, *Theor. Chem. Acc.* **2010**, *125*, 245–252. b) T. van der Wijst, C. Fonseca Guerra, M. Swart, F. M. Bickelhaupt, B. Lippert, *Angew. Chemie Int. Ed.* **2009**, *48*, 3285–3287.

(19) a) Y. Connolly Martin, *J. Comput. Aided. Mol. Des.* **2009**, *23*, 693–704. b) Roger A. Sayle, *J. Comput. Aided. Mol. Des.* **2010**, *24*, 485–496.

(20) a) T. H. Rehm, C. Schmuck, *Chem. Soc. Rev.* **2010**, *39*, 3597. b) M. Ma, D. Bong, *Langmuir* **2011**, *27*, 8841–53. c) B. J. Cafferty, I. Gállego, M. C. Chen, K. I. Farley, R. Eritja, N. V. Hud, *J. Am. Chem. Soc.* 2013, *135*, 2447–2450.

(21) a) A. Klamt and G. Schüürmann, *J. Chem. Soc., Perkin Trans. 2* **1993**, *799.* b) A. Klamt, *J. Phys. Chem.* **1995**, *99*, 2224. c) C. C. Pye, T. Ziegler, *Theor. Chem. Acc.* **1999**, *101*, 396.

(22) N. Akai, T. Harada, K. Shin-ya, K. Ohno, M. Aida, *J. Phys. Chem. A* **2006**, *110*, 6016–6022.

(23) I. Reva, M. J. Nowak, L. Lapinski, R. Fausto, *J. Phys. Chem. B* **2012**, *116*, 5703–5710.

(24) a) W. M. Padgett, W. F. Hamner, *J. Am. Chem. Soc.* **1958**, *80*, 803–808. b) B. V. Lotsch, W. Schnick, *Z. Anorg. Allg. Chem.* **2006**, *632*, 1457–1464.

(25) P. V. Bernhardt, E. J. Hayes, *Inorg. Chem.* **1998**, *37,* 4214–4219.

(26) C. Fonseca Guerra, H. Zijlstra, G. Paragi, F. M. Bickelhaupt, *Chem. - A Eur. J.* **2017**, *17*, 12612–12622.

(27) A. N. Petelski, N. M. Peruchena, S. C. Pamies, G. L. Sosa, *J. Mol. Model.* **2017**, *23*, 263.

(28) S. C. C. van der Lubbe, C. Fonseca Guerra. *Chem. - A Eur. J.* **2017**, *23*, 10249–10253.

(29) L. P. Wolters, N. W. G. Smits, C. Fonseca Guerra, *Phys. Chem. Chem. Phys.* **2015**, *17*, 1585–1592.

Table S1. Geometrical parameters (in Å) of single rosettes with C_{2h} symmetry (ZORA-BLYP-D3(BJ)/TZ2P level of theory)

Rosette	gas phase			water		
	d_i(D···A)[a]	d_o(D···A) [b]	d_{hole}[c]	d_i(D···A)	d_o(D···A)	d_{hole}
M_6	2.95	2.97	7.71	2.97	2.98	7.66
M'_6	2.81	2.84	7.44	2.84	2.86	7.45
M''_6	2.80	2.80	7.46	2.83	2.83	7.46
a-AM_6	2.82	2.82	6.98	2.80	2.82	7.08
a-AM'_6	2.84	2.81	7.61	2.89	2.83	7.38
b-AM_6	2.83	2.85	7.53	2.83	2.83	7.22
b-AM'_6	2.77	2.81	7.42	2.81	2.88	7.37

[a] Average inner hydrogen bond distances D(H)···A. [b] Average outer hydrogen bond distances D(H)···A. [c] Average diameter of the cavity taken between the nitrogen/oxygen atoms.

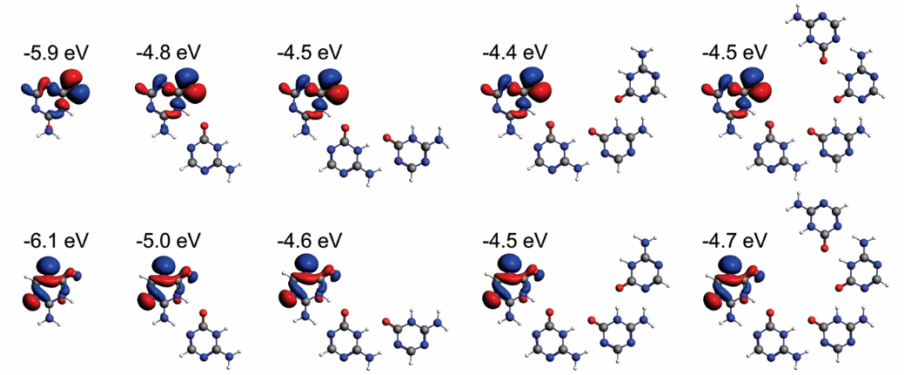

Figure S1. Oxigen (top) and Nitrogen (down) lone-pair orbitals and their energies [eV] of the front atoms of *a*-AM'$_n$ (n = 1, 2, 3, 4, 5) in the geometry they adopt in the C_{2h}-symmetric structure, computed at the BLYP-D/TZ2P level of theory

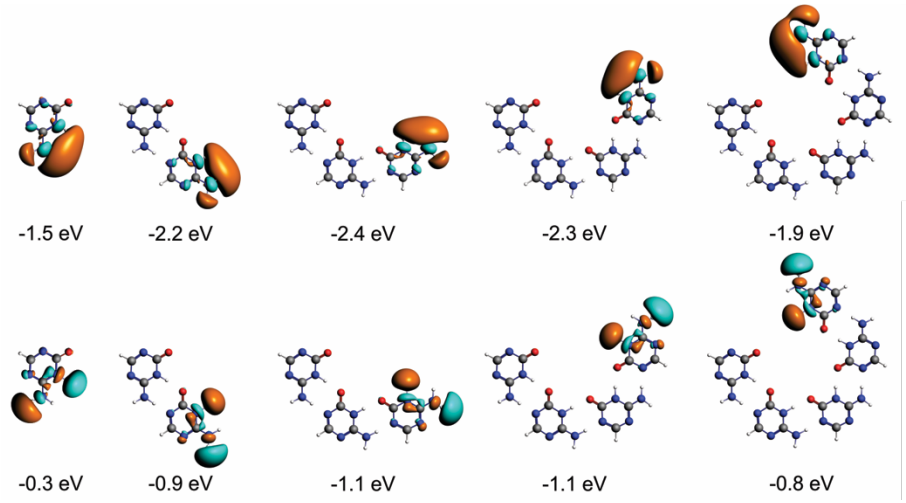

Figure S2. Top: Unoccupied orbitals of the N–H bonds (σ_{LUMO}) and their energies [eV] of the front atoms. Down: σ_{HOMO-1} orbitals and their energies [eV] of the front atoms. ZORA-BLYP-D3(BJ)/TZ2P level of theory.

Table S2. Energy decomposition for the formation of M'$_n$ from M'$_{n-1}$ + M' in stepwise one-way direction (n = 2, 3, 4, 5, 6).

Steps	ΔE_{int}	ΔV_{elstat}	ΔE_{Pauli}	ΔE_{oi}		ΔE_{disp}
				ΔE_{σ}	ΔE_{π}	
M'$_2$	-21.5	-38.4	46.2	-21.8	-2.1	-5.3
M'$_3$	-30.0	-43.2	45.3	-23.7	-2.9	-5.4
M'$_4$	-34.0	-45.6	45.0	-24.7	-3.3	-5.5
M'$_5$	-39.2	-48.8	45.0	-25.6	-4.3	-5.5
M'$_6$	-80.0	-95.9	93.7	-57.5	-9.5	-10.9
ΔE_{syn}	-57.8	-24.5	-2.3	-21.9	-9.2	0.0

Table S3. Energy decomposition for the formation of M''$_n$ from M''$_{n-1}$ + M'' in stepwise one-way direction (n = 2, 3, 4, 5, 6).

Steps	ΔE_{int}	ΔV_{elstat}	ΔE_{Pauli}	ΔE_{oi}		ΔE_{disp}
				ΔE_{σ}	ΔE_{π}	
M''$_2$	-22.2	-41.6	53.2	-25.5	-2.8	-5.5
M''$_3$	-30.8	-48.2	54.6	-28.1	-3.6	-5.6
M''$_4$	-34.9	-50.9	54.9	-29.3	-4.1	-5.6
M''$_5$	-39.8	-54.7	55.3	-30.4	-4.3	-5.7
M''$_6$	-84.7	-102.1	106.8	-66.3	-11.8	-11.3
ΔE_{syn}	-66.2	-35.9	5.5	-26.4	-9.5	0.0

Table S4. Energy decomposition for the formation of *b*-AM'$_n$ from *b*-AM'$_{n-1}$ + *b*-AM' in stepwise one-way direction (n = 2, 3, 4, 5, 6).

Steps	ΔE_{int}	ΔV_{elstat}	ΔE_{Pauli}	ΔE_{oi}		ΔE_{disp}
				ΔE_{σ}	ΔE_{π}	
b-AM'$_2$	-19.5	-35.7	44.5	-20.9	-2.4	-5.0
b-AM'$_3$	-27.5	-39.7	43.4	-22.9	-3.1	-5.1
b-AM'$_4$	-31.0	-41.7	43.0	-23.8	-3.4	-5.2
b-AM'$_5$	-35.6	-44.6	42.9	-24.7	-3.9	-5.3
b-AM'$_6$	-75.2	-88.7	89.1	-55.5	-9.7	-10.3
ΔE_{syn}	-59.8	-25.1	-4.5	-22.1	-8.2	0.0

VII. MELAMINE AND AMMELINE ROSETTES FOR SELECTIVE ION RECOGNITION

"Persist and believe in your vision even if it defies an accepted norm. Originality and hard work are the two things that are important"

Martin Karplus

To be submitted

VII.1. Introduction

Non-covalent synthesis is an elegant approach in supramolecular chemistry to construct highly complex structures with well-defined properties.[1] Their strategies require a fundamental understanding of molecular interactions as well as the thermodynamics of the process. Thus, by manipulating and tuning intermolecular forces chemists could master the controlled design of new materials. That is why the physicochemical information about structural issues and interaction properties, which can be obtained by theoretical calculations, constitute a valuable background for experimentalists.[2]

An emerging topic in the field of supramolecular chemistry is the use of cyclic rosette complexes[3] to build large structures. In this context, 1,3,5-triazine-2,4,6-triamine or melamine (M), which is also very well-known for its uses in the plastic industry,[4] has been considered a very versatile building block for creating a great diversity of sophisticated functional materials.[5] Their rosettes can stack on top of each other to form one dimensional wires or columnar arrays,[6] and 3D network structures.[7] Besides, self-assembled monolayers of melamine and some related compounds over Au(111)[8] and highly oriented pyrolytic graphite[9] surfaces have also been obtained and characterized. These materials could have potential applications in the

functionalization of surfaces,[10] hydrogels,[11] non-covalent polymers and nanoelectronics.[12]

On the other hand, it is known that the presence of ions induces a change on the hydrogen-bonding pattern,[13] and they can assist the self-assembly process.[14] For instance, guanine (G) molecules self-assemble in quartets by the inclusion of a K^+ cation in the center.[15] They can also form the well-known G-quadruplexes (GQ), which are arranged by three or four stacked layers of G-quartets with cations in between. Even more, Kotlyar *et al.*[16] have obtained long G-wires, with and without potassium cations in between, with promising applications in nanoelectronics. However, when it comes to anions, there are just a few examples in the literature about anion recognition by supramolecules itself. The first cases in this context are the Adenine quartets, which were shown to coordinate F^-, Cl^- and Br^-.[17] Then, Paragi *et al.*[18] have proposed with theoretical predictions that 7-methyl-guanine cyclic rings are also able to coordinate anions like Cl^-, Br^- and NO^{3-}.

In the previous chapter, we have shown that ammeline (AM) has a stronger self-assembling capacity than melamine (M). This is due to a stronger pair interactions and the fact that AM rosettes experience a considerable synergetic effect. In this work, we investigated if M or AM can coordinate ions in the same way as GQs and G-wires coordinate cations. With this aim, we have explored a model set of seven rosette like supramolecules, as shown in Schemes 1 and 2, and their interactions with various monovalent anions (Cl^-, Br^- and I^-) as well as cations (Na^+, K^+ and Rb^+). The computations are based on dispersion-corrected density functional theory (DFT-D). Our investigations cover the situation of single rosettes and stacked complexes. In both cases, we also consider conditions in gas phase and aqueous solution.

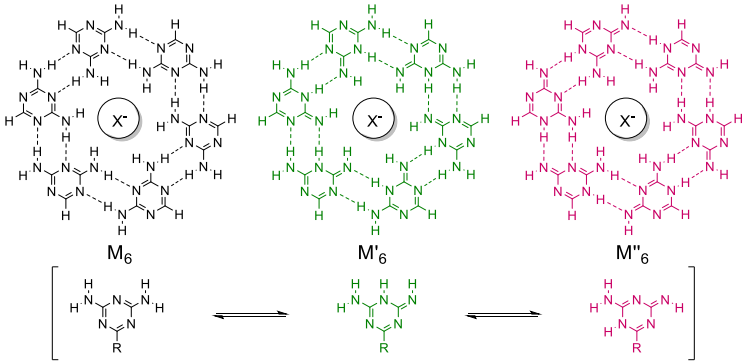

Scheme 1. Molecular structures of M rosettes. $X^- = Cl^-, Br^-, I^-$

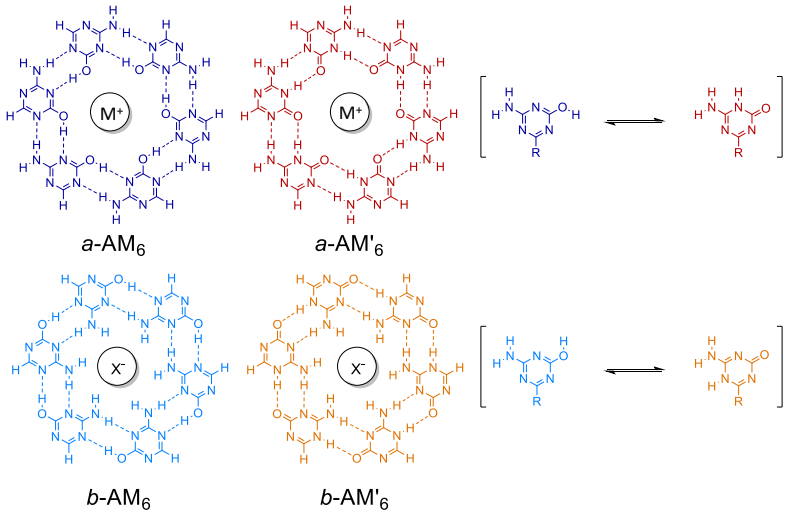

Scheme 2. Molecular structures of AM rosettes. $M^+ = Na^+, K^+, Rb^+$ and $X^- = Cl^-, Br^-, I^-$

VII.2. Computational Methods

All calculations were performed using the Amsterdam Density Functional (ADF) program developed by Baerends *et al.*,[19] based on dispersion-corrected relativistic density functional theory at the ZORA-BLYP-D3(BJ)/TZ2P level for geometry optimizations and energies,[20] which was shown to accurately reproduce hydrogen bond strengths and structures.[21] In order to mimic either a surface environment or a stacking arrangement, a planar symmetry (C_s) was imposed on the rosettes. This

approach provides also a clear σ–π separation, which is more informative. The stacked systems were optimized with C_2 symmetry enforced.

Since recognition and assembly processes in aqueous media are still challenging issues for chemists, and water is considered a green solvent by excellence,[22] solvent effects in this medium have been estimated using the conductor-like screening model[16a,23] (COSMO), as implemented in the ADF program. Radii of anions and cations have been computed according to the procedure presented in ref. (16a) to reproduce the solvation energy of the cation. Gibbs free energy of solvation and formation were computed at the ZORA-BLYP-D3(BJ)/DZP.

Bonding energy analysis

We defined the energy of formation of the rosette according to [Eq. (1)]:

$$\Delta E_f = \mathrm{E}_{\mathrm{R@I}} - n \times E_{\mathrm{m}} - E_{\mathrm{I}} \quad (1)$$

where $E_{\mathrm{R@I}}$ is the energy of the rosette with a specific symmetry (either C_S or C_2), n the number of monomers (either 6 or 12), E_{m} the energy of the most stable tautomer conformation of the isolated monomer and E_{I} the energy of the isolated ion; therefore, this equation expresses the relative stability of the rosettes.

The bonding energy is defined as:

$$\Delta E_{\mathrm{bond}}^{C\mathrm{X}} = E_{\mathrm{R@I}} - n \times E_{\mathrm{m}}^{*} - E_{\mathrm{I}} \quad (2)$$

here, E_{m}^{*} is the energy of the isolated tautomer. The superscript C_{X} is either C_{S} or C_2 symmetry. Then, the overall bonding energy is made up of two major components:

$$\Delta E_{\mathrm{bond}}^{C\mathrm{X}} = \Delta E_{\mathrm{prep}} + \Delta E_{\mathrm{int}} \quad (3)$$

The preparation energy ΔE_{prep} is the amount of energy required to deform the

separate tautomers from their equilibrium structure to the geometry that they acquire in the rosette. The interaction energy ΔE_{int} corresponds to the actual energy change when the prepared units are combined to form the rosettes.

All the interaction energy terms were examined in the framework of the Kohn–Sham Molecular Orbital model using a quantitative energy decomposition analysis[24] (EDA) into electrostatic interaction, Pauli-repulsive orbital interactions, and attractive orbital interactions:

$$\Delta E_{int} = \Delta V_{elstat} + \Delta E_{Pauli} + \Delta E_{oi} + \Delta E_{disp} \quad (5)$$

The term ΔV_{elstat} corresponds to the classical electrostatic interaction between the unperturbed charge distributions of the prepared (that is, deformed) units and is usually attractive. The Pauli repulsion ΔE_{Pauli} comprises the destabilizing interactions between occupied orbitals and is responsible for any steric repulsion. The orbital interaction ΔE_{oi} accounts for charge transfer (that is, donor–acceptor interactions between occupied orbitals on one moiety with unoccupied orbitals of the other, including the HOMO–LUMO interactions) and polarization (empty/occupied orbital mixing on one fragment due to the presence of another fragment). The term ΔE_{disp} accounts for the dispersion corrections. The orbital interaction energy can be further decomposed into the contributions from each irreducible representation Γ of the interacting system [eqn (6)].

$$\Delta E_{oi} = \Delta E_{\sigma} + \Delta E_{\pi} \quad (6)$$

VII.3. Results and discussion

VII.3.1. Rosettes with central ion

In this section we address the situation in a surface environment, under the constraint of C_{2h} symmetry, and the capacity of the systems to coordinate anions or cations.

Structure and relative stabilities

In Chapter VI, we have already established that, among all tautomers, M_6 and *a*-AM'$_6$ are the most stable rosettes both in gas phase and in water. As shown in Tables 1a and b, the formation energies suggest, again, that the most stable systems are $M_6@X^-$ and *a*-AM'$_6@M^+$, either in gas phase or in water. With regards to the other tautomers, the ions add an extra stabilization factor, but it is not enough to stabilize the rosettes, neither in gas phase nor water. Besides, rosettes with Cl^- and Na^+ show the greatest ΔE_{bond} in gas phase, but the affinity for ions changes in water, since the rosettes with I^- and Rb^+ show the greatest bonding and formation energies. Even though AM was shown to be a more robust building block than M, with or without solvation, we show in this chapter two new positive sides of these self-assembling molecules. While M coordinates only anions, AM could be used to form rosettes able to recognize mainly cations.

Table 1.a Analysis of the interaction energies (in kcal mol^{-1}) of rosettes with C_s symmetry (ZORA-BLYP-D3(BJ)/TZ2P level of theory).

Rosette	Ion	ΔE_f	ΔE_{bond}^{Cs}	ΔE_{coor}	ΔE_{HB}	ΔE_{int}	ΔE_f^w	ΔE_{bond}^w
M_6	no ion	-79.3	-79.3	0.0	-79.3	-86.8	-44.3	-44.3
	Cl^-	-143.6	-143.6	-69.1	-74.5	-153.5	-53.1	-53.1
	Br^-	-140.9	-140.9	-65.6	-75.3	-150.5	-53.4	-53.4
	I^-	-136.4	-136.4	-60.0	-76.4	-145.6	-57.2	-57.2
M'$_6$	no ion	-36.3	-180.1	0.0	-180.1	-204.7	1.6	-77.3
	Cl^-	-81.2	-224.9	-50.2	-174.8	-257.2	-2.9	-81.8
	Br^-	-78.5	-222.2	-47.0	-175.2	-252.9	-2.6	-81.5
	I^-	-73.9	-217.6	-42.1	-175.5	-245.7	-5.4	-84.3
M''$_6$	no ion	-13.3	-178.9	0.0	-178.9	-212.4	16.6	-74.7
	Cl^-	-86.3	-251.8	-78.7	-173.1	-289.7	5.1	-86.2
	Br^-	-82.4	-248.0	-73.6	-174.4	-284.9	5.2	-86.2
	I^-	-75.8	-241.3	-65.7	-175.6	-276.8	2.1	-89.2

Table 1.b Analysis of the interaction energies (in kcal mol^{-1}) of rosettes with C_s symmetry (ZORA-BLYP-D3(BJ)/TZ2P level of theory).

Rosette	Ion	ΔE_f	$\Delta E_{\text{bond}}^{C_S}$	ΔE_{coor}	ΔE_{HB}	ΔE_{int}	ΔE_f^{w}	$\Delta E_{\text{bond}}^{\text{w}}$
a-AM$_6$	no ion	-101.5	-101.5	0.0	-101.5	-120.7	-23.3	-67.9
	Na^+	-163.3	-163.3	-66.5	-96.8	-185.5	-28.9	-73.5
	K^+	-157.9	-157.9	-60.8	-97.1	-179.7	-31.4	-76.0
	Rb^+	-158.1	-158.1	-60.5	-97.6	-179.6	-34.6	-79.2
a-AM'$_6$	no ion	-128.1	-141.8	0.0	-141.8	-161.1	-63.8	-63.8
	Na^+	-198.0	-211.8	-79.4	-132.4	-238.5	-67.5	-67.5
	K^+	-192.7	-206.5	-72.3	-134.2	-232.3	-70.4	-70.4
	Rb^+	-192.7	-206.5	-71.4	-135.1	-232.0	-73.3	-73.3
b-AM$_6$	no ion	-81.8	-85.5	0.0	-85.5	-101.1	-15.3	-60.0
	Cl^-	-165.9	-165.9	-88.9	-77.1	-187.0	-29.0	-73.7
	Br^-	-161.5	-161.5	-83.5	-78.0	-181.8	-28.3	-73.0
	I^-	-153.8	-153.8	-75.2	-78.6	-173.1	-29.9	-74.6
b-AM'$_6$	no ion	-84.6	-163.1	0.0	-163.1	-188.8	-40.5	-62.6
	Cl^-	-170.4	-248.8	-92.2	-156.7	-280.6	-54.2	-76.2
	Br^-	-166.0	-244.5	-86.3	-158.2	-275.3	-53.9	-76.0
	I^-	-158.5	-237.0	-77.4	-159.7	-266.4	-56.6	-78.6

Table 2 collects the parameters that define the structural effects of the ions, that is, the hydrogen bond distances and the size of the cavity. The most remarkable consequence of introducing them in the center is the contraction of the rosettes. This means that upon addition of Cl^- or Na^+ the size of the cavity and H-Bond distances are reduced. With the subsequent addition of the bigger ions (X^- = Br^-, I^-; M^+ = K^+, Rb^+) those distances gradually increase until they reach almost the size of the empty scaffold.

Both formation and bonding energies reveal the ions add an extra stabilization factor to the system, so they are interacting with the functional groups of the cavity.

Table 2.a. Geometrical parameters (in Å) of single rosettes with C_{2h} symmetry (ZORA-BLYP-D3(BJ)/TZ2P level of theory).

Rosette	Ion	gas phase			water		
		d_i(D···A)[a]	d_o(D···A)[b]	d_{hole}[c]	d_i(D···A)	d_o(D···A)	d_{hole}
M_6	empty	2.95	2.97	7.71	2.97	2.98	7.66
	Cl^-	2.91	2.92	7.43	2.94	2.95	7.50
	Br^-	2.92	2.93	7.50	2.95	2.96	7.55
	I^-	2.94	2.96	7.62	2.97	2.98	7.65
M'_6	empty	2.81	2.84	7.44	2.84	2.86	7.45
	Cl^-	2.74	2.80	7.39	2.82	2.85	7.43
	Br^-	2.75	2.81	7.47	2.82	2.85	7.50
	I^-	2.77	2.83	7.59	2.83	2.87	7.61
M''_6	empty	2.80	2.80	7.46	2.83	2.83	7.46
	Cl^-	2.79	2.79	7.17	2.81	2.82	7.32
	Br^-	2.80	2.80	7.26	2.82	2.83	7.38
	I^-	2.81	2.82	7.41	2.83	2.84	7.50

[a] Average inner hydrogen bond distance D(H)···A. [b] Average outer hydrogen bond distance D(H)···A. [c] Average diameter taken between the nitrogen/oxygen atoms of the cavity.

Therefore, we have partitioned the overall bonding energy of the complexes [Eqn. (9)] into two main components: the coordination energy ΔE_{coor}, which is straight related to the recognition process, and the hydrogen bond energy ΔE_{HB} [Eqn. (10)].

$$\Delta E_{bond}^{CS} = E_{R@I} - 6\times E_m^* - E_I \quad (9)$$

$$\Delta E_{bond}^{CS} = \left(E_{R@I} - E_R^{R@I} - E_I\right) + \left(E_R^{R@I} - 6\times E_m^*\right) = \Delta E_{coor} + \Delta E_{HB} \quad (10)$$

In these equations $E_{R@I}$ is the energy of the rosette@ion coordination complex and $E_R^{R@I}$ is the energy of the empty rosette in the structure of the rosette@ion coordination complex, so the superscript indicates the considered geometry. All the

bonding energy terms are also shown in Table 1.

Table 2.b. Geometrical parameters (in Å) of single AM rosettes with C_{2h} symmetry (ZORA-BLYP-D3(BJ)/TZ2P level of theory).

Rosette	Ion	gas phase			water		
		d_i(D···A)[a]	d_o(D···A)[b]	d_{hole}[c]	d_i(D···A)	d_o(D···A)	d_{hole}
a-AM_6	empty	2.82	2.82	6.98	2.80	2.82	7.08
	Na^+	2.73	2.77	6.82	2.77	2.79	6.90
	K^+	2.74	2.78	6.83	2.76	2.79	6.89
	Rb^+	2.74	2.78	6.87	2.76	2.79	6.91
a-AM'_6	empty	2.84	2.81	7.61	2.89	2.83	7.38
	Na^+	2.81	2.78	6.97	2.85	2.80	7.11
	K^+	2.82	2.79	7.05	2.86	2.81	7.19
	Rb^+	2.82	2.79	7.09	2.86	2.80	7.14
b-AM_6	empty	2.83	2.85	7.53	2.83	2.83	7.22
	Cl^-	2.81	2.81	7.07	2.81	2.81	7.12
	Br^-	2.83	2.83	7.16	2.82	2.83	7.19
	I^-	2.85	2.86	7.31	2.85	2.86	7.32
b-AM'_6	empty	2.77	2.81	7.42	2.81	2.88	7.37
	Cl^-	2.76	2.80	7.08	2.79	2.86	7.21
	Br^-	2.77	2.81	7.18	2.80	2.87	7.29
	I^-	2.79	2.83	7.34	2.82	2.89	7.43

[a] Average inner hydrogen bond distance D(H)···A. [b] Average outer hydrogen bond distance D(H)···A. [c] Average diameter taken between the nitrogen/oxygen atoms of the cavity.

Our partitioning scheme reveals that introducing either anions or cations in the cavity weakens the H-Bonds within the rosettes (see ΔE_{HB} values in Table 1). The biggest ions (I^- and Rb^+) are less distortive but the coordination energy is lower. In addition, this approach let us discriminate which system will perform better for a

specific ion. For instance, the formation energies suggest that AM will recognize only cations, but it is worth pointing out the differences in anion recognition between M and AM. From Table 2, one can see that *b*-AM_6 coordinates anions more strongly than M_6 (see ΔE_{coor} values). In addition, the bonding energies both in gas phase and in water are larger for the former system. Therefore, we show again the superior capacity of AM for designing new supramolecular systems, but, with the ability to recognize anions. In this context, a conceivable alternative to this structure could be the isocytosine rosette,[25] since they share the same molecular skeleton and might show cooperativity.

Energy decomposition analysis

The nature of the interactions was evaluated by an energy decomposition of each interaction energy term. Values for ΔE_{coor} are collected in Table 3, and values for ΔE_{HB} are collected in Table S1. This analysis reveals that, in all cases, the coordination is mostly electrostatic in nature, providing around 60% of all attractive interactions. Nevertheless, the orbital component ΔE_{oi} contributes with around 30% and together with the dispersion correction (around 10%), the three components explain the attractive nature of the ion recognition.

The charge transfer component, which is obtained as the addition of the gross Mulliken population of the lowest unoccupied molecular orbitals (LUMO) orbitals, are also shown in Table 3. These values confirm there is a charge transfer as a consequence of the orbital interactions. Halide ions transfer charge to the N–H antibondings, while the metals receive charge donation from carbonyl oxigens. Figure 1 shows the orbitals involved in these interactions for M and AM rosettes. As can be seen in Figure 1, the lowest unoccupied MOs of M_6 that receives electronic density from X^- is entirely localized in the center of the rosette. Therefore, this picture reinforces the fact that, when the rosette is formed, M and its tautomers have a strong capacity to recognize anions. The same can be seen for the *a*-AM'$_6$ system, in which all the oxygen lone pairs (σ_{HOMO-3}) donate charge to the metal.

Table 3. Energy decomposition analysis of ΔE_{coor} (in kcal mol^{-1}) and charge transfer of rosettes with C_S symmetry in gas phase (ZORA-BLYP-D3(BJ)/TZ2P level of theory).

Rosette	Ion	ΔE_{coor}	ΔV_{elstat}	ΔE_{Pauli}	ΔE_{oi}		ΔE_{disp}	$P_{virtuals}$[a]
					ΔE_{σ}	ΔE_{π}		
M_6	Cl^-	-69.1	-51.9	14.7	-18.2	-8.0	-5.9	0.24
	Br^-	-65.6	-53.7	22.3	-18.8	-7.7	-7.7	0.22
	I^-	-60.0	-56.1	34.7	-20.5	-7.5	-10.5	0.28
M'_6	Cl^-	-50.2	-33.0	15.9	-18.6	-8.4	-6.1	0.19
	Br^-	-47.0	-35.6	23.7	-19.0	-8.1	-8.0	0.20
	I^-	-42.1	-39.5	36.5	-20.4	-7.8	-10.9	0.22
M''_6	Cl^-	-78.7	-63.9	21.7	-21.6	-8.2	-6.6	0.26
	Br^-	-73.6	-65.8	31.5	-22.9	-7.9	-8.6	0.24
	I^-	-65.7	-67.8	46.7	-25.4	-7.6	-11.6	0.33
a-AM_6	Na^+	-66.5	-38.3	0.7	-10.1	-6.9	-11.9	0.07
	K^+	-60.8	-38.6	2.9	-9.9	-6.9	-8.2	0.05
	Rb^+	-60.5	-39.0	4.9	-10.0	-6.9	-9.5	0.07
a-AM'_6	Na^+	-79.4	-52.0	0.6	-9.2	-7.3	-11.4	0.06
	K^+	-72.3	-51.2	2.2	-8.8	-7.2	-7.4	0.03
	Rb^+	-71.4	-47.3	3.6	-8.8	-7.1	-8.2	0.04
b-AM_6	Cl^-	-88.9	-75.5	24.4	-22.0	-9.0	-6.9	0.26
	Br^-	-83.5	-77.7	35.2	-23.4	-8.7	-8.8	0.26
	I^-	-75.2	-80.3	51.5	-26.1	-8.4	-11.9	0.35
b-AM'_6	Cl^-	-92.2	-79.0	25.0	-22.8	-8.4	-6.9	0.26
	Br^-	-86.3	-80.4	35.3	-24.2	-8.1	-8.9	0.26
	I^-	-77.4	-81.6	50.6	-26.7	-7.7	-11.9	0.37

[a] $P_{virtuals}$ is the sum of the gross Mulliken population of the lowest unoccupied MOs. For systems with X^-, LUMOs correspond to N–H antibonding orbitals. For systems with M^+, LUMOs correspond to the metal.

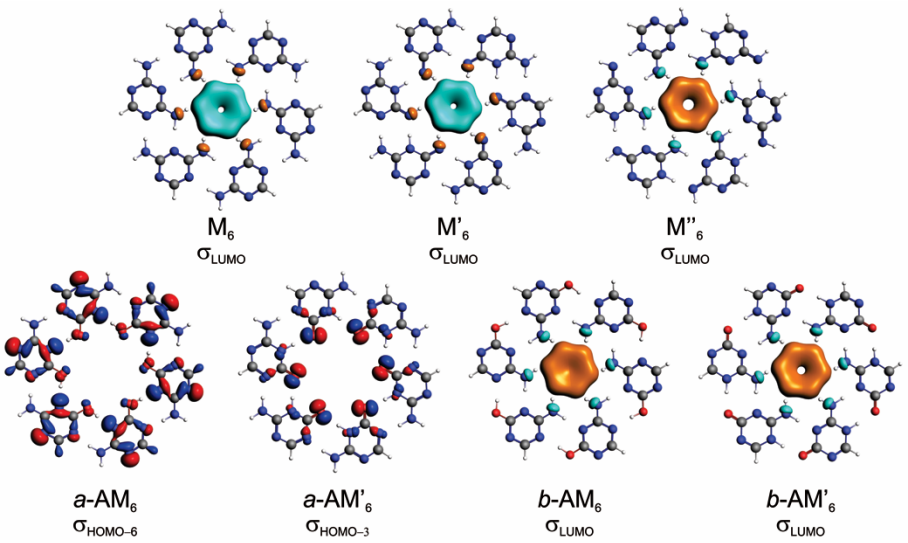

Figure 1. Highest occupied and lowest unoccupied MOs of M and AM rosettes (C_s-symmetry), that contribute to the orbital interactions with either the halides or metals.

3.3. Stacked rosettes

Structure and relative stabilities

The stacking arrangement does not change the trend in the stability. As shown in Table 4, the formation energies indicate that $M_{12}@X^-$ and *a*-$AM'_{12}@M^+$ will predominate both in gas phase and in water. The systems with the greatest formation and bonding energies in water are those, again, for I^- and Rb^+.

Figures 2 and 3 show the molecular structures in gas phase of M and AM stacked rosettes, respectively. A glance at these figures immediately reveals that the empty systems adopt an almost planar stacking. Besides, both anions and cations show a clear templation effect. This means that after introducing the ion in the empty scaffold, all the structures experience a structural rearrangement. In most cases, the systems become more planar; specially M_{12}, M''_{12}, *b*-AM_{12} and *b*-AM'_{12}. When introducing anions in the cavity, all the amine groups pyramidalize in such a way that all the hydrogen atoms point toward the anion. However, when introducing cations within *a*-AM_{12}, the system bends, adopting a saddle shape.

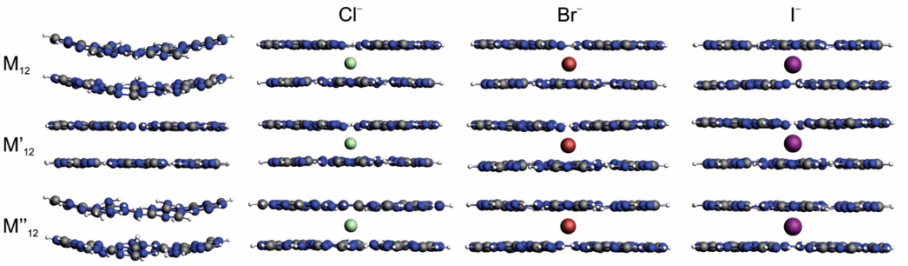

Figure 2. Structures of M stacked rosettes in gas phase optimized at ZORA-BLYP-D3(BJ)/TZ2P with C_2 symmetry.

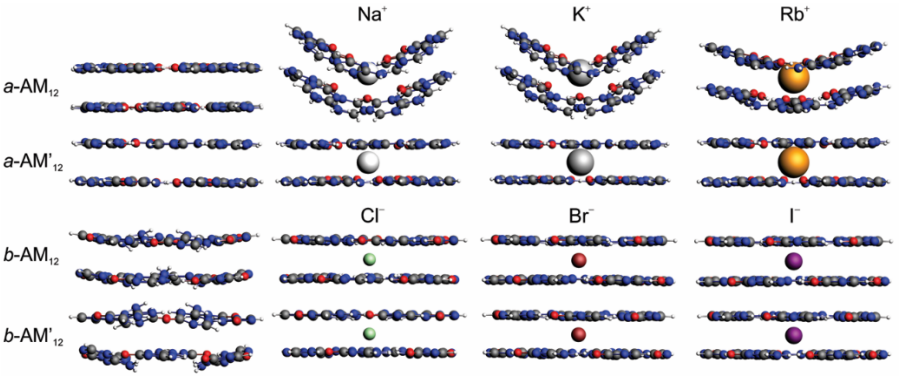

Figure 3. Structures of AM stacked rosettes in gas phase optimized at ZORA-BLYP-D3(BJ)/TZ2P with C_2 symmetry.

To look further into the structure, we measured the average inner and outer hydrogen-bonding distances, and the size of the cavities (see Table S2). The general trend is the same as that in the planar rosettes: the average diameter of the cavities decreases upon addition of Cl^-/Na^+, and then it gradually increases with the successive ions.

Next, we analyzed the systems in an aqueous environment, as shown in Figures 4 and 5. In general, the complexes keep their original gas phase structures, except, surprisingly, the *a*-AM'$_{12}$ system. This aggregate adopts almost the same structure as that of its imidate-like counterpart, for Na^+ and Rb^+, but not for K^+. So then, we tackled

the query where does this behavior come from. If we look at the size of the cavity, when adding Na^+ to the empty scaffold the rosette is contracted, then with K^+ is expanded again, and finally it is slightly contracted with Rb^+ (see d_{hole} values in Table S3). To shed light on these structures, we analyzed the preparation energy by our approach in previous work,[26] which consists in partitioning the preparation energy into the preparation of the H-Bond energy $\Delta E_{prep,HB}$, and the preparation of the stacking $\Delta E_{prep,stack}$ (see Table S3). Both components are the smallest ones for *a*-AM'$_{12}K^+$ of 2.7 and 1.5 kcal mol^{-1}, which means that K^+ is less distorting for this system. Furthermore, we computed the planarization energy for the bent systems (*a*-AM'$_{12}Na^+$, *a*-AM'$_{12}Rb^+$), which is around 4 kcal mol^{-1}. This suggests that the transition from bend to planar is very shallow; thus, within a more realistic system with more layers, like a nanowire, the rosettes may adopt a planar structure. We analyze the electronic structure of this phenomenon with more detail in the section hereafter.

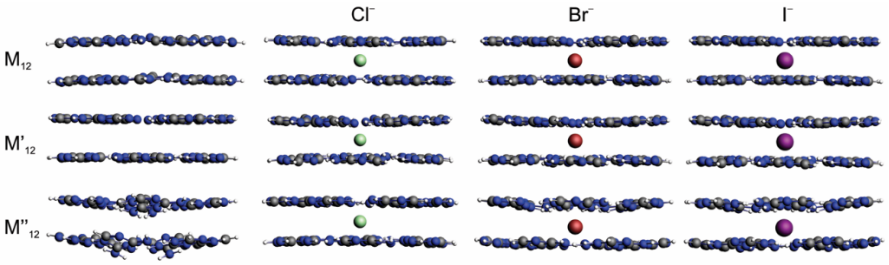

Figure 4. Structures of M stacked rosettes in water optimized at ZORA-BLYP-D3(BJ)/TZ2P with C_2 symmetry.

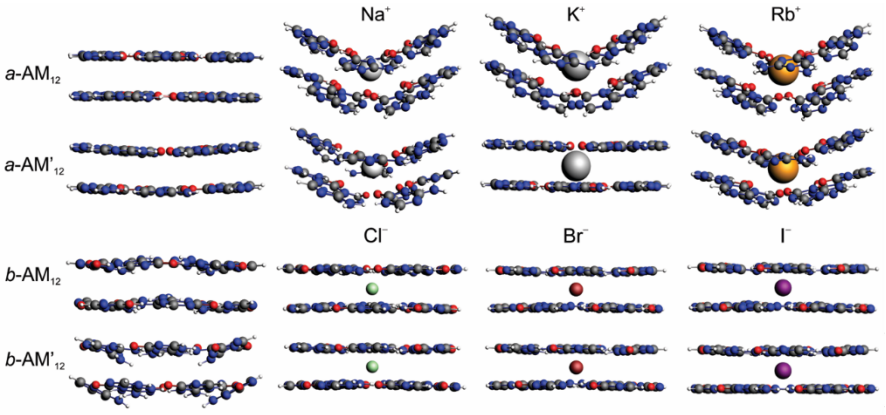

Figure 5. Structures of AM stacked rosettes in water optimized at ZORA-BLYP-D3(BJ)/TZ2P with C_2 symmetry.

Partitioning of the bond energy

The partitioning of the bond energy allows us to dissect the consequences of introducing ions within the cavity. With that in mind, the bonding energy in the stacking environment [eqn (10)] can also be decomposed in three main components: coordination energy ΔE_{coor}, stacking energy ΔE_{stack} and hydrogen-bond energy ΔE_{HB}, according to eqn (11) (see also Scheme 3).

$$\Delta E_{bond}^{C_2} = E_{R[I]R} - 12\times E_m^* - E_I \qquad (10)$$

$$\begin{aligned}\Delta E_{bond}^{C_2} &= \left(E_{R[I]R} - E_{R[\,]R}^{R[I]R} - E_I\right) + \left(E_{R[\,]R}^{R[I]R} - 2\times E_R^{R[I]R}\right) + \left[2\left(E_R^{R[I]R} - 6\times E_m^*\right)\right] \\ &= \Delta E_{coor} + \Delta E_{stack} + \Delta E_{HB} \qquad (11)\end{aligned}$$

In these formulas, $E_{R[I]R}$ is the energy of the stacked rosette with an interlayer ion, $E_{R[\,]R}$ is the energy of the empty scaffold, and the superscripts indicate the considered geometry. All these values, which are listed in Table 4, show that the stacking and the H-Bond energies are slightly weakened. When looking the coordination strengths, the trends observed for the single rosettes are the same for the stacked systems. Besides, the addition of a second rosette improves the coordination energy

by around 25 to 45%. The same observations, as those described for single rosettes, can be clearly seen on the basis of our bonding partitioning. For instance, the fact that AM will perform better than M to coordinate anions is conserved.

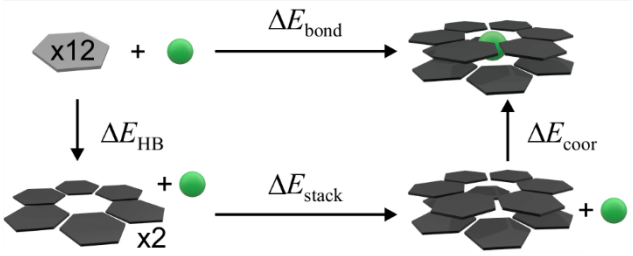

Scheme 3. Partitioning of the bond energy of the stacked rosettes.

Table 4. Analysis of the bonding energies (in kcal mol^{-1}) of stacked rosettes with C_2 symmetry (ZORA-BLYP-D3(BJ)/TZ2P level of theory).

Complex	Ion	ΔE_f	$\Delta E_{bond}^{C_2}$	ΔE_{coor}	ΔE_{stack}	ΔE_{HB}	ΔE_{int}
M_{12}	no ion	-209.6	-209.6	0.0	-52.8	-156.8	-228.3
	Cl^-	-291.3	-291.3	-91.5	-47.7	-152.1	-308.9
	Br^-	-290.1	-290.1	-89.9	-47.7	-152.5	-307.5
	I^-	-288.5	-288.5	-87.4	-47.7	-153.4	-305.8
M'_{12}	no ion	-40.6	-415.8	0.0	-56.8	-359.0	-467.1
	Cl^-	-44.0	-473.4	-64.4	-55.7	-353.3	-533.2
	Br^-	-47.4	-472.1	-62.9	-55.7	-353.5	-531.2
	I^-	-53.8	-470.3	-60.6	-55.8	-354.0	-528.0
M''_{12}	no ion	-12.0	-416.8	0.0	-59.6	-357.1	-489.9
	Cl^-	-22.7	-506.5	-103.2	-51.9	-351.5	-581.3
	Br^-	-26.7	-504.9	-100.7	-52.0	-352.2	-578.8
	I^-	-34.4	-502.1	-96.4	-52.6	-353.1	-574.6
a-AM_{12}	no ion	-87.8	-250.8	0.0	-48.8	-202.0	-291.3
	Na^+	-97.3	-338.0	-95.3	-44.1	-198.6	-391.6
	K^+	-103.2	-330.5	-88.0	-44.1	-198.3	-384.1
	Rb^+	-108.5	-328.8	-83.3	-45.9	-199.6	-372.6

Complex	Ion	ΔE_f	$\Delta E_{bond}^{C_2}$	ΔE_{coor}	ΔE_{stack}	ΔE_{HB}	ΔE_{int}
a-AM'$_{12}$	no ion	-162.5	-327.2	0.0	-44.7	-282.6	-367.4
	Na^+	-164.9	-418.7	-100.0	-43.2	-275.4	-466.8
	K^+	-172.3	-417.0	-92.5	-43.8	-280.7	-462.0
	Rb^+	-173.8	-414.3	-94.4	-43.4	-276.5	-461.7
b-AM$_{12}$	no ion	-71.4	-216.4	0.0	-51.3	-165.0	-264.1
	Cl^-	-88.4	-321.2	-118.7	-43.8	-158.7	-363.4
	Br^-	-91.1	-319.0	-115.6	-44.2	-159.2	-360.1
	I^-	-97.5	-315.1	-110.4	-44.8	-160.0	-355.5
b-AM'$_{12}$	no ion	-117.8	-386.1	0.0	-56.5	-329.6	-440.7
	Cl^-	-131.7	-490.2	-119.7	-50.0	-320.5	-550.1
	Br^-	-134.8	-488.5	-117.0	-50.6	-321.0	-547.9
	I^-	-142.1	-485.6	-112.2	-51.8	-321.6	-543.9

Energy decomposition analysis

The nature of the coordination does not change in the stacks, and the trends are preserved. The average contributions to the attractive interactions are the same as those in the planar systems, that is, 60% electrostatic, 30% orbital and 10% dispersive (see Table 5, and Table S4). Besides, as expected, the stacking energy is mostly dispersive in nature (around 70%), with an electrostatic and orbital contribution of 20% and 10%, respectively.

The charge transfer component ($P_{virtuals}$) does not increase very much in the stack environment. The most representative orbitals are displayed in Figure 6. The presented orbitals provide a clear indication that the LUMO in M_6, which receives charge donation from halides, is mostly localized at the center of the rosette and displaying a cylinder-like form. This is very interesting, since in a pillar array this orbital will be longitudinally localized, like in a coaxial wire. Hence, this suggests that the supramolecular wire could capture anions along all its longitude.

In the systems with cations, the metal receives less charge donation than in the planar systems. In this case, we can bring up a very familiar system: the GQ. If we compare $P_{virtaul}$ values of *a*-AM'$_{12}$@M$^+$ (0.03, 0.01, 0.01) with those obtained for GQ@M$^+$ (0.25, 0.13, 0.15) for the same metals[26] (Na$^+$, K$^+$ and Rb$^+$ respectively), it can be noticed that the charge transfer component is superior for the GQ. When analyzing the size of their cavities, as shown in Figure S1, the size of the pore is much larger in *a*-AM'$_{12}$ which could explain these values. However, their shapes are almost the same.

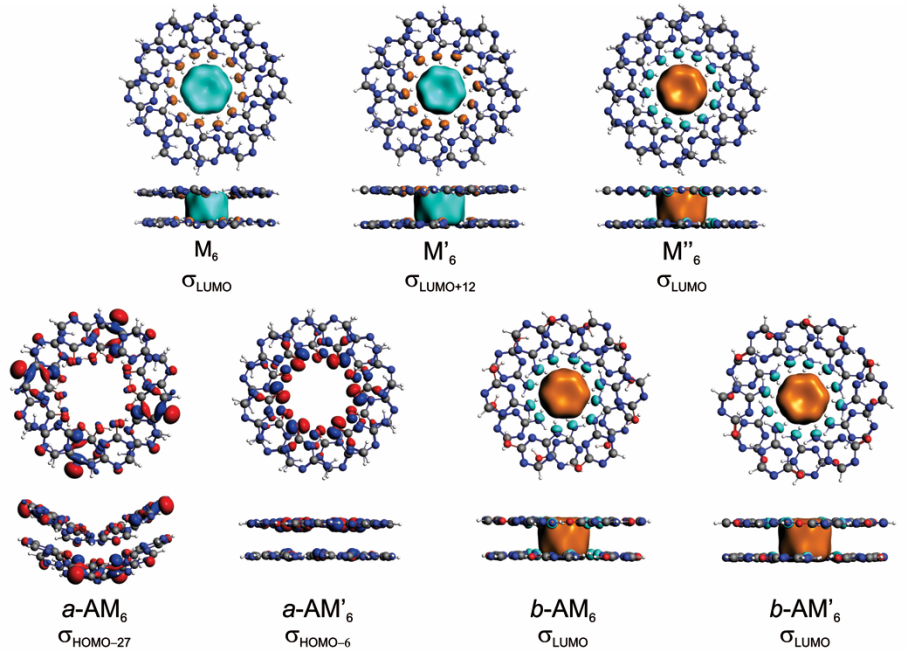

Figure 6. Highest occupied and lowest unoccupied MOs of M and AM rosettes, that contribute to the orbital interactions with either the halides or metals.

Table 5. Energy decomposition analysis of ΔE_{coor} (in kcal mol^{-1}) and charge transfer of stacked rosettes with C_2 symmetry in gas phase (ZORA-BLYP-D3(BJ)/TZ2P level of theory).

Rosette	Ion	ΔE_{coor}	ΔV_{elstat}	ΔE_{Pauli}	ΔE_{oi}	ΔE_{disp}	$P_{virtuals}$
M_{12}	Cl^-	-91.5	-66.1	11.9	-28.8	-8.5	0.25
	Br^-	-89.9	-69.3	19.5	-28.5	-11.6	0.23
	I^-	-87.4	-74.6	34.0	-30.1	-16.7	0.23
M'_{12}	Cl^-	-64.4	-38.5	13.6	-30.4	-9.1	0.26
	Br^-	-62.9	-42.4	22.1	-30.2	-12.4	0.20
	I^-	-60.6	-49.1	38.1	-31.9	-17.8	0.27
M''_{12}	Cl^-	-103.2	-78.5	16.4	-31.5	-9.7	0.28
	Br^-	-100.7	-82.2	26.3	-31.7	-13.1	0.26
	I^-	-96.4	-88.2	44.2	-33.9	-18.5	0.31
a-AM_{12}	Na^+	-95.3	-53.3	0.8	-22.4	-20.4	0.07
	K^+	-88.0	-54.0	3.2	-22.6	-14.7	0.03
	Rb^+	-83.3	-51.2	3.9	-20.4	-15.6	0.03
a-AM'_{12}	Na^+	-100.0	-65.7	0.4	-18.4	-16.4	0.03
	K^+	-92.5	-60.3	1.2	-16.7	-16.7	0.01
	Rb^+	-94.4	-65.4	2.5	-18.1	-13.4	0.01
b-AM_{12}	Cl^-	-118.7	-95.2	19.3	-32.4	-10.3	0.28
	Br^-	-115.6	-99.6	30.7	-33.0	-13.8	0.26
	I^-	-110.4	-106.3	51.0	-35.6	-19.4	0.31
b-AM'_{12}	Cl^-	-119.7	-95.7	17.0	-31.3	-9.8	0.25
	Br^-	-117.0	-99.3	27.0	-31.4	-13.2	0.23
	I^-	-112.2	-104.6	44.6	-33.5	-18.6	0.27

Finally, and going back to the fact that the system *a*-$AM'_{12}@Na^+$ is bended in water, we analyzed the coordination energy within the structure in water solution but taken here in the gas phase. Our MO analysis shows that this effect improves the coordination (ΔE_{coor} = -106.0 kcal mol^{-1}) by increasing the charge transfer by just

0.01 electrons. In addition, unlike *a*-AM'$_{12}$ in the gas phase, two HOMO orbitals donate charge to the metal.

Gibbs free energy of formation

At this stage, we have pinpointed the consequences of introducing ions within the interlayer stacked rosettes. However, according to the thermodynamic principles of self-assembly, it is known that the process will proceed spontaneously only if the change in Gibbs free energy (ΔG) is negative. For this reason, we have computed the changes in Gibbs free energy of formation in water and solvation, for the most stable complexes with Cl^- and Na^+, as shown in Table 6. A related case recently reported by Zaccaria *et al.*[27] has shown a ΔG_f of –45.3 kcal mol^{-1} for a GQ with an interlayer K^+ at the same level of theory. This result, which is comparable to that of *a*-AM'$_{12}Na^+$**,** suggest that the assembly could be experimentally feasible in water. Nevertheless, the monomers should be equipped with side chains to direct and improve the assembly, which is a current proceeding. It should also be mentioned that stacked rosettes of melamine have never been obtained experimentally without any covalent modification.[6,22c]

Table 6. Gibbs free energy (in kcal mol^{-1}) for the most stable rosettes. (ZORA-BLYP-D3(BJ)/DZP level of theory).

Rosette	Ion	ΔE_{bond}	ΔG_f[a]	ΔH_f[b]	$-T\Delta S_f$[c]	ΔG_{solv}[d]
M_{12}	Cl^-	-214.8	-21.3	-199.7	178.4	-72.2
a-AM'$_{12}$	Na^+	-233.3	-43.1	-222.3	179.2	-79.2

[a-c] Thermodynamic properties of formation in water, [d] Gibbs free energy of solvation.

VII.4. Conclusions

Our DFT-D calculations predict that M and AM rosettes can coordinate ions in a feasible way alike the naturally occurring guanine quadruplexes and nanowires. While M can only recognize anions, AM rosettes can recognize both anions and

cations. Therefore, ammeline could be used to recognize either anions or cations with the selection of the appropriate salt. In addition, based on the formation energies, M and AM could constitute a potent binary mixture for dual-receptor strategies.

Since thermodynamics govern the self-assembly process, our results suggest that the most stable structures, in gas phase and in water solution, are those of melamine in its amino-like form and ammeline in its amide-like form (protonated at position 1, *a*-AM').

Finally, all the ions have shown to organize the assemblies in a particular arrangement, with respect to the empty systems, both in gas phase and in water. Hence, they could be used as an external factor to direct the self-assembly, and they can be part of the final ensemble. These results could also assist the rational design of self-assembling materials with tunable properties by the presence of different ions. The predicted planar structures are suitable models to construct self-assembling monolayers with the ability to capture anions and cations. Whereas the predicted stacked rosettes, with ions in between, suggest that pillar arrays or nanowires could be experimentally obtained. Nevertheless, in order to achieve a more robust complex with a stronger binding energy, some covalent modifications over M and AM should be taken into account. For instance, one amine group could be replaced by long chains (in general alkylic chains with aromatic groups) for further stabilization with van der Waals and/or π-π interactions. Preorganization techniques also constitute a viable method. We think that this study could be generalized to other systems based on amine-substituted triazines like diaminopyrimidines, cytosine and iso-cytosyne.

VII. References

(1) a) G. M. Whitesides, E. E. Simanek, J. P. Mathias, C. T. Seto, D. N. Chin, M. Mammen, D. M. Gordon, *Acc. Chem. Res.,* **1995**, *28*, 37–44. b) L. J. Prins, D. N. Reinhoudt, P. Timmerman, *Angew. Chemie - Int. Ed.,* **2001**, *40*, 2382–2426. c) X. Li, Y. Gao, C. E. Boott, M. A. Winnik, I. Manners, *Nat. Commun.,* **2015**, *6*, 1–8.

(2) a) J. Zhou, B. T. Roembke, G. Paragi, A. Laguerre, H. O. Sintim, C. Fonseca Guerra, D. Monchaud, *Sci. Rep*., **2016**, **6**, 33888. b) G. Paragi, Z. Kupihár, G. Endre, C. Fonseca Guerra, L. Kovács, *Org. Biomol. Chem.,* **2017**, *15*, 2174–2184.

(3) a) S. I. Stupp, L. C. Palmer, *Chem. Mater.,* **2014**, *26*, 507–518. b) M. J. Mayoral, N. Bilbao, D. González-Rodríguez, *ChemistryOpen,* **2016**, *5*, 10–32. c) R. L. Beingessner, Y. Fan, H. Fenniri, *RSC Adv.,* **2016**, *6*, 75820–75838. d) B. Adhikari, X. Lin, M. Yamauchi, H. Ouchi, K. Aratsu, S. Yagai, *Chem. Commun.,* **2017**, *53*, 9663–9683.

(4) H. Diem, G. Matthias, R. A. Wagner, in Ullmann's Encycl. Ind. Chem., Wiley-VCH Verlag GmbH & Co. KGaA, Weinheim, Germany, **2010**.

(5) B. Roy, P. Bairi, A. K. Nandi, *RSC Adv.,* **2014**, *4*, 1708.

(6) a) P. Jonkheijm, A. Miura, M. Zdanowska, F. J. M. Hoeben, S. De Feyter, A. P. H. J. Schenning, F. C. De Schryver, E. W. Meijer, *Angew. Chemie - Int. Ed.,* **2004**, *43*, 74–78. b) K. E. Maly, C. Dauphin, J. D. Wuest, *J. Mater. Chem.,* **2006**, *16*, 4695.

(7) a) S. SeethaLekshmi, T. N. Guru Row, *CrystEngComm,* **2011**, *13*, 4886. b) N. E. Braml, A. Sattler, W. Schnick, *Chem. - A Eur. J.,* **2012**, *18*, 1811–1819. c)S. J. Makowski, M. Lacher, C. Lermer, W. Schnick, *J. Mol. Struct.,* **2012**, *1013*, 19–25.

(8) a) P. A. Staniec, L. M. A. Perdigão, B. L. Rogers, N. R. Champness, P. H. Beton, *J. Phys. Chem. C,* **2007**, *111*, 886–893. b) W. Xu, M. Dong, H. Gersen, E. Rauls, S. Vázquez-Campos, M. Crego-Calama, D. N. Reinhoudt, I. Stensgaard, E. Laegsgaard, T. R. Linderoth, et al., *Small,* **2007**, *3*, 854–8. c) F. Silly, A. Q. Shaw, M. R. Castell, G. a. D. Briggs, M. Mura, N. Martsinovich, L. Kantorovich, *J. Phys. Chem. C,* **2008**, *112*, 11476–11480. d) M. Mura, N. Martsinovich, L. Kantorovich, *Nanotechnology,* **2008**, *19*, 465704. e) H. Zhang, Z. Xie, L. Long, H. Zhong, W. Zhao, B.-W. Mao, X. Xu, L.-S. Zheng, *J. Phys. Chem. C,* **2008**, *111*, 4209–4218.

(9) a) N. Katsonis, H. Xu, R. M. Haak, T. Kudernac, Ž. Tomović, S. George, M. Van Der Auweraer, A. P. H. J. Schenning, E. W. Meijer, B. L. Feringa, S. De Feyter, *Angew. Chemie - Int. Ed.,* **2008**, *47*, 4997–5001. b) A. Minoia, Z. Guo, H. Xu, S. J. George, A. P. H. J. Schenning, S. De Feyter, R. Lazzaroni, *Chem. Commun.,* **2011**, *47*, 10924–10926. c) A. Ciesielski, S. Haar, G. Paragi, Z. Kupihár, Z. Kele, S. Masiero, C. Fonseca Guerra, F. M. Bickelhaupt, G. P. Spada, L. Kovács, P. Samorì, *Phys. Chem. Chem. Phys.,* **2013**, *15*, 12442.

(10) Y. Li, K. Zhao, Y. Yang, K. Deng, Q. Zeng, C. Wang, *Nanoscale,* **2012**, *4*, 148

(11) a) A. Kohlmeier, L. Vogel, D. Janietz, *Soft Matter*, **2013**, *9*, 9476–9486. (b) L. Niu, J. Song, J. Li, N. Tao, M. Lu, K. Fan, *Soft Matter*, **2013**, *9*, 7780.

(12) A. P. H. J. Schenning, P. Jonkheijm, F. J. M. Hoeben, J. Van Herrikhuyzen, S. C. J. Meskers, E. W. Meijer, L. M. Herz, C. Daniel, C. Silva, R. T. Phillips, R.H. Friend, D. Beljonne, A. Miura, S. De Feyter, M. Zdanowska, H. Uji-i, F.C. De Schryver, Z. Chen, F.Würthner, M. Mas-Torrent, D. den Boer, M. Durkut, P. Hadley, *Synth. Met.,* **2004**, *147*, 43–48.

(13) a) R. Varghese, S. J. George, A. Ajayaghosh, *Chem. Commun. (Camb.)* **2005**, *1*, 593–595. b) A. Ciesielski, S. Lena, S. Masiero, G. P. Spada, P. Samorì, *Angew. Chemie Int. Ed.,* **2010**, *49*, 1963–1966.

(14) a) C. Fonseca Guerra, H. Zijlstra, G. Paragi, F. M. Bickelhaupt, *Chem. - A Eur. J.,* **2011**, **17**, 12612–12622. b) J. Szolomájer, G. Paragi, G. Batta, C. F. Guerra, F. M. Bickelhaupt, Z. Kele, P. Pádár, Z. Kupihár, L. Kovács, *New J. Chem.,* **2011**, *35*, 476–482.

(15) a) E. Buhler, N. Sreenivasachary, S. J. Candau, J. M. Lehn, *J. Am. Chem. Soc.,* **2007**, *129*, 10058–10059. b) V. Venkatesh, N. K. Mishra, I. Romero-Canelón, R. R. Vernooij, H. Shi, J. P. C. Coverdale, A. Habtemariam, S. Verma, P. J. Sadler, *J. Am. Chem. Soc.,* **2017**, *139*, 5656–5659.

(16) A. B. Kotlyar, N. Borovok, T. Molotsky, H. Cohen, E. Shapir, D. Porath, *Adv. Mater*., 2005, *17*, 1901–1905.

(17) a) T. Van Der Wijst, C. Fonseca Guerra, M. Swart, F. M. Bickelhaupt, B. Lippert, *Angew. Chemie - Int. Ed.,* **2009**, *48*, 3285–3287. b) T. Van Der Wijst, B. Lippert, M. Swart, C. Fonseca Guerra, F. M. Bickelhaupt, *J. Biol. Inorg. Chem.,* **2010**, *15*, 387–397.

(18) G. Paragi, Z. Kupihár, C. Guerra, F. Bickelhaupt, L. Kovács, *Molecules,* **2012**, *18*, 225–235.

(19) a) G. te Velde, F. M. Bickelhaupt, E. J. Baerends, S. J. A. van Gisbergen, C. Fonseca Guerra, J. G. Snijders and T. Ziegler, *J. Comput. Chem.* **2001**, *22*, 931–967. b) E. J. Baerends, et al., ADF2014.01, SCM, Theoretical Chemistry, Vrije Universiteit, Amsterdam, The Netherlands, http://www.scm.com.

(20) a) S. Grimme, J. Antony, S. Ehrlich, H. Krieg, *J. Chem. Phys.* **2010**, *132*, 154104. b) S. Grimme, S. Ehrlich, L. Goerigk, *J. Comput. Chem.* **2011**, *32*, 1456–1465. c) S. Grimme, *J. Comput. Chem.* **2004**, *25*, 1463–1473. d) S. Grimme, *J. Comput. Chem.* **2006**, *27*, 1787–1799.

(21) a) C. Fonseca Guerra, T. van der Wijst, J. Poater, M. Swart, F. M. Bickelhaupt, *Theor. Chem. Acc.* **2010**, *125*, 245–252. b) T. van der Wijst, C. Fonseca Guerra, M. Swart, F. M. Bickelhaupt, B. Lippert, *Angew. Chemie Int. Ed.* **2009**, *48*, 3285–3287.

(22) a) T. H. Rehm, C. Schmuck, *Chem. Soc. Rev.* **2010**, *39*, 3597. b) M. Ma, D. Bong, *Langmuir* **2011**, *27*, 8841–53. c) B. J. Cafferty, I. Gállego, M. C. Chen, K. I. Farley, R. Eritja, N. V. Hud, *J. Am. Chem. Soc.,* **2013**, *135*, 2447–2450.

(23) (a) A. Klamt and G. Schüürmann, J. Chem. Soc., *Perkin Trans. 2*, ***1993***, 799; (b) A. Klamt, *J. Phys. Chem.*, **1995**, *99*, 2224; (c) C. C. Pye and T. Ziegler, *Theor. Chem. Acc.*, **1999**, *101*, 396.

(24) a) T. Ziegler, A. Rauk, *Inorg. Chem.,* **1979**, *18*, 1755; b) T. Ziegler, A. Rauk, *Inorg. Chem.,* **1979**, *18*, 1558; c) T. Ziegler, A. Rauk, *Theor. Chim. Acta,* **1977**, **46**, 1. F. M. Bickelhaupt and E. J. Baerends, in Rev. Comput. Chem., ed. K. B. Lipkowitz and D. B. Boyd, Wiley-VCH, New York, **2000**, vol. 15, pp. 1–86.

(25) A. Ciesielski, S. Colella, L. Zalewski, B. Bruchmann, P. Samorì. *CrystEngComm*, **2011**, *13*, 5535–5537.

(26) F. Zaccaria, G. Paragia, C. Fonseca Guerra, *Phys. Chem. Chem. Phys.*, **2016**, *18*, 20895–20904.

(27) F. Zaccaria, C. Fonseca Guerra. *Chem. –A Eur. J.* **2018**. DOI: 10.1002/chem.201803530

Table S1. Energy decomposition analysis (in kcal mol^{-1}) of rosettes with C_{2h} symmetry in gas phase (ZORA-BLYP-D3(BJ)/TZ2P level of theory).

Rosette	Total	Coordination					HB				
	ΔE_{int}	ΔV_{elstat}	ΔE_{Pauli}	ΔE_{oi}		ΔE_{disp}	ΔV_{elstat}	ΔE_{Pauli}	ΔE_{oi}		ΔE_{disp}
				ΔE_{σ}	ΔE_{π}				ΔE_{σ}	ΔE_{π}	
M_6							-145.9	180.3	-84.6	-6.3	-30.4
M_6@Cl^-	-153.5	-51.9	14.7	-18.2	-8.0	-5.9	-169.5	209.1	-86.7	-4.7	-32.5
M_6@Br^-	-150.5	-53.7	22.3	-18.8	-7.7	-7.7	-165.1	201	-84.2	-4.7	-32
M_6@I^-	-145.6	-56.1	34.7	-20.5	-7.5	-10.5	-157.1	186.7	-79.4	-4.6	-31
M'_6							-247.3	278.3	-172.8	-30.3	-32.6
M'_6@Cl^-	-257.2	-33	15.9	-18.6	-8.4	-6.1	-273.7	348.6	-226.8	-21	-34.2
M'_6@Br^-	-252.9	-35.6	23.7	-19	-8.1	-8	-268.6	336	-219	-20.6	-33.7
M'_6@I^-	-245.7	-39.5	36.5	-20.4	-7.8	-10.9	-259.1	313.5	-205.1	-20	-32.8
M''_6							-261.5	318.6	-198.3	-37.4	-33.8
M''_6@Cl^-	-289.7	-63.9	21.7	-21.6	-8.2	-6.6	-280.6	328.1	-179.4	-43.7	-35.4
M''_6@Br^-	-284.9	-65.8	31.5	-22.9	-7.9	-8.6	-274.3	316.4	-175.3	-43.5	-34.7
M''_6@I^-	-276.8	-67.8	46.7	-25.4	-7.6	-11.6	-263.2	295.4	-166.8	-42.7	-33.7
a-AM_6							-198.4	246.3	-128.7	-9.8	-30.2
a-AM_6@Na^+	-185.5	-38.3	0.7	-10.1	-6.9	-11.9	-228.6	309.5	-160	-7.5	-32.5
a-AM_6@K^+	-179.7	-38.6	2.9	-9.9	-6.9	-8.2	-226.4	304.8	-157.6	-7.4	-32.3
a-AM_6@Rb^+	-179.6	-39	4.9	-10	-6.9	-9.5	-224.6	300.3	-155.4	-7.4	-32.1
a-AM'_6							-195.1	220	-136.1	-23.2	-26.8
a-AM'_6@Na^+	-238.5	-52	0.6	-9.2	-7.3	-11.4	-220	257.3	-138.8	-27.9	-29.7
a-AM'_6@K^+	-232.3	-51.2	2.2	-8.8	-7.2	-7.4	-216.5	249	-135.7	-27.7	-29.2
a-AM'_6@Rb^+	-232	-47.3	3.6	-8.8	-7.1	-8.2	-218.8	245.6	-134.5	-27.6	-28.9
b-AM'_6							-177.8	241.7	-124.3	-8.3	-32.4
b-AM'_6@Cl^-	-187	-75.5	24.4	-22	-9	-6.9	-203.4	263.7	-119.7	-4.6	-34
b-AM'_6@Br^-	-181.8	-77.7	35.2	-23.4	-8.7	-8.8	-195.2	248.8	-114.2	-4.5	-33.2
b-AM'_6@I^-	-173.1	-80.3	51.5	-26.1	-8.4	-11.9	-181.1	223.8	-104.4	-4.2	-32
b-AM'_6							-225.3	266.7	-168.1	-31.2	-30.9
b-AM'_6@Cl^-	-280.6	-79	25	-22.8	-8.4	-6.9	-250.5	284.7	-154.4	-35.1	-33.1
b-AM'_6@Br^-	-275.3	-80.4	35.3	-24.2	-8.1	-8.9	-243.9	272.4	-150.3	-34.9	-32.3
b-AM'_6@I^-	-266.4	-81.6	50.6	-26.7	-7.7	-11.9	-232.5	250.9	-141.9	-34.4	-31.1

Table S2. Geometrical parameters (in Å) of stacked rosettes with C_2 symmetry (ZORA-BLYP-D3(BJ)/TZ2P level of theory)

Rosette	Ion	gas phase			water		
		d_i(N···N)	d_o(N···N)	d_{hole}	d_i(N···N)	d_o(N···N)	$d_{hole\text{-}w}$
M_{12}	no ion	2.94	2.96	7.53	2.95	2.96	7.59
	Cl^-	2.91	2.92	7.46	2.93	2.93	7.45
	Br^-	2.92	2.93	7.48	2.93	2.94	7.47
	I^-	2.92	2.93	7.52	2.93	2.94	7.50
M'_{12}	no ion	2.81	2.84	7.39	2.82	2.84	7.40
	Cl^-	2.76	2.80	7.38	2.80	2.83	7.35
	Br^-	2.77	2.81	7.40	2.80	2.83	7.37
	I^-	2.77	2.81	7.45	2.80	2.83	7.42
M''_{12}	no ion	2.82	2.77	7.35	2.85	2.78	7.43
	Cl^-	2.79	2.78	7.22	2.80	2.79	7.27
	Br^-	2.79	2.78	7.25	2.80	2.80	7.30
	I^-	2.80	2.79	7.31	2.81	2.80	7.35
a-AM_{12}	no ion	2.81	2.81	7.05	2.79	2.81	7.04
	Na^+	2.68	2.85	6.46	2.69	2.85	6.52
	K^+	2.68	2.85	6.45	2.68	2.85	6.47
	Rb^+	2.74	2.80	6.80	2.69	2.85	6.52
a-AM'_{12}	no ion	2.83	2.80	7.58	2.86	2.82	7.34
	Na^+	2.81	2.78	7.21	2.77	2.84	6.77
	K^+	2.84	2.81	7.45	2.86	2.82	7.40
	Rb^+	2.81	2.78	7.25	2.79	2.82	6.95
b-AM_{12}	no ion	2.84	2.80	7.12	2.83	2.78	7.11
	Cl^-	2.81	2.81	7.08	2.8	2.79	7.07
	Br^-	2.81	2.81	7.11	2.80	2.80	7.10
	I^-	2.82	2.82	7.17	2.81	2.80	7.15
b-AM'_{12}	no ion	2.81	2.76	7.46	2.81	2.79	7.35
	Cl^-	2.76	2.79	7.17	2.78	2.83	7.18
	Br^-	2.76	2.80	7.21	2.78	2.83	7.21
	I^-	2.77	2.81	7.28	2.79	2.84	7.27

Table S3. Partitioning of the preparation energy according ref. [a]

Rosette	Ion	$\Delta E_{prep,HB}$	$\Delta E_{prep,stack}$
M_{12}	Cl^-	4.8	9.8
	Br^-	4.5	9.4
	I^-	3.6	8.5
M'_{12}	Cl^-	5.7	6.8
	Br^-	5.4	6.5
	I^-	5.0	6.0
M''_{12}	Cl^-	5.5	13.3
	Br^-	4.9	12.4
	I^-	3.9	10.9
a-AM_{12}	Na^+	3.4	8.1
	K^+	3.6	8.3
	Rb^+	2.7	5.3
a-AM'_{12}	Na^+	6.8	8.6
	K^+	1.5	2.7
	Rb^+	5.6	7.3
b-AM_{12}	Cl^-	6.3	13.9
	Br^-	5.7	13.0
	I^-	4.9	11.6
b-AM'_{12}	Cl^-	9.4	15.5
	Br^-	8.8	14.4
	I^-	8.1	12.6

[a] F. Zaccaria, G. Paragia, C. Fonseca Guerra, *Phys. Chem. Chem. Phys.*, **2016**, *18*, 20895–20904.

Table S4. Energy decomposition analysis (in kcal mol^{-1}) of stacked rosettes with C_2 symmetry in gas phase (ZORA-BLYP-D3(BJ)/TZ2P level of theory).

		ΔE_{int}	ΔE_{stack}					ΔE_{HB}				
			Total	ΔV_{elstat}	ΔE_{Pauli}	ΔE_{oi}	ΔE_{disp}	Total	ΔV_{elstat}	ΔE_{Pauli}	ΔE_{oi}	ΔE_{disp}
M$_{12}$	empty	-228.3	-52.8	-37.1	78.4	-13.0	-81.2	-175.5	-305.9	381.3	-188.3	-62.6
	Cl-	-308.9	-47.7	-32.9	83.7	-12.9	-85.6	-169.7	-318.1	419.8	-206.9	-64.6
	Br-	-307.5	-47.7	-32.8	83.4	-12.8	-85.5	-169.8	-316.2	415.8	-205.1	-64.3
	I-	-305.8	-47.7	-31.9	81.1	-12.5	-84.4	-170.6	-311.5	405.3	-200.7	-63.6
M'$_{12}$	empty	-467.1	-56.8	-39.6	81.6	-12.7	-86.0	-410.2	-500.7	569.5	-413.2	-65.9
	Cl-	-533.2	-55.7	-42.6	90.6	-13.6	-90.1	-413.1	-540.0	658.7	-463.9	-67.9
	Br-	-531.2	-55.7	-42.2	89.7	-13.5	-89.7	-412.7	-537.1	652.3	-460.3	-67.6
	I-	-528.0	-55.8	-41.1	87.2	-13.2	-88.7	-411.7	-530.7	638.4	-452.5	-66.9
M"$_{12}$	empty	-489.9	-59.6	-46.3	87.8	-17.6	-83.5	-430.3	-531.7	646.6	-476.6	-68.7
	Cl-	-581.3	-51.9	-36.9	89.8	-15.2	-89.5	-426.3	-536.4	674.4	-494.0	-70.3
	Br-	-578.8	-52.0	-36.4	88.4	-15.0	-88.9	-426.1	-533.1	665.7	-488.9	-69.9
	I-	-574.6	-52.6	-35.9	85.7	-14.7	-87.8	-425.6	-526.3	648.4	-478.6	-69.1
a-AM$_{12}$	empty	-291.3	-48.8	-31.3	72.3	-12.0	-77.9	-242.5	-405.4	509.1	-285.1	-61.1
	Na+	-391.6	-44.1	-25.7	70.1	-11.1	-77.5	-252.1	-448.8	606.0	-344.5	-64.9
	K+	-384.1	-44.1	-25.6	70.1	-11.1	-77.5	-252.0	-448.7	605.7	-344.1	-64.9
	Rb+	-372.6	-45.9	-28.5	73.7	-11.7	-79.4	-243.3	-436.5	579.9	-322.9	-63.9
a-AM'$_{12}$	empty	-367.4	-44.7	-25.2	68.0	-11.7	-75.8	-322.7	-400.0	461.1	-329.6	-54.3
	Na+	-466.8	-43.2	-23.9	74.0	-13.4	-79.8	-323.5	-414.2	505.5	-357.3	-57.5
	K+	-462.0	-43.8	-23.1	67.3	-12.0	-76.0	-325.7	-395.3	453.1	-328.8	-54.7
	Rb+	-461.7	-43.4	-23.6	72.6	-13.2	-79.1	-323.9	-410.7	495.9	-352.2	-57.0
b-AM$_{12}$	empty	-264.1	-51.3	-33.3	75.1	-15.1	-78.0	-212.8	-377.5	504.4	-273.2	-66.6
	Cl-	-363.4	-43.8	-26.3	82.4	-15.6	-84.3	-200.9	-382.5	544.0	-294.3	-68.1
	Br-	-360.1	-44.2	-25.9	80.7	-15.3	-83.7	-200.3	-377.6	533.9	-289.1	-67.5
	I-	-355.5	-44.8	-25.1	77.4	-14.8	-82.2	-200.3	-368.7	514.4	-279.4	-66.6
b-AM'$_{12}$	empty	-440.7	-56.5	-41.8	78.5	-18.6	-74.6	-384.2	-447.8	517.8	-392.6	-61.7
	Cl-	-550.1	-50.0	-32.0	87.0	-18.5	-86.6	-380.4	-464.1	570.9	-422.3	-64.8
	Br-	-547.9	-50.6	-32.0	85.9	-18.4	-86.1	-380.3	-460.9	562.2	-417.3	-64.3
	I-	-543.9	-51.8	-32.0	83.2	-18.1	-84.9	-379.9	-454.3	545.1	-407.4	-63.3

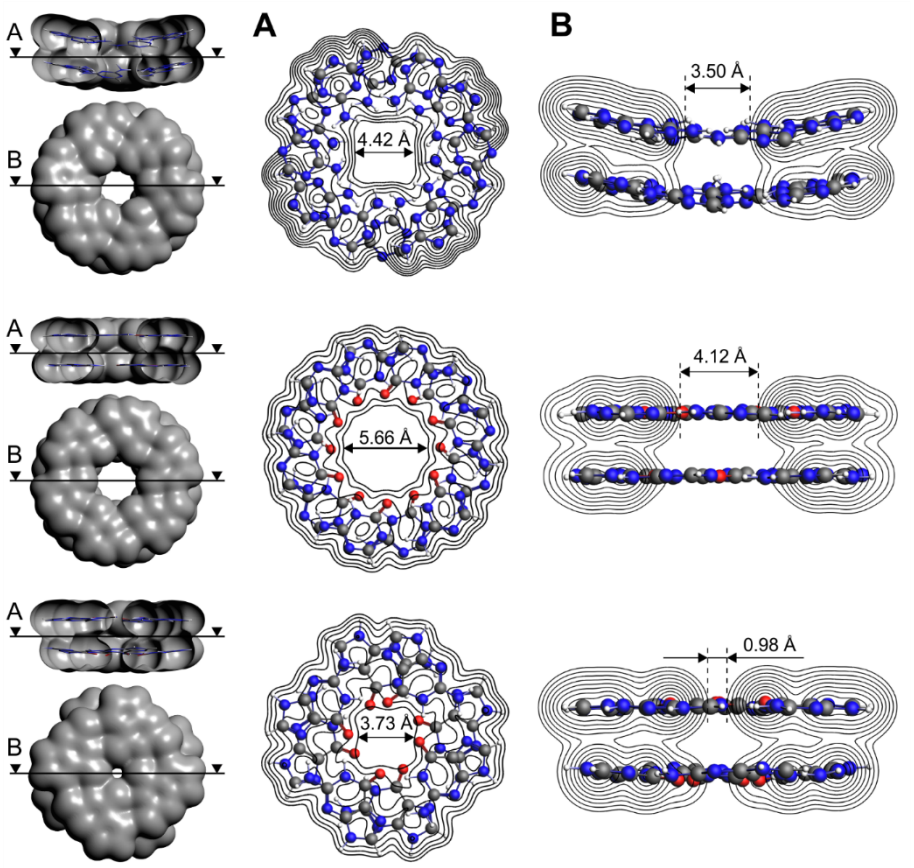

Figure S1. Longitudinal (A) and cross-sections (B) of electron density surfaces ρ(r) (isosurface ρ(r) = 0.001 a.u.). Top: M_{12}, middle: *a*-AM'_{12}, and bottom: guanine quadruplex. Computed at ZORA-BLYP-D3(BJ)/TZ2P in gas phase.

VII. GENERAL CONCLUSIONS

"The science of today is the technology of tomorrow"

Edward Teller

The aim of the present thesis was to examine the non-covalent interactions in supramolecules of mainly melamine (M) and cyanuric acid (CA), two daily chemical compounds. This thesis was also undertaken to evaluate the electronic and structural properties of some supramolecules in order to explain the self-assembling phenomenon. Therefore, the further purpose is the rational design of new materials.

Despite its exploratory nature, this study offers some insight into the self-assembly of M and CA. Firstly, both compounds are able to assemble each other through halogen bonds, being the brominated CA the best option. However, the analogue with Iodine should also be verified. It is interesting to highlight that the halogenated derivatives of cyanuric acid have been widely used as halogenating reagents in organic synthesis, but they were never tested as self-assembling building blocks. Hence, this could bring new properties to a well-known material.

Second, it has been shown that, within the M-CA adduct, the hydrogen bonds lead to a reinforcement of the intramolecular interactions of both monomers. In addition, the study of bonding energies suggest that the self-assembly of the mentioned compounds does not follow a preferential path, and it does not show cooperativity effects, as it is usually assumed. Nevertheless, the formation of the rosette is conducted by a localized cooperativity in the outer region of the supramolecule, although there is no observable preference for cyclic arrangements.

The third point is that the complex M_3AC_1 was shown to be more energetically and topologically favored than the M_1AC_3 tetramer. This is in line with the experimental observation of a new phase of self-assembled monolayer of M:CA (1:1) over Au(111).

The theoretical results shown herein provide also insights into the self-assembly of CA. This compound generates three different topologies when it is deposited as a monolayer, and they can coexist within the same layer. The computations have shown that one of those phases displays positive cooperativity, while the other one possess a stronger pair interaction. Therefore, during the self-assembling steps some competition between both arrangements may arise.

Finally, the most outstanding finding of this thesis is that the first hydrolysis by-product of melamine, which is called ammeline (AM), performs better than the former as a self-assembling building block for the construction of hexameric rosettes. This is because not only does AM has a larger pair interaction energy than M but also it displays a great synergy. This is the first study of AM which examines its self-assembling capacities, providing a theoretical framework for designing supramolecular materials. Our results have also established a quantitative background for the ion recognition properties of M and AM. Whilst the hexameric rosettes of the former will only recognize anions, AM could coordinate both cations and anions. These findings provide a way in the field of rational design of materials, and therefore further experimental research needs to examine more closely the self-assembling properties of M and AM.

ACKNOWLEDGEMENTS

The words of the inaugural address given by the physicist Albert Einstein to the Prussian Academy of Sciences fit perfectly to this letter of gratitude, simply because I have felt myself deeply identified with his speech:

> *"I have to thank you most heartily for conferring the greatest benefit on me that anybody can confer on a man like myself. By electing me to your Academy you have freed me from the distractions and cares of a professional life and so made it possible for me to devote myself entirely to scientific studies. I beg that you will continue to believe in my gratitude and my industry even when my efforts seem to you to yield but a poor result."*[1]
>
> Albert Einstein

Firstly, I deeply thank to my family, my biggest emotional support (and a few times my financial support): my mother Graciela, my sister Alexandra, my stepfather Guille, and my boyfriend Gustavo.

I acknowledge the National Council of Scientific and Technical Research (CONICET), the *Academy* that made this research to be possible, and by extension, my gratitude is also directed toward my country. I feel myself a very lucky person.

I also thank the big UTN family and the Secretary of Science and Technology of Facultad Regional Resistencia (FRRe), who not only did make a large contribution of funds to support the research of this thesis, but provided me the workplace where it was materialized. Once again, thank you country. If you ask yourself where your taxes are going to, a large part is invested in SCIENCE.

I enormously thank my mentors from Argentina, my professors of this scientific way: my supervisors Dr. Gladis Laura Sosa and Dr. Nélida María Peruchena. Two

[1] Albert Einstein. In *Einstein's essays in science.* Dover Publications Inc. Mineola. New York. 2009

beautiful people to whom I have a great affection and admiration. I do appreciate their instructions and for all the time they have spent with me, because *if I have seen further than others, it is by standing upon the shoulders of giants.*

I express my gratitude to my third home, my third *Academy*, in which a part of this research was possible. Firstly, I greatly thanks Prof. Dr. Célia Fonseca Guerra for having believed in me, and by extension, thank Prof. Dr. Matthias Bickelhaupt for having given me the opportunity to continue my dreams in their group. It is and it has been a great privilege. Thanks to the giant SCM team behind the ADF program. The Vrije Universiteit Amsterdam (VU) for having offered me a very warm and welcoming work place to materialize my ideas, and the Surfsara services for having provided me all their powerful computational resources. I also thank to the TC group for their company and friendship, and especially to Francesco Zaccaría, Stephanie van der Lubbe, Lando Wolters, and Ayush Narsaria for their invaluable help with the computations. A big thank you to Eva for all the Tea talks we had during our breaks, and Noelia for having helped me with the clusters.

To my uncle Nestor, my aunt Mirta and my cousins Bubi and Manu: thank you for having accompanied and supported me in this way. You have shared with me topics like supramolecular chemistry, molecular modeling and nanotechnology; thank you for having host this future Doctor. On the other side of the city, I sincerely thank my aunt Eunice, and all my cousins, nephews and nieces: Eli, Giampi, Ro, Luli, Eze, Valen, Sofi, Giuli and Isabelita. To my family from the Patagonian corner: Maxi, Agos, Sandra and “el Negro”. All of you made my trips happier.

To my big family from the QUITEX UTN group, thanks for your friendship and your advices. I feel very proud of the group I belong to.

To all my friends for all their support, they are uncountable. Hakunas, El Valle, the cinema, Nacional, and 54. Thanks for being there and listening my theoretical chemistry things.

To my collegues of the LEMYP group (Laboratorio de Estructura Molecular y Propiedades): Dr. Darío J. R. Duarte and MSc. Gabriel J. Buralli, thanks for the uncountable talks and the teamwork; Dr. Emilio Angelina and Dr. Fernanda Zalazar, thanks for having given me valuable advices.

To my English teacher Madia Burgos for all her positive wishes and her constant support; and also to my translator Chabela Rodriguez, who is an accomplice of most of my works.

PUBLICATIONS

2019 – **Designing self-assembling rosettes: Why ammeline is a superior building block than melamine.** Petelski, Andre N.; Fonseca Guerra, C. *ChemistryOpen,* **2019**, *8*, 135 – 142. (Front Cover and Cover Profile)

2017 – **Insights into the self-assembly steps of Cyanuric Acid toward rosette motifs. A DFT Study.** Petelski, Andre N.; Peruchena, Nélida M.; Pamies, Silvana C.; Sosa, Gladis L. Sosa. *Journal of Molecular Modeling,* **2017**, *23*, 263. (Topical Collection QUITEL 2016)

2016 – **Evolution of the hydrogen-bonding motif in the melamine-cyanuric acid co-crystal: A topological study.** Petelski, A. N.; Peruchena, N. M.; Sosa, G. L. *Journal of Molecular Modeling,* **2016***, 22*, 202.

2015 – **Intermolecular perturbation in the self-assembly of melamine.** Petelski, A. N.; Duarte, D. J. R.; Pamies, S. C.; Peruchena, N. M.; Sosa, G. L. *Theoretical Chemistry Accounts,* **2015***, 135*, 65. (Special collection of articles "CHITEL 2015 - Torino - Italy")